DISSERTATION

MOLECULAR CONSEQUENCES OF FETAL BVDV PERSISTENT INFECTION: TALES FROM THE PLACENTA AND SPLEEN

Submitted by

Hanah Michale Georges

Department of Biomedical Sciences

In partial fulfillment of the requirements

For the Degree of Doctor of Philosophy

Colorado State University

Fort Collins, Colorado

Summer 2021

Doctoral Committee:

Advisor: Thomas R. Hansen

Hana Van Campen
Helle Bielefeldt-Ohmann
Ann M. Hess

ABSTRACT

MOLECULAR CONSEQUENCES OF FETAL BVDV PERSISTENT INFECTION: TALES FROM THE PLACENTA AND SPLEEN

Introduction. Molecular consequences of viral vertical transmission have been heavily studied to understand how maternal viral infection contributes to the developmental origin of adult health and disease concept. Despite this research, knowledge on the molecular mechanisms behind congenital malformations and pathologies is limited due to a lack of in vivo models. Bovine viral diarrhea virus (BVDV), when infecting a pregnant female, crosses the placenta and infects the fetus. Maternal infection in early gestation results in persistently infected (PI) calves which shed the virus throughout their postnatal lives, making PI animals the main reservoir of BVDV today. Oftentimes, PI animals present with congenital malformations including immune system dysfunction, bone, neural, and heart abnormalities, as well as intrauterine growth restriction (IUGR) of fetuses. Many of these pathologies are also observed in human fetuses following placental inflammation, making the BVDV model unique and relevant to human and animal health. It was hypothesized that an attenuation of the fetal adaptive immune response occurs in the later stages of gestation (days 190 to 245), as measured in fetal spleen mRNA (Aim 1), fetal spleen methylation and protein (Aim 2), as well as in placental tissue protein (Aim 3), contributing to the fetal immunotolerance and PI of BVDV.

Approach. Forty-six BVDV naïve heifers were bred via artificial insemination and confirmed pregnant. At day 75 of gestation, 23 of those heifers were intranasally inoculated with non-cytopathic (ncp) BVDV type 2 as the PI group and the other 23 heifers were sham inoculated with media as a control group. Fetuses were sacrificed and collected via cesarian section at multiple timepoints throughout gestation: days 82, 89, 97, 190, and 245. Fetal spleens, maternal caruncles, and fetal cotyledons were frozen for molecular analysis as well as embedded in paraffin wax for immunohistochemical and histological analysis. Molecular analyses included mRNA, protein, and DNA methylation measurement for the splenic tissues and protein measurement for the placental tissues (maternal caruncle and fetal cotyledons).

Aim 1 Results. Experiment I: Immune response in PI fetal spleens throughout gestation. Day 82 PI fetal spleens did not exhibit significant changes in immune marker expression. By day 97, PI fetal spleens had a robust induction of the innate immune system and antigen presentation as confirmed by increased mRNA expression of *DDX58* (*RIGI*), *IRF7*, *ISG15, STAT4, IFI30, PSMB8/9.* On day 190, a drastic downregulation of the immune system had occurred, observed through the significant ($p < 0.05$) decrease in *IFNB, STAT4, IFI30, PSMB8/9, CD4, CD8A/B,* and *CD79B* mRNA concentrations in PIs when compared to controls. By day 245, only *ISG15* mRNA was significantly different (upregulated) in PI fetal spleens compared to controls.

Aim 2 Results. DNA methylation and proteomic analysis of day 245 fetal spleens. There were 2,641 differentially methylated regions; 1,951 hypermethylated regions and 691 hypomethylated regions in PI fetal spleens compared to controls. IPA identified several pathways associated with differentially methylated regions including bone

development, immune cell migration, as well as heart and brain development. Proteomic analysis revealed 12 differentially expressed proteins; TMA7, PEPD, NUDC, TMOD3, and SNRPF were increased (associated with protein processing) whereas THY1, HNRPC, CSRP1, VAPB, CSTB, AKAP2, and CNN2 (associated with immune development) were decreased in PI fetal spleens compared to controls.

Aim 3 Results. Protein analysis of maternal and fetal placental tissues throughout gestation. Infected maternal caruncles exhibited an interferon (IFN) response on day 82, 7 days post maternal inoculation. On days 89 and 97, infected caruncles had differential protein expression associated with nutrient exchange. However, on day 190, infected caruncles had an increased IFN response and a decrease in general cell signaling. By day 245, infected caruncles exhibited a change in proteins associated with mTOR , actin cytoskeleton, FAT10, EIF2, and phagosome signaling. In contrast, infected fetal cotyledons did not show differences on day 82 of gestation but by day 89, had an increase in type I and II IFN signaling proteins. By day 97, differential protein expression associated with cell survival, immune signaling, and nutrient exchange were observed to be mostly decreased in infected cotyledons compared to controls. Day 190 was the final day of protein abundance differences seen in infected cotyledons, including proteins associated with decreased cell proliferation, increased immune signaling, and altered nutrient exchange.

Conclusions. BVDV vertical transmission has drastic effects on fetal development, including immune dysfunction, bone, heart, and brain development. It is clear that the upregulation of immune genes seen in PI placental tissue on day 97 may be a result of both BVDV viral stimulation as well as a response to general placental inflammation. The

immune response of the PI fetus results in an attenuation of the innate and adaptive immune system in the fetal spleen, possibly regulated either/both Treg cells or DNA methylation. Additionally, the pathways associated with osteoclast differentiation/maturation was significantly altered in these PI fetuses, suggesting a reason for the observed osteopetrosis in postnatal PI animals. The altered osteoclast numbers are theorized to be the cause of extramedullary splenic hematopoiesis, severely hindering the development and mobilization of immune cells in the PI fetus, potentially causing the observed immune dysfunction, brain and heart abnormalities in PI animals.

ACKNOWLEDGEMENTS

I would like to acknowledge all of the wonderful people who have made my time and experience at CSU so memorable. First, my advisor, Dr. Hansen whose first email response to me was “Hello fellow Aggie!”, immediately making me feel welcome. Despite my initial hesitation, I fell in love with the BVDV project and had incredible support throughout it. His thoughtfulness, support, trust, and willingness to try something new has made quite the impact on myself and my career; allowing me to submit/work on several grants, develop and manage an amazing side project, helping me through the times where techniques randomly failed for no immediately apparent reason, and his recommendation for my postdoctoral position. Dr. Hana Van Campen, a committee member who always “wow-ed” me with her wonderful stories working with viral outbreaks in cattle. She has always been a welcoming light with a wealth of knowledge should it be needed. Jeanette Bishop who is a great sounding board and an incredible resource to learn any technique or develop protocols. Dr. Katie Knapek who also welcomed me and was happy to teach the way of the lab when it came to the BVDV samples and techniques. A great friend, office mate, snowboarding/hiking buddy, she definitely helped keep me enjoying life outside the lab. Dr. Helle Bielefeldt-Ohmann, a committee member who is also a great advisor and mentor, gracefully hosting me in her lab in Australia for a month, teaching me IHC and letting me give a few carrots to her rabbits. Dr. Ann Hess, a committee member with endless patience, happily meeting with Dr. Hansen and I about appropriate statistics and big data analysis on incredibly complicated data sets (at least, for me they were complicated). All the wonderful people at ARBL, not only helping with

the administrative work, but also for the lunches, chili cook-offs, valentine's day bake-offs and even more, they kept ARBL light and fun, making it a great place to work. Finally, my lovely therapy dog who kept me sane throughout my college career, demanding pats and walks when I needed them most. All of these incredible individuals make it extremely difficult to leave CSU but they will always hold a special place in my heart.

DEDICATION

To my fabulous family who have supported me in all my endeavors. From showing goats to a Ph.D, I couldn't have done it without you. A "thank you" will never be sufficient enough to express how grateful I am to you all.

TABLE OF CONTENTS

ABSTRACT II
ACKNOWLEDGEMENTS VI
DEDICATION VIII
CHAPTER 1: LITERATURE REVIEW 12
HISTORY OF BVDV 12
VIROLOGY 13
VIRAL REPLICATION 16
THE MAMMALIAN IMMUNE SYSTEM IN RESPONSE TO VIRAL INFECTION 20
BVDV ECONOMICS 22
VACCINE 24
THE GREAT DEBATE: PATHOGENESIS OF BVDV TO ESTABLISH PERSISTENT INFECTION 26
In Vitro: BVDV inhibits the innate immune response 26
In Vivo: IFN responses prior to immunotolerance in PI animals 28
CHAPTER 2: ATTENUATED LYMPHOCYTE ACTIVATION LEADS TO THE DEVELOPMENT OF IMMUNOTOLERANCE IN BOVINE FETUSES PERSISTENTLY INFECTED WITH BVDV 35
OVERVIEW: 35
IMPORTANCE: 36
INTRODUCTION 36
MATERIALS AND METHODS 39
Animals, viral infections, and fetal collections 39
Microarray 41
Transcriptional Analysis by RT-qPCR 41
Protein Analysis by Western Blot 43
Histology and Immunohistochemistry 44
Statistical Analysis and Data Management 45
RESULTS 46
Microarray 46
RT-qPCR 47
Western Blot 53
Histology and Immunohistochemistry 54
DISCUSSION 56
CHAPTER 3: EPIGENOMIC AND PROTEOMIC CHANGES IN BOVINE VIRAL DIARRHEA VIRUS PERSISTENTLY INFECTED FETAL SPLEENS: REPERCUSSIONS FOR THE DEVELOPING IMMUNE SYSTEM, BONE, BRAIN, AND HEART. 62
OVERVIEW: 62
INTRODUCTION 63
METHODS 65

Animals, viral infections, and fetal collections *65*
Reduced Representation Bisulfite Sequencing *66*
Methylation Bioinformatics and Pathway Analysis *67*
Protein Sample Preparation *67*
Liquid Chromatography and Mass Spectrometry *68*
Proteomics Data Analysis and Instrument Quality Control *69*
RESULTS 70
Reduced Representation Bisulfite Sequencing *70*
Proteomics *72*
DISCUSSION 72
Fetal BVDV PI alters the expression of genes that influence lymphocyte development. *73*
BVDV fetal infection alters osteoclastogenesis resulting in extramedullary splenic hematopoiesis *77*
Methylation patterns and protein expression in the PI fetal spleen are related to neural defects in PI fetuses. *85*
Genes affecting cardiac development are hypermethylated in the spleen of BVDV PI fetuses *87*
BVDV Replication and Immune Evasion *89*
CONCLUSIONS 91
CHAPTER 4: VERTICAL TRANSMISSION OF BVDV LEADS TO CYCLICAL PLACENTAL INFLAMMATION AND INTRAUTERINE GROWTH RESTRICTION IN INFECTED BOVINE FETUSES. 94
OVERVIEW: 94
INTRODUCTION 95
METHODS 98
Animals, BVDV inoculation, and tissue collection *98*
Sample preparation for LC-MS *99*
Liquid chromatography mass spectrometry and proteomic analysis *101*
Data Analysis *101*
Statistical and pathway analyses *102*
RESULTS 103
Caruncle *103*
Cotyledon *106*
DISCUSSION 108
Placental inflammation and hindered nutrient transport in early infection sets the stage for IUGR *108*
Placental cellular stress responses inhibited; fetal protective mechanism, direct inhibition by BVDV, or viral immunotolerance? *111*
Placental IFN and inflammatory response to BVDV is cyclical *114*
CONCLUSIONS 117
CHAPTER 5: CONCLUSIONS 120
BIBLIOGRAPHY 126
APPENDIX 145

TABLE OF ABBREVIATIONS 173

Chapter 1: Literature Review

History of BVDV

A mysterious disease was discovered in a New York dairy herd in 1946 and rapidly spread to 5 more herds [1, 2]. Clinical presentations being the cattle became anorexic, exhibited diarrhea, had elevated body temperatures, and developed ulcers on mucosal tissue [1, 2]. The veterinarians recorded that some animals showed mild symptoms while others were much more severe [1]. During the same year, an “X disease” was identified in Western Canada, presenting as acute or subacute infections [3, 4]. Although clinical signs of X disease were consistent with the New York disease, an important distinction was that the New York disease could be experimentally transmitted whereas X disease could not for unknown reasons [1, 3, 4]. Following the success of the experimental transmission of the New York disease, researchers determined that the disease was viral and affected animals differently; some presenting with no symptoms and others presenting with severe pyrexia, diarrhea, nasal discharge, leukopenia, and mouth ulcers [1, 4]. Interestingly, the animals that succumbed to the virus diarrhea was found to have postmortem findings very similar to those found in cattle infected with X disease [4]. After the successful experimental transmission of the New York virus, it was termed virus diarrhea of cattle [4]. At an Iowa farm, another disease broke out similar to virus diarrhea; however, mucus discharge was not consistent with virus diarrhea and experimental transmission was not achieved [4]. Due to the mucosal lesions found in the Iowa cattle, the disease was termed mucosal disease by veterinarians [4].

In 1957, the virus from mucosal disease was propagated in cell culture for the first time [2, 4, 5]. This particular isolated virus was cytopathic (cp) to the cultured cells.

Another group at Cornell also propagated the virus from virus diarrhea which was found to be non-cytopathic to cells in culture [4]. By this time, the virus had been isolated in the US, Canada, Germany, and the United Kingdom [2]. Following the propagation virus from of several different cases of virus diarrhea and mucosal disease, it was found that the antibodies from cattle infected with virus diarrhea could neutralize the cytopathic effects of mucosal disease. By 1960, researchers determined that despite differences in mortality and experimental transmission, virus diarrhea and mucosal disease were related viruses. In the 1960s-1970s, virus diarrhea and mucosal disease became known as bovine viral diarrhea mucosal disease complex, later changed to bovine viral diarrhea virus (BVDV). In the 1980s, BVDV, border disease virus, and classical swine fever virus were classified together in the pestivirus genus, part of the *Togaviridae* family. In 1991, after advances in molecular techniques, BVDV and other pestiviruses were reclassified from the *Togaviridae* family to the *Flaviviridae* family.

Virology

The identification and classification of BVDV has a long history which includes mis-classification. However, with the advancement of technology, proper taxonomic classification was achievable and assisted in the understanding of BVDV replication. Although BVDV had similar organization and replication as other viruses in the Flaviviridae family, it does contain several unique characteristics. Such characteristics have made the understanding of the virus difficult but several studies to have been done in attempt to uncover these mysteries.

The Flaviviridae family of viruses contains three genera: Hepacivirus, Flavivirus, and Pestivirus [6, 7]. The viruses classified in the Flaviviridae family are enveloped, nonsegmented, single positive strand RNA viruses with a single large open reading frame (ORF) [7]. Viral genomes of the family range from 8.9-13 kb depending on the genus and individual viruses [7]. The flaviviral family virion contains a single core/capsid protein and 2-3 envelope glycoproteins [7].

The pestivirus genus of the *Flaviviridae* family contains four viruses, all affecting the agricultural industry: BVDV-1, BVDV-2, Classical Swine Fever Virus (CSFV), and Border Disease Virus (BDV) [6]. Viruses in this genus, known as pestiviruses, are typically transmitted through respiratory droplets, urine, or feces, causing subclinical or enteric disease [7].

BVDV is a complex classification of several viruses, containing 2 (controversially 3) different genotypes, several subgenotypes, and 2 biotypes. Although complex, many attributes of the viruses are conserved among subgenotypes and biotypes. Interestingly, infection with different BVDV genotypes, subgenotypes, and biotypes often leads to the hosts' production of cross-neutralizing antibodies which results in the inability to recognize serological subgroups [8, 9]. This led to the identification of BVDV strains based on genomic and cell culture differences.

Like most viruses in the *Flaviviridae* family, BVDV species have large ORF regions flanked by both a 5' and 3' untranslated region (UTR)/non-coding region [4, 7]. BVDV translation is mediated by an internal ribosome entry site (IRES) which begins translation at the first protein in the BVDV genome, Npro [10]. Npro is a viral protease which once translated, will cleave the other BVDV viral proteins along with endogenous cellular

proteases [4]. Following the Npro region of the BVDV genome are a capsid protein, three structural envelope glycoproteins (E^{rns}, E1, and E2), and 5-6 nonstructural proteins (NS2/3, NS4A, NS4B, NS5A, and NS5B). The differences between BVDV 1 and 2, recently changed to Pestivirus A and Pestivirus B, respectively, and subgenotypes stem from genomic differences and mutations [11]. Genotypes for BVDV 1 and BVDV 2 differ significantly in the 5' UTR. Although this is not a coding region, the UTR differences implement distinctive strategies for the initiation of viral translation. There are other conserved genomic differences between the BVDV 1 and 2 species which further their distinction from one another and allow the different genotypes to evade the hosts' immune system [4, 12]. These viruses are often referred to as simply BVDV in clinical settings with further classification occurring after further diagnostic tests.

Minor point mutations in BVDV genotypes result in BVDV subgenotypes. Genome differences in BVDV subgenotypes are seen mostly in the Npro and E2 (envelope protein) coding regions [13]. The glycoprotein encoded by the E2 region is the dominant target for host antibody responses and mutations in this region provide new opportunities for BVDV isolates to evade host antibodies [13]. Overall, there are currently 21 subgenotypes of BVDV-1 (BVDV-1a to BVDV-1u) and four subgenotypes of BVDV-2 (BVDV-2a to BVDV2-d) [13]. These subgenotypes are associated with geographical regions. However, the most prevalent BVDV subgenotype in the Americas, Asia, and Europe is BVDV-1b followed by BVDV-1a [9, 13-15]. The most predominant BVDV subgenotype in Africa is BVDV-1a [13]. Certain subgenotypes, BVDV-1m to BVDV-1p and BVDV-1q, have only been found in Asia [13]. Subgenotypes BVDV-1f to -1h, -1k, -1l, and -1r to -1t have only

been reported in Europe [13]. For BVDV-2, the primary subgenotype in the world is BVDV-2a; BVDV-2c has only been isolated in Europe and the Americas [13, 16].

In addition to point mutations, BVDV and other RNA viruses are prone to homologous and non-homologous recombination events. The noncytopathic (ncp) biotype of BVDV is the most prevalent biotype in natural infections. In persistently infected animals (see pages 15-17), animals originally infected with ncp BVDV *in utero*, a recombination event may occur that leads to the introduction of a non-regulated cleavage site in non-structural protein NS2/3 [4, 17-20]. With the introduction of a new cleavage site, NS2/3 is cleaved into NS2 and NS3(p80) which creates the cytopathic (cp) biotype of BVDV in the already infected PI animal [4, 17-20]. The cp biotype of BVDV is named for its cytopathic abilities in cell culture while ncp biotypes does not have cytopathic abilities [4]. A PI animal with ncp and cp biotypes will develop mucosal disease (see pages 15-17) [4, 18, 19]. This biotype mutation also occurs in other pestiviruses and is usually a result of extensive replication of the ncp pestivirus biotype, seen in PI animals [4, 18, 19].

Viral Replication

Viral infection occurs with the interaction of virions with cellular receptors and co-receptors. The virus fuses with the cell membranes and releases the viral genomic RNA into the cellular cytoplasm. The viral genomic RNA acts as a template for the translation of viral polyproteins, which is post-translationally cleaved by both viral and cellular proteases [7]. After translation of cleavage of the polyprotein, the virion is assembled, transported via cytoplasmic vesicles, and exocytosed from the cell [7].

The specific method by which BVDV binds to the cell to begin host cell invasion and replication and then spread to other cells has been debated recently. The BVDV E^{rns} protein has been reported to interact with heparan sulphates that bind to bovine CD46 receptor for cellular entry by endocytosis [21-23]. However, in a CD46 knockout in vitro model, BVDV remained capable of infecting the cells, although, at a reduced rate [24]. Interestingly, with additional passaging of the virus in the CD46 knockout cell line, the research group found that the virus developed mutations in the BVDV E^{rns} protein which increased the virus's infectivity in the knockout cells [24]. Additionally, the over-expression of CD46 reduced BVDV infectivity rate, indicating that an additional cellular entry factor is needed for optimal infectivity [21]. In another study, BVDV was shown to have a preference for CD46 independent methods of cell to cell transmission [21, 25]. BVDV cell-to-cell transmission is proposed to occur through the accumulation of exocytic vesicles containing virions at the site of cellular junctions [25]. Through clathrin-dependent endocytosis, BVDV E2 on the virion membrane binds to coreceptors on the susceptible uninfected cell and induces internalization of the virion [25]. It is currently theorized that the CD46 receptor assists in the entry of free BVDV virions into susceptible cells through its interaction with BVDV E^{rns} protein. Although CD46 is not required for cellular entry, it certainly improves the efficiency by which free virus infects susceptible cells. Following the initial infection of susceptible cells, BVDV then rapidly spreads through the host using cell-to-cell transmission through the interaction of BVDV E2 protein with cellular junctions.

While the structural proteins of BVDV are necessary for viral entry into cells, the non-structural proteins are critical for viral replication and pathogenicity. As discussed above in the BVDV biotypes section, the cleavage of autoprotease NS2/3 differentiates

ncp from cp BVDV biotypes. However, it has been shown the ncp BVDV has highly regulated NS2/3 cleavage which occurs early in infection [26]. The NS2 protease, when in the presence of cellular chaperone “Jiv” (J domain protein interacting with viral protein), will cleave the ncp BVDV NS2/3 [20, 26-28]. Cleaved NS2 and NS3 proteases are present in cells infected with ncp BVDV up to 9 hours post infection [20, 26-28]. Both cleaved products result in high viral replication; however, after the first few hours of ncp BVDV infection, this cleavage diminishes after cellular Jiv is consumed by this process [20, 26-28]. At this point, un-cleaved NS2/3 is used for the formation of the virion [29]. A possible explanation for this phenomenon is for BVDV to quickly establish viral replication then drastically reduce the process in order to evade the hosts’ immune system [28]. In an infection with cp BVDV, NS3 accumulates at all times during the infection, indicating a non-regulated cleavage of NS2/3 due to a genomic mutation. In certain in-vitro studies, it was observed that cp BVDV depended on a “helper” virus, usually the ncp BVDV virus which the cp strain mutated from, for efficient replication [28]. Despite this finding, an experimental in vivo cp BVDV infection did result in serological responses in both dams and fetuses but did not result in a PI animal [30]. Although cp BVDV can infect without ncp BVDV, the natural prevalence and efficient replication of cp BVDV is enhanced in the presence of ncp BVDV.

Very little is known about the functions of BVDV NS4A, NS4B, and NS5A in viral replication. However, it is known that they are needed for virion packaging. NS4A has been identified as a cofactor for NS3 to assist in the processing of other downstream proteins [31]. Additionally, NS4A along with NS5B are necessary for efficient virion assembly [29, 32]. Single stranded RNA viruses, such as BVDV, have a double stranded

RNA (dsRNA) intermediate in the infected cell's cytoplasm during viral replication [33]. In this case, BVDV NS4A has been identified as a binding site for adenosine deaminase acting on RNA (ADAR) [33]. ADAR hyperedits dsRNA as part of the innate immune system in response to large RNA viruses [33]. The binding of ADAR limits its ability to hyperedit dsRNA; therefore, the ability of BVDV NS4A to bind to ADAR may be an evolutionary trait for BVDV to evade the host's immune system [33]. NS4B has been found to induce alterations in cellular membranes for the formation of the BVDV replication complex [34]. NS4B has also been shown to induce autophagy and the formation of autophagosomes which increases viral replication [35]. NS5A has been shown to interact with NIK- and IKK β binding protein (NIBP) and inhibit NFKB activation *in vitro*, suggesting another route of host immune system evasion [36]. As is the case with most of the NS BVDV viral proteins, NS5A is also an important component of the viral replicase and efficient viral replication process [37].

While the functions of BVDV viral proteins NS4A-NS5A are not fully understood, the function of NS5B is well known and critical for the success of BVDV replication. BVDV NS5B is an RNA dependent RNA polymerase (RdRp) [38]. In addition to the RNA polymerase activity, it has been suggested that NS5B may also have a role in the viral encapsidation and virion assembly [39].

Additional research on the functions of BVDV NS proteins is still needed. However, mounting evidence suggests that every NS protein is critical for the efficient replication of BVDV, mostly virion assembly. There also seems to be several different host immune system evasion techniques that the individual NS proteins are needed for, attributing to the incredible infectivity and immunosuppressive abilities of BVDV.

The Mammalian Immune System in Response to Viral Infection

The mammalian immune system is extremely complex, with branches and sub-branches which are differentially activated based on the stimulus. The first, front line defense to infection is the innate immune branch, mostly associated with inflammation [40]. Should the innate system be unable to clear the pathogen within a few hours, the adaptive branch is stimulated and usually clears the invading pathogen using pathogen specific responses, including the generation of antibodies [40]. Although very different, these branches work together to rid the mammal of the infecting pathogen as quickly as possible, while “learning” the pathogen to generate memory for future, more robust responses.

The innate branch of the immune system is the first line of defense against pathogens, responding to the invading pathogen within hours of pathogen entry. The innate immune response recognizes pathogen-associated molecular patterns (PAMPs) on microbes and molecules from damaged cells, damage-associated molecular patterns (DAMPs) through pattern recognition receptors (PRRs) on cells [41, 42]. These PRRs include toll like receptors (TLRs), nucleotide binding oligomerization domains (NOD), retinoic acid inducible gene 1 like receptors (RLR/RIGI), and C type lectin receptors (CLRs) [41]. Most of these PRR receptors activate pathways associated with inflammatory responses, specifically, the transcription of proinflammatory cytokines, type I interferons (IFNs), chemokines, and pathway modulators [43]. Of particular interest is the type I IFN response, which has a central role in antiviral responses. Once a PRR is activated by the invading virus, IFN transcriptional regulators nuclear factor kappa B

(NFKB), interferon regulator factors (IRF) 3 and 7, are activated and induce the transcription of type I IFNs, IFNA and IFNB [44, 45]. IFNA and IFNB then bind to neighboring cells through their receptors, IFNAR1 and IFNAR2 [45]. IFNAR 1 and 2 form a heterodimer, activating the janus kinase (JAK) and signal transducer and activator of transcription (STAT) pathway. Following the JAK STAT pathway, STAT1 and 2 bind to IRF9 forming the interferon stimulating gene factor 3 (ISGF3) complex [45]. The ISGF3 complex binds to interferon stimulated gene (ISG) promotors to induce their transcription [45]. ISG expression leads to an antiviral state in the cell, promoting inflammation, inhibiting viral replication, and activating the adaptive immune response [45].

Cross communication from the innate to adaptive branches of the immune response involves several different cells and signal pathways. In a viral response, type I IFNs, along with interleukin 12, promote CD8 T cell activation and expansion through STAT4 and IFNG signaling [46, 47]. IFNG further promotes CD8 T cell expansion by promoting major histocompatibility complex (MHC) class I expression through the induction of PSMB8 and 9, which presents antigens to CD8 T cells [48, 49]. In addition to CD8 T cell activation, IFNG is further produced by antigen presenting cells for CD4 T helper cell differentiation [50]. IFNG also stimulates IFI30 lysosomal thiol reductase (IFI30/GILT) which promotes the expression of MHC class II expression on CD4 T cells [51]. Active CD4 T helper cells activate B cells for the production of virus specific antibodies and the production of memory B cells to protect the host from future infection if it comes in contact with the same virus [52].

BVDV Economics

The worldwide economic impact of BVDV is considerable and is recognized as a large cost to the cattle industry. However, estimations of the economic impact are difficult due to dependencies on geographical conditions, country/region eradication efforts, differing vaccination strategies, management differences, and many other factors. It is accepted that economic losses due to BVDV include not only the death of animals but also production loss / additional infection due to immunosuppression, reproductive failures (reduced conception and abortions), calf deformities, and reduced gain/milk production [53-56].

Several studies have estimated that a BVDV outbreak would cost a producer anywhere from $20-$103/animal while the worldwide loss to BVDV was estimated to be between $1.5 and $2.5 billion [57-60]. Despite this drastic loss due to BVDV, one major hurdle identified to the control of BVDV in the US was the cost vs. benefit to cow calf producers for testing and culling for BVDV. With an estimated 4% of US cattle herds having a PI animal and national PI prevalence being 0.6%, cow-calf producers are hesitant to continuously test for PI cattle [15, 58, 61]. Most costs due to BVDV PI animals are incurred in the feedlot setting, where the high concentration of animals allows the virus to spread quickly, even with a low prevalence of PI animals [58]. An estimated 0.3% of feedlot animals are PI for BVDV, which seems minor; however, with 77% of cattle being produced in a feedlot with a capacity over 1000 animals, approximately 3 or more of those cattle in a single feedlot at any given time are PI for BVDV [62, 63]. That type of confinement and concentration of cattle allows for BVDV to spread rapidly, despite BVDV vaccination of animals upon feedlot entry [62]. The presence of PI animals in a feedlot lead to a 43% increase in treatment for respiratory disease in animals exposed to a PI

animal, and a 15.9% increase in feedlot wide respiratory tract disease [62]. With the generation of PI animals occurring at the cow-calf level while most of the costs are incurred at the feedlot level, how can the US cattle industry promote BVDV testing and eradication at the cow-calf level?

In a recent cost benefit analysis/review, the authors sought to understand the benefit, if there was one, of cow-calf producers testing for BVDV [58]. The authors found that for the cow-calf operators that did not have a BVDV infection (96% of operations), the cost of testing and management resulted in a loss of $54.25 per cow [58]. However, infected herds (4% of operations) gained $278.28 per cow with the more intensive management [58]. Without any type of premium offered for animals managed intensively for BVDV, the industry, as a whole, would lose $40.95/cow due to the low amount of BVDV infected herds [58]. There is not currently a premium offered for BVDV tested animals [58]. Despite this, a premium may be offered for a VAC 24/34/45 program which is a program of intensive vaccinations before the cattle reach the feedlot [58]. The average premium for VAC cattle is $9.90 / 100kg which would result in a gain of $54.29/ cow if a similar premium was offered for BVDV intensive management [58]. In the past, there have been voluntary BVDV eradication programs in the US, some of which offered assistance to cover the cost of PI testing [64]. Unfortunately, these programs have not had a substantial impact on BVDV prevalence in the US, most likely due to testing costs and producer effort in monitoring. Economically, the intensive testing for BVDV PI cattle is costly to the cow-calf producer but with a widespread implementation of a premium for BVDV managed cattle, cow calf producers may be willing to test and cull their PI animals, which in turn, would benefit the feedlot sector and the national cattle industry as well.

Vaccine

Since the beginning of BVDV vaccine use in the 1960s, producers have been unsuccessful in BVDV eradication from vaccine use alone due to the heterogeneity of BVDV and the ability of the virus to be vertically transmitted [65-68]. Several vaccines are available commercially, including both killed vaccines (KV) and modified-live viral (MLV) vaccines [69]. Most BVDV vaccines have shown protection against clinical disease and PI generation in controlled experimental settings; however, the rapid mutation rate of the virus and less controlled vaccination protocols in normal cattle production offer yet another difficult hurdle in BVDV control. Due to this hurdle, most modern BVDV vaccines contain both BVDV1 and BVDV2 isolates to increase protection against BVDV field strains [65, 70, 71]. Although several vaccination options are available, the efficacy and safety of the vaccines are controversial. Despite this controversy, BVDV vaccination is centered around two goals, to prevent disease and symptoms of BVDV after exposure and to prevent herd transmission and vertical transmission of BVDV from dam to fetus [65, 66, 69]. With these goals in mind, producers must decide which type of vaccine, KV or MLV, fits their program the best and offer the most protection to their cattle.

BVDV KV is primarily used for its increased safety, as KV is not able to cause immunosuppression or replicate in the host [69]. This offers an advantage to MLV since it has a lower risk of BVDV PI generation should the vaccine be given to pregnant females [69]. Despite the increased safety of the KV, the immune stimulation and BVDV protection is significantly less than what is observed with MLV. The KV vaccine mostly recognizes BVDV structural proteins (Erns, E2), stimulating an antibody and T helper cell immune response. Despite this, cross protection and duration of immunity with the KV is limited, requiring the use of several boosters (reviewed in [65, 69]).

In contrast to the KV, the MLV vaccine offers superior protection, particularly to fetuses if an appropriate vaccination schedule is used, but at the risk of PI animal generation and possible immunosuppression of the animal if proper vaccination scheduling is not performed. MLV elicits higher levels of antibodies and a more robust T cell response (Thelper and Tcytotoxic), as well as a more rapid protective response [65, 69, 70, 72]. MLV vaccines are shown to be more similar to natural BVDV infections, causing the host's immune system to recognize and target both structural and nonstructural BVDV proteins, including the capsid protein, Erns, E1, E2 and NS2/3 [65]. Additionally, MLV vaccines allow protection against BVDV for more than one year, with boosters required less frequently than with KV (reviewed in [70]). Despite the seemingly superior protection that MLV BVDV vaccine offers, due safety concerns such as immunosuppression, BVDV contamination of fetal bovine serum used in the generation of MLV vaccines, and the possible generation of PI animals, MLV vaccines are not recommended to give to pregnant females unless the females were vaccinated prior to breeding (reviewed in [65]).

BVDV vaccines do offer protection; however, vaccination alone is not robust enough to achieve eradication. Strict vaccination schedules for maximum protection against clinical disease and PI generation is generally recommended. Vaccinated animals have been shown to generate PI animals [73]. Both KV and MLV BVDV vaccines have been shown to offer incomplete fetal protection from BVDV vertical transmission but they have both also been shown to significantly reduce abortions and PI births [69, 74]. The eradication and control of BVDV in the US will require more than vaccination strategies,

it will also necessitate biosecurity measures and the identification and elimination of PI animals from the national cattle herd [65].

The Great Debate: Pathogenesis of BVDV to establish Persistent Infection

Due to its persistence in the cattle industry, BVDV has been heavily studied in both in vitro and in vivo models. Interestingly, the in vitro and in vivo models don't always agree with each other, leading to robust debates among BVDV groups on the pathogenesis of establishing PI by BVDV. Despite this, it's important to consider both models when attempting to understand the complicated pathogenesis of BVDV.

In Vitro: BVDV inhibits the innate immune response

Several groups have identified potential methods of action for the ability of ncpBVDV to evade the host's innate immune response, specifically, the induction of type I interferons (IFN). In 2001, a group from Switzerland infected bovine turbinate cells, Madin-Darby bovine kidney cells (MDBK), and monocyte derived macrophages with a ncpBVDV strain then followed infection with a poly I:C transfection to induce type I IFNs [75]. In BVDV infected cells, IFNA and IFNB expression was lower than mock infected cells; however, following poly I:C transfection, IFNA and IFNB expression was higher than mock infected controls [75]. The authors concluded that BVDV doesn't inhibit IFN response but rather, evades it and does not induce apoptosis [75]. Contrarily, in 2002, another group infected calf testis cells with ncp BVDV followed by poly I:C treatment or infection with Semliki Forest virus) [76]. They found that ncp BVDV did inhibit IFN production (measured by MX1) in both BVDV and SFV infection, through blocking

transcriptional regulator IRF3 binding to DNA, thus inhibiting IFN transcription, as opposed to the evasion concluded in the 2001 study [76]. In what seems to be a rebuttal, the Switzerland group published another study in 2006 in which they found that MX1 can be induced independently of type I IFNs [77]. The authors maintained the conclusion that cp and ncp BVDV evade the host's IFN response, contributing the differences between the two published results to differences in BVDV strain and cell lines [77].

Additionally, a group that infected human epithelial (Hep2) and African green monkey kidney cells (Vero) with ncp BVDV found that the Npro BVDV protein blocked activation of IRF3 to inhibit type I IFN response [78]. The Switzerland group followed this study up with another that found ncp BVDV Erns protein may prevent IFN induction in uninfected cells neighboring BVDV infected cells, thus an inhibition of communication between cells in response to BVDV infection [79]. Interestingly, a group in South Dakota found that ncp BVDV Npro protein associates with DAMP S100A9 to prevent its activity, supporting the conclusion that ncp BVDV inhibits cellular communication between infected and noninfected cells [80]. The study found that with inhibition of S100A9, BVDV replication was enhanced and IFN production was hindered [80].

In vitro work can be very valuable to understand viral mechanisms of infection. However, in vitro infections are not a perfect model as the studies are limited by the availability of established cell lines such as bovine placental cells. To support the idea that the availability immortalized bovine cell lines limit the understanding of BVDV infection, one group harvested cells directly from bovine lymph nodes and identified that non-T/B cell populations were able to produce type I IFNs following ncp BVDV infection in vitro [81]. Additionally, establishing a persistently infected cell model, to mimic what is

seen in PI fetuses, is not achievable due to the many organ systems and immune changes involved to create a PI animal. Despite these limitations, the in vitro work may give insight into possible mechanisms involved in the establishment of immunotolerance seen in vivo.

In Vivo: IFN responses prior to immunotolerance in PI animals

The generation of in vivo models for intrauterine infection with BVDV is costly and complicated. However, it is needed for a complete understanding of the establishment of BVDV PI and its effects on fetal development. Only a few groups have been able to create in vivo models for PI infection ours being one of them. The time needed for the transmission of BVDV from the dam to the fetus has been shown to be dependent on the BVDV strain used and the infection model. In a sheep model, BVDV was transmitted from dam to fetus in 72 hours following intranasal inoculation [82]. In a bovine model in which the dams were intravenously infected very early in gestation (day 26), BVDV was found in placental membranes and allantoic fluid 6 days post maternal inoculation [83]. However, the authors concluded that BVDV infected the embryo prior to complete implantation/placentation [83]. The method of inoculation may have also decreased the transmission time as BVDV is not transmitted intravenously in nature. In a PI study in which pregnant heifers were intranasally inoculated on day 75 of gestation, maternal viremia was present seven days post inoculation and cleared by two weeks post inoculation [84]. Fetal viremia was present two weeks post maternal inoculation and was consistently present throughout gestation [84].

With the acceptance that maternal infection with BVDV takes seven days and vertical transmission takes 14 days after initial exposure to the virus, the mystery of the IFN responses was studied. One group directly infected fetuses by performing laparotomies, aspirating amniotic fluid, adding ncp BVDV to the amniotic fluid, then adding the BVDV containing amniotic fluid back into the amniotic cavity [85]. The group found ncp BVDV in the fetal spleens 7 days post infection; however, MX1 was not increased from those spleens when compared to uninfected controls [85]. With this data, the authors concluded that the IFN response to BVDV was inhibited by the virus in PI fetuses [85]. The short timeframe from infection to collection and the lack of collections past the 7 day mark may not have given the fetus enough time to respond to the viral infection, thus leading the authors to jump to conclusions based on the published in vitro data.

Maternally, the virus is quickly cleared through a complete immune response from the dam, as determined by a measurement of ISGs in the maternal blood starting 3 days post inoculation and ending approximately 7-10 days post inoculation [84]. Additionally, *ISG15* mRNA was found in maternal placental tissue (caruncle) starting at 2 weeks post inoculation and persisting for 117 days post inoculation [84]. The induction of ISG15 in the caruncle after maternal clearing of BVDV is not well understood but may shed light on the stimulation of immune pathways in maternal tissues from BVDV PI fetal crosstalk at the placentome. *ISG15* mRNA expression was significantly increased in the blood of PI fetuses at 2 weeks and 117 days post maternal inoculation. Intracellular sensor DDX58/RIGI and MDA5 was increased in the PI fetal blood at the 2 week mark [84]. In the fetal placental membranes, IFNA, IFNB, and ISG15 were all significantly upregulated

117 days post maternal inoculation, possibly contributing to the stimulation of ISG15 in maternal tissues [84]. IFNG, a type II IFN, is induced after the activation of the innate immune system. IFNG works to stimulate communication with the adaptive branch of the immune system, through activation of antigen presentation and T cell proliferation. In previous studies, IFNG expression was found to be upregulated in maternal blood, PI fetal blood, and PI amniotic fluid 2 weeks post maternal inoculation [86]. With the knowledge that BVDV is present in both maternal and fetal blood, as well as its ability to induce type I IFNs in both the maternal and fetal placental tissues, it is clear that BVDV vertical transmission occurs approximately two weeks post maternal infection, causing placental inflammation and possibly, long term fetal pathologies.

To understand the effects of BVDV on PI fetal immune development and the molecular mechanisms behind immunotolerance to the virus, the fetal lymphoid tissues were investigated. BVDV was present in fetal thymus, liver, spleen, blood (discussed above), and even in neural tissue following vertical transmission [86-88]. In the fetal spleen, STAT1, important for type I IFN signal transduction, was upregulated in PI fetuses 21 days post maternal inoculation and downregulated at 117 days post maternal inoculation [86]. Chemokine ligands (CXCL) CXCL10, CXCL16, chemokine receptor (CXCR) 6, and interferon gamma inducible protein (IFI16) were all upregulated in the PI fetal spleens 21 days post maternal inoculation when compared to uninfected controls [86]. In a separate study, PI fetal spleens exhibited a downregulation of nuclear factor kappa B (NFKB), cluster of differentiation (CD)4, and CD8B 117 days post maternal inoculation [89]. These trends are indicative of a type I IFN response in the fetal spleen

after vertical transmission; however, the reason for the down regulation of the innate and adaptive responses by 117 days post maternal inoculation has yet to be elucidated.

In the fetal thymus, early PI fetal responses were not measured. However, when the mRNAs associated with type I IFN responses were measured 117 days post maternal inoculation, NFKB and IFNB were found to be significantly down regulated in the PI fetal thymuses when compared to controls [89]. Additionally, PSMB8 and 9 (associated with antigen presentation), as well as T cell markers CD4 and CD8A/B, and B cell marker CD79B were all significantly down regulated in PI fetal thymuses 117 days post maternal infection when compared to controls [89]. It is clear that there is some direct inhibition of the fetal immune system at this time point, possibly due to the establishment of immunotolerance.

Fetal brains from PI fetuses were evaluated for BVDV antigen presence and ISG15 response. Antigen was found in PI fetal brains, specifically amoeboid glial cells, as early as 14 days post maternal inoculation [87]. Vasculopathy was also observed in PI fetal brains beginning at 14 days post maternal inoculation [87]. ISG15 protein was found in the PI fetal neural microvasculature at 14 days post maternal infection and in most cells by 117 days post maternal inoculation [87]. Interestingly, BVDV antigen and ISG15 protein was only seen in 2/4 of the PI fetal brains at the 2 week time point, indicating that some PI fetuses may be slightly delayed in viral transmission and spread to the fetal brain [87].

The fetal liver houses large numbers of immature lymphocytes and is a critical lymphoid organ. One group looked at the PI fetal liver in response to BVDV maternal infection. As expected, BVDV antigen was not found in livers 7 days post maternal

inoculation [88]. BVDV antigen was present in PI fetal livers 14 days post maternal inoculation and persisted at all other timepoints [88]. Additionally, MHCI and MHCII containing cells were measured via flow cytometry and revealed that PI fetal livers, 14 days post maternal inoculation, had a larger population of cells expressing MHCI and MHCII proteins, with an increase in MHCII indicating increased antigen presentation [88]. Hepatic Kupffer cells, which express both MHCI and MHCII, were confirmed to be infected with BVDV in the PI fetuses [88]. Although they were not able to confirm Kupffer cell expression of immunotolerant cytokines, the authors suggested that Kupffer cells, which express both MHCI and II, in the liver may contribute to the immunotolerance of PI animals to BVDV [88].

The bone marrow is an important lymphoid organ for the development of immune cells, producing many immune cell progenitors and educating/maturing others. Abnormal bone development and bone marrow lesions in PI animals have been described previously [90-92]. The pathology consistently seen in both experimental and in natural infections is osteopetrosis, which is often found in the context of genetic disorders in humans and animals [90-92]. Femurs from PI fetuses 117 days post maternal inoculation had medullary spaces that were significantly smaller and had greater femur wall thickness compared to controls [92]. Also at this time point, radio-dense transverse bands were seen in the PI fetuses, indicative of recurring impaired resorption of calcified cartilage [91]. Decreased numbers of osteoclasts were also observed in the PI fetal bones, providing an explanation for the impaired resorption of PI fetal bone [91]. Without proper bone remodeling in the PI fetus and a decrease in medullary space, hematopoiesis is shunted to other organs, such as the spleen. The effects of this shift to extramedullary

hematopoiesis is not well understood but in some instances, is a good hematopoietic substitute in the absence of an appropriate bone marrow niche [93, 94]. However, in chronic disease states, extramedullary hematopoiesis can contribute to inflammation, splenomegaly, or organ rupture [93, 94]. The consequences of this osteopetrotic pathology on PI immune development has yet to be explored.

BVDV vertical transmission has been known to cause smaller fetuses compared to uninfected counterparts. When measured 117 days post maternal inoculation, PI fetuses exhibited significantly smaller ponderal index, weight, heart girth, and crown rump length when compared to uninfected controls [92]. Although indicative of intrauterine growth restriction (IUGR), the molecular causes of IUGR following BVDV vertical transmission remains unknown.

Frequently, PI animals, both fetal and postnatal calves, will exhibit congenital malformations as a consequence of transplacental transmission of the virus. For example, some PI animals are healthy, but others appear small, weak, have decreased weight gain, and stunted growth, possibly due to the IUGR discussed previously [95-97]. Several pathologies involve the brain and neural development, including cerebellar hypoplasia, hydranencephaly, hydrocephalus, as well as other lesions in central nervous system, ocular nerves, chorioretinopathy, and cataracts (reviewed in [97]). Interestingly, heart septal defects and thymic hypoplasia has also been observed in PI animals [96, 97]. Despite several studies and case reports on PI animals, the molecular explanations for these pathologies are still unknown. Theories have included viral inhibition of IFNs, viral stimulation of IFNs, general inflammation, immune cell population abrogation, and many more [90-92, 95-100].

Further investigation into molecular mechanisms of BVDV persistence in PI fetuses was needed to further our understanding of viral vertical transmission. In attempt to help the cattle industry overcome BVDV losses and to also help the advancement of human medicine by furthering the understanding of transplacental virus infection on fetal development, DNA methylation, mRNA expression, and protein abundance was measured in BVDV PI fetal spleens and BVDV infected placental tissues.

Chapter 2: Attenuated lymphocyte activation leads to the development of immunotolerance in bovine fetuses persistently infected with BVDV

Overview:

Bovine viral diarrhea virus (BVDV) continues to cost the cattle industry millions of dollars each year despite control measures. The primary reservoirs for BVDV are persistently infected (PI) animals, which are infected *in utero* and shed the virus throughout their lifetime. The difficulty in controlling the virus stems from a limited understanding of transplacental transmission and fetal development of immunotolerance. In this study, pregnant BVDV naïve heifers were inoculated with BVDV on day 75 of gestation and fetal spleens were collected on gestational days 82, 97, 190, and 245. Microarray analysis on splenic RNA from days 82 and 97 revealed an increase in signaling for the innate immune system and antigen presentation to T cells in day 97 PI fetuses compared to controls. RT-qPCR on select targets validated the microarray revealing a downregulation of type I interferons and lymphocyte markers in day 190 PI fetuses compared to controls. Protein was visualized using western blot and tissue sections were analyzed with H&E staining and immunohistochemistry. Data collected indicates that fetal immunotolerance to BVDV developed between days 97 and 190, with mass attenuation of the immune system on day 190 of gestation. Furthermore, lymphocyte transcripts were initially unchanged then downregulated, suggesting that immunotolerance to the virus stems from a blockage in lymphocyte activation and hence an inability to clear the virus. The identification of lymphocyte derived immunotolerance will aid in the development of preventative and viral control measures to implement before or during pregnancy.

Importance:

BVDV is an infectious RNA virus which is a major cause of production losses in cattle due to its contribution to bovine respiratory disease in feedlot animals and reproductive losses in cow-calf (breeding) herds. Persistently infected (PI), immunotolerant animals are the main source of BVDV infections in cattle. The generation of PI animals by vertical transmission of BVDV during early pregnancy has been known for over 50 years; however, the mechanisms responsible for the immunotolerance to and persistence of BVDV in PI animals have not been elucidated [1-3]. This *in vivo* study provides not only a unique perspective on the development of immunotolerance to BVDV in PI fetuses but contributes to our understanding the development of the bovine fetal immune system.

Introduction

Bovine viral diarrhea virus (BVDV), a single-stranded RNA virus, was first isolated in 1957 and has continued to plague the U.S cattle industry despite attempted control measures [101]. BVDV, family Flaviviridae and genus *Pestivirus*, has two main biotypes: cytopathic and non-cytopathic [102, 103]. The non-cytopathic biotype predominates in nature while the cytopathic biotypes are mutants that arise in PI cattle with a non-cytopathic biotype and are associated with mucosal disease [5]. Additionally, there are 2 genotypes of BVDV, BVDV1 and BVDV2, both of which have subtypes [8]. In recent studies, BVDV has been estimated to cost cow-calf (breeding herd) operators $119.42 per bred cow and the US cattle industry $1.5-2.5 billion annually [58, 59]. Inactivated and modified live viral (MLV) vaccines are used by 80% of producers in the USA to prevent

losses due to BVDV infections; however, substantial losses continue to occur both nationally and internationally [64, 104]. BVDV can be transmitted vertically across the placenta, infecting the fetus and if fetal infection occurs before day 30 of pregnancy, abortion, resorption, or fetal mummification can be induced [105]. If fetal infection occurs between days 42 and 125 of gestation, the fetus is unable to clear the virus and the calf remains persistently infected (PI), shedding the virus throughout its lifetime. Although the majority of PI calves are born without obvious malformations, congenital defects such as cerebellar hypoplasia, cranial deformation, lenticular cataracts, intrauterine growth restrictions occur in a subset of calves [105].

PI animals have been identified as the primary reservoir for BVDV, exposing naïve and unprotected animals within their proximity [106]. In a meta-analysis conducted in 2018, worldwide prevalence of PI animals was estimated to be 0.36% while the worldwide prevalence of cattle herds with PI animals was estimated to be 18.88% [107]. More specifically, the prevalence of PI herds in the US ranges from 20-40% while the prevalence in Europe ranges from 10-60% with the exception of Denmark at 0% due to eradication efforts [107]. Antibody positive herds (herds exposed to BVDV) prevalence ranged from 60-80% in the US and 20-80% in Europe (varies by country due to eradication efforts in some) [107]. Approximately 0.2-0.4% of cattle entering feedlots are PI with BVDV, which equates to approximately 62% of cattle in direct contact with a PI animal [60, 62]. The resulting immunosuppressive effects of BVDV infection provides a unique opportunity for the viruses and bacteria included in the Bovine Respiratory Disease (BRD) complex to cause disease in exposed animals. Cattle directly exposed to cattle PI with BVDV were 43% more likely to exhibit and receive treatment for BRD clinical

signs, thus contributing to the industry loss of approximately $800-900 million annually due to BRD [62, 108]. Overall, losses due to BVDV exposure amount to $93.52/animal from performance loss including cost of treatment, prolonged feeding period, decreased rate of gain, and increased mortality [60]. These costs in both the beef and dairy industries mandate the need for further research to understand the cellular and molecular mechanisms leading to development of persistent BVDV infection in the bovine fetus.

Previously, we developed an *in vivo* model of fetal infection by inoculating naïve pregnant heifers with BVDV on gestational day 75 to generate PI fetuses [109, 110]. Fetuses were collected by cesarean section on days 82, 97, 190, and 245 of gestation. Fetal viremia peaked on day 97, which is 22 days post-maternal inoculation, at levels 23,000 times greater than maternal viral titers at their peak on day 85 of gestation [84]. There also was an upregulation of the type I interferon (IFN) response in PI fetuses. This finding directly contradicted *in vitro* studies, which concluded that BVDV suppressed the PI innate immune system [75, 84, 111].

The aim of this study was to elucidate possible mechanisms of immunotolerance and viral persistence in bovine fetal spleens PI with BVDV. It was hypothesized that PI fetal spleens would exhibit a chronically upregulated innate immune response with an attenuated adaptive immune response throughout gestation. Using spleens from previously generated PI fetuses, microarray transcriptome analysis was performed on splenic samples from day 82 and 97 of gestation to elucidate pathways associated with PI infection before and after transmission to the fetus [84, 86]. Selected targets were validated by reverse transcription quantitative polymerase chain reaction (RT-qPCR) and protein analysis by western blots for gestational days 82, 97, 190, and 245. An active and

responsive innate immune system was present by day 97 of gestation (22 days post maternal infection) but by day 190, both the innate and adaptive branches of the immune system were attenuated in PI fetuses. This attenuation of the fetal immune system is interpreted as the development of immunotolerance by day 190 of gestation, 115 days post inoculation of the dam.

Materials and Methods

Animals, viral infections, and fetal collections

All experiments using cattle were approved by the Institutional Animal Care and Use Committee at Colorado State University (IACUC) and the Colorado State University Biosafety Committee (BSL1 and 2 approval 19-037B for BVDV). Virus inoculations and fetal collections are described in previous reports [84, 86]. Briefly, a power analysis was performed and determined that a samples size of 3-4 animals per treatment groups was sufficient for an experimental power of 1. Therefore, 45 BVDV naïve, unvaccinated Hereford heifers (1 year old, >700 lbs) were purchased from a source which did not vaccinate against BVDV. All heifers were confirmed to be seronegative and virus negative for BVDV1 and BVDV2 upon arrival by virus neutralization assay and ear-notch extract BVDV antigen capture ELISA, respectively [84, 92]. All heifers were artificially inseminated with pregnancies confirmed by ultrasound examination 35 and 70 days after insemination.

Twenty-two randomly assigned heifers were inoculated intranasally with 2 mL ncp BVDV2 strain 96B2222 at 4.4 $\log_{10}$ $TCID_{50}$/mL in Minimal Essential Media (MEM) on day 75 of gestation [112]. The other 23 naïve heifers, in the control group, were inoculated with 2 mL of MEM media intranasally. Control and PI heifer groups were kept in widely

separated pens to eliminate chance of virus transmission. To avoid viral transmission to control animals or any other animals in the facility, infected cattle were fed last at the end of the day, allowing animal workers to change clothes prior to interacting with non-infected animals the following day. Control heifers were confirmed BVDV free throughout gestation while BVDV infected heifers were confirmed infected, by RT-qPCR and serum neutralization assay, with a series of blood samples taken from each animal at days 75, 78, 82, 85, 89, 97, 103, 115 of gestation and every two weeks thereafter [84].

Forty-four fetuses were collected via Cesarean section on gestational days 82 (control n = 4, PI n = 3), 97 (control n = 4, PI n = 4), 190 (control n = 7, PI n = 7), and 245 (control n = 4, PI n = 3). One calf in the day 245 PI group was aborted for reasons unrelated to BVDV infection and excluded from the analyses. Day 82 and 97 of fetal collection were chosen based on high maternal viremia (82) and viral entry into the fetus (97) [84]. Day 190 of fetal collections were based on expected maternal seroconversion while day 245 of collections were chosen for its proximity to parturition and to avoid pre-term birth [84]. During surgeries, control animals were handled first, then infected animals. Standard sterile surgical packs were replaced between each animal. Pathological findings of the fetuses can be found in previously published papers [84, 87].

Spleens were sampled to ensure presence of both red and white pulp. In the early fetuses (days 82 and 97) this meant the whole spleen, while in older fetuses, samples were taken from the middle part of the organ. Samples were halved then: 1) snap frozen in liquid nitrogen and stored at -80^{o}C for RNA and protein extraction, and 2) fixed for 48 hours in 10% neutral-buffered formalin and routine paraffin embedded.

Microarray

RNA was isolated from 100μg of frozen fetal spleens, collected on days 82 and 97 (n=4 control/ 3 PI for day 82, n=4 control/ 4 PI for day 97), and mechanically homogenized in TRI-Reagent per manufacturer's instructions (50mg/mL reagent) (Sigma St. Louis, MO). Further cleanup was performed using RNeasy MinElute cleanup kit and treatment with RNase free DNase (Qiagen Hilden, Germany). RNA was biotin labeled and used for library preparation, as outlined in [86], then subjected to transcriptional profiling with the Affymetrix bovine DNA chip (#900562, Affymetrix, Santa Clara, CA, USA) at the Genomics and Microarray Core, University of Colorado-Anschutz Medical Campus. On-chip controls include hybridization controls, poly-A controls, and control gene probes. Microarray results are reported as log 2 fold changes.

Transcriptional Analysis by RT-qPCR

RNA was isolated from days 82 (50 μg), 97 (100μg), 190 (100μg), and 245 (100μg) frozen fetal spleens (n=4 control/ 3 PI for day 82, n=4 control/ 4 PI for day 97, n=7control/7PI for day 190, n=4 control/3 PI for day 245) as described above and quantified using the NanoDrop 2000 Spectrophotometer (Thermo Scientific Waltham, MA). A total of 0.5 μg RNA (days 82 and 97 spleens) or 1 μg RNA (days 190 and 245 spleens), was reverse transcribed to cDNA with iScript cDNA synthesis kit according to manufacturer's protocol (RNase H+, Bio-Rad, USA) in 20μl reactions. iQ SYBR Green Supermix was utilized for amplification according to the manufacturer's instructions (Bio-Rad Hercules, CA) and amplified in 384 well plates (adhesive seal, Bio-Rad Hercules, CA) at a volume of 10μl per reaction using a LightCycler489 (days 82 and 97) (Roche

Basel, Switzerland) or a CFX384 (days 190 and 245) (Bio-Rad Hercules, CA). The switch from one machine to the other was beyond our control and splenic samples were not abundant enough for repeated analysis on the CFX384. Due to the statistical design, discussed below, comparisons between days was not feasible, therefore, the difference in the aforementioned machines should not have biased results since complete day groups were able to be completed on one machine or the other. Samples were amplified in technical duplicates and plates were biologically replicated three times. Cycling conditions: 1) 95°C for 3 minutes, 2) 95°C for 15 seconds, 3) 58°C for 30 seconds, 4) 72°C for 30 seconds, 5) repeat steps 2-4 for 41 cycles, 6) melt curve from 65°C to 95°C. Targets included DExD/H-Box Helicase 58 (*DDX58;* intracellular receptor RIGI*),* Interferon Regulatory Factor *(IRF7),* Interferon *(IFNB),* Interferon Stimulated Gene *(ISG15),* Signal Transducer and Activator of Transcription *(STAT4),* Interferon Gamma Inducible Protein *(IFI30),* Proteasome Subunit Beta *(PBSMB8), PSMB9,* Cluster of Differentiation Factor *(CD4), CD8A, CD8B,* and *CD79B* (Appendix Table 1). Amplification of BVDV was performed with previously published primers [92].

Reference genes included Glyceraldehyde-3-Phosphate Dehydrogenase (*GAPDH)* and Tyrosine 3-Monooxygenase (*YWHAZ)* for days 82 and 97 samples and *18S* for days 190 and 245 samples. Reference genes consistent throughout our samples were not found, variation occurred either between day groups or between treatment groups within a day. Reference genes tested included *GAPDH, TBP, YWHAZ, Pol2, RPL19*, and *18S.* Reference genes were chosen based on the lack of significant difference between control and PI groups on any given day. Reference genes *GAPDH* and *YWHAZ* were not affected by PI status for days 82 and 97, nor were they different

between days 82 and 97. Reference gene *18S* was the only reference gene found unaffected by PI status during days 190 and 245 but was significantly different between days 190 and 245.

Approximately 3-4 primer sets per target were chosen via NCBI Primer Blast tool based on annealing temperatures of 60°C, 100-200 base pair amplicons, and minimal self-complementarity scores. Primers were purchased from Integrated DNA Technologies (Coralville, IA), validated by RT-qPCR standard curves, gel electrophoresis, and amplicon sequencing. Primer sets per target were chosen by: 1) correct amplicon amplification, 2) single amplicon amplification, 3) amplification efficiencies (ideally between 90-110%), and 4) single, appropriate melt curve peak. When available, intron spanning primers were chosen. Some target primer sets (*RIGI, IRF7, NFKB, ISG15, IFI30, LMP2, LMP7,* and *CD79B*) were outside of the ideal efficiency range. Due to limitations on available primer sets for those targets, primer sets closest to the ideal efficiency range were chosen. Fold change ($2^{-\Delta\Delta Ct}$), calculated from raw C_q values, was analyzed for statistical significance in GraphPad Prism 8 (San Diego, CA). MIQE guidelines were generally followed for nomenclature and validation [113].

Protein Analysis by Western Blot

Protein from frozen splenic tissues, days 82, 97, 190, and 245 (n=4 control/ 3 PI for day 82, n=4 control/ 4 PI for day 97, n=7 control/ 7 PI for day 190, n=4 control/ 3 PI for day 245), was isolated utilizing RIPA Lysis and Extraction Buffer (Thermo Scientific Waltham, MA) and Halt Protease and Phosphatase Inhibitor Cocktail (10 μl HALT/1 mL RIPA; Thermo Scientific Waltham, MA). Approximately 25 mg of tissue/ mL of RIPA buffer

for days 82 and 97 and 100 mg of tissue/mL of RIPA buffer for days 190 and 245 were homogenized and protein extracted according to manufacturer's instructions. Protein was quantified using a Pierce BCA Assay (Thermo Scientific Waltham, MA) according to the manufacturer's instructions. Protein (45 μg) was separated on 12% acrylamide gels, cast according to manufacturer's instructions for TGX Fastcast Acrylamide Kit (Bio-Rad Hercules, CA). Samples were transferred to nitrocellulose membranes and incubated with appropriate primary and secondary antibodies (Appendix Table 2). Antibodies for western blot were chosen for validation of RNA data and for their cross reactivity to bovine protein. Chemiluminescence was detected using Clarity Western ECL Substrate (Bio-Rad Hercules, CA) and imaged/analyzed using a ChemiDoc XRS+ and Image Lab Software (Bio-Rad Hercules, CA). Anti-actin beta (ACTB) conjugated with horseradish peroxidase (HRP) was used as a loading control and results are reported as target/ACTB ratio. Validation of antibodies and controls consisted of 1) no primary antibody controls (for secondary antibodies) and 2) no secondary antibody controls (for primary antibodies). Results are reported as relative quantitation with treatment group means, standard deviation (SD), and standard error of the mean (SEM).

Histology and Immunohistochemistry

Paraffin embedded tissue samples, from days 82, 97, 190, and 245 (n=4 control/ 3 PI for day 82, n=4 control/ 4 PI for day 97, n=7control/7PI for day 190, n=4 control/3 PI for day 245) were sectioned (4-5 μm) and processed for either histological analysis or immunohistochemical (IHC) analysis. The sections prepared for histological analysis were stained with hematoxylin and eosin (H&E), then assessed microscopically with

special attention to the reticulo-endothelial network, myeloid and lymphoid cells and their location in the organ primordium. Sections (days 97, 190, and 245) prepared for IHC analysis were processed for antigen retrieval using citrate or EDTA depending on antibody optimization (Appendix Table 2). Sections were blocked with peroxidase, 0.15 M glycine in PBS and DAKO Antibody Blocking Reagent, followed by incubation with antibody according to antibody optimization (Appendix Table 2), antibody binding visualized with AEC chromogen, and sections counterstained with Meyer's hematoxylin [114, 115]. IHC sections were imaged at 100X and 200X magnification at 5 randomly selected fields of view. Images were analyzed using FIJI/ImageJ software which separated and counted positive (chromogen stained) cells as well as negative (hematoxylin only stained) cells (macro script available on GitHub detailed below). Statistical analysis was performed using GraphPad Prism (San Diego, CA).

Statistical Analysis and Data Management

Microarray data were analyzed in R utilizing Bioconductor packages affy, gcrma, and limma [116-118]. The package gcrma was implemented for background adjustment of sequence reads, the affy R package was utilized for probe/oligonucleotide analysis. Data were adjusted for False discovery rate using the Benjamini and Hochberg method in the limma R package. Ingenuity Pathway Analysis (IPA, Qiagen Hilden, Germany) was utilized to visualize pathways of differentially expressed genes from the microarray. Parameters for IPA analysis include a p-value cutoff of <0.05 and log2 fold change cutoff of 1 (below -1 or above 1, equivalent to a 2-fold change cutoff). RT-qPCR, western blot, and IHC data were analyzed in GraphPad Prism (San Diego, CA) using unpaired two

tailed T-tests to compare control and PI data for each day. Due to the everchanging transcriptional landscape of the developing fetus, one suitable reference gene across all timepoints was not found, therefore, comparisons between days were not feasible. Additionally, two-way ANOVAs were performed with treatment groups (Control and PI) and fetal sex as factors. Fetal sex was not a significant factor nor was there interaction between fetal sex and treatment groups. Raw data for this study is available to the public on the NCBI Gene Expression Omnibus (GEO) repository (GEO Accession GSE148323). FIJI IHC analysis scripts produced for this project are available to the public on GitHub (https://github.com/hanahm1/imagej_analysis) [119].

Results

Microarray

The microarray transcriptome analysis of day 82 and 97 control and PI fetal spleens, revealed several differentially expressed pathways and genes, as determined by IPA, in the day 97 fetuses but not in the day 82 PI vs. control fetal spleens. Several canonical pathways were significantly upregulated ($p < 0.05$) in day 97 PI fetuses compared to controls including IFN signaling, helper T cell signaling, immune cell communication, and others (Table 1). The top pathway identified was IFN signaling, which included several upregulated genes in PI fetal spleens. The top differentially expressed genes (1 log2 fold or greater) associated with type I IFN signaling were *STAT1, STAT2,* Interferon Induced Protein with Tetratricopeptide Repeats 1 (*IFIT1)*, 2'-5'-Oligoadenylate Synthetase 1 *(OAS1),* Interferon-induced GTP-binding protein *(MX1), IRF9, IFI35, PSMB8,* and Transporter associated with Antigen Processing (*TAP1)* ($p < 0.05$) (Fig. 1).

Additionally, several upregulated genes, which were not included in an IPA pathway, were identified in day 97 PI fetal spleens: *DDX58, IRF7, ISG15, STAT4, PSMB8, PSMB9,* as well as the significantly downregulated B-cell receptor subunit *CD79B* gene ($p < 0.05$).

Table 1: Top pathways altered in d97 BVDV PI fetuses compared to control fetuses as identified by IPA analysis of the microarray data.

Top Pathways	Change in PIs	Immune Function
CD28 Signaling in helper T Cells	Upregulated	CD4 helper T cell activation
Interferon Signaling	Upregulated	Type I and II IFN signaling for inhibition of viral replication
FCG Receptor Mediated Phagocytosis in Macrophages and Monocytes	Upregulated	Activation of Macrophage and Monocyte phagocytosis of infected cells
EIF2 Signaling	Downregulated	Regulation/Inhibition of type I IFN signaling
mTOR Signaling	Upregulated	Immune system activation in response to viral infection

RT-qPCR

BVDV viral transcripts were present in PI fetal spleens starting at day 97 and continuing to day 245. These viral transcripts were not present in control animals at any point in gestation.

Genes involved in type I IFN signaling of the innate immune system were examined to determine innate immune signaling throughout gestation in response to persistent BVDV infection. Transcripts for *DDX58*, *IRF7,* and *ISG15* were significantly upregulated in PI fetal spleens by day 97 compared to controls (Fig. 2, Table 2), corroborating the microarray data. However, by day 190, these transcripts were no longer

significantly different between PI and control spleens. *IFNB* transcripts trended toward an upregulation ($p = 0.06$) in PI spleens compared to controls on day 97 but were significantly downregulated, compared to controls, on day 190. On day 245 of gestation, only *ISG15* was differentially expressed and was significantly upregulated in PI fetal spleens compared to controls (Fig. 2, Table 2).

Transcripts of *STAT4* and antigen presentation genes*, IFI30, PSMB8,* and *PSMB9* were all significantly upregulated on day 97 in PI fetal spleens compared to controls (Fig. 3, Table 2), as also seen in the microarray. These same genes were significantly downregulated in PI spleens by day 190 when compared to day 190 control spleens, but by day 245, significant differences in antigen presentation transcripts between PI and controls were no longer evident (Fig. 3, Table 2).

All three T-cell CD-markers were downregulated, compared to controls, on day 190 with no difference in expression by day 245 of gestation when compared to day 245 control spleens (Fig. 3, Table 2). B-cell receptor subunit *CD79B* trended towards being downregulated ($p = 0.09$) in PI fetuses on day 97 compared to controls, and was significantly downregulated on day 190 compared to controls (Fig. 3, Table 2)

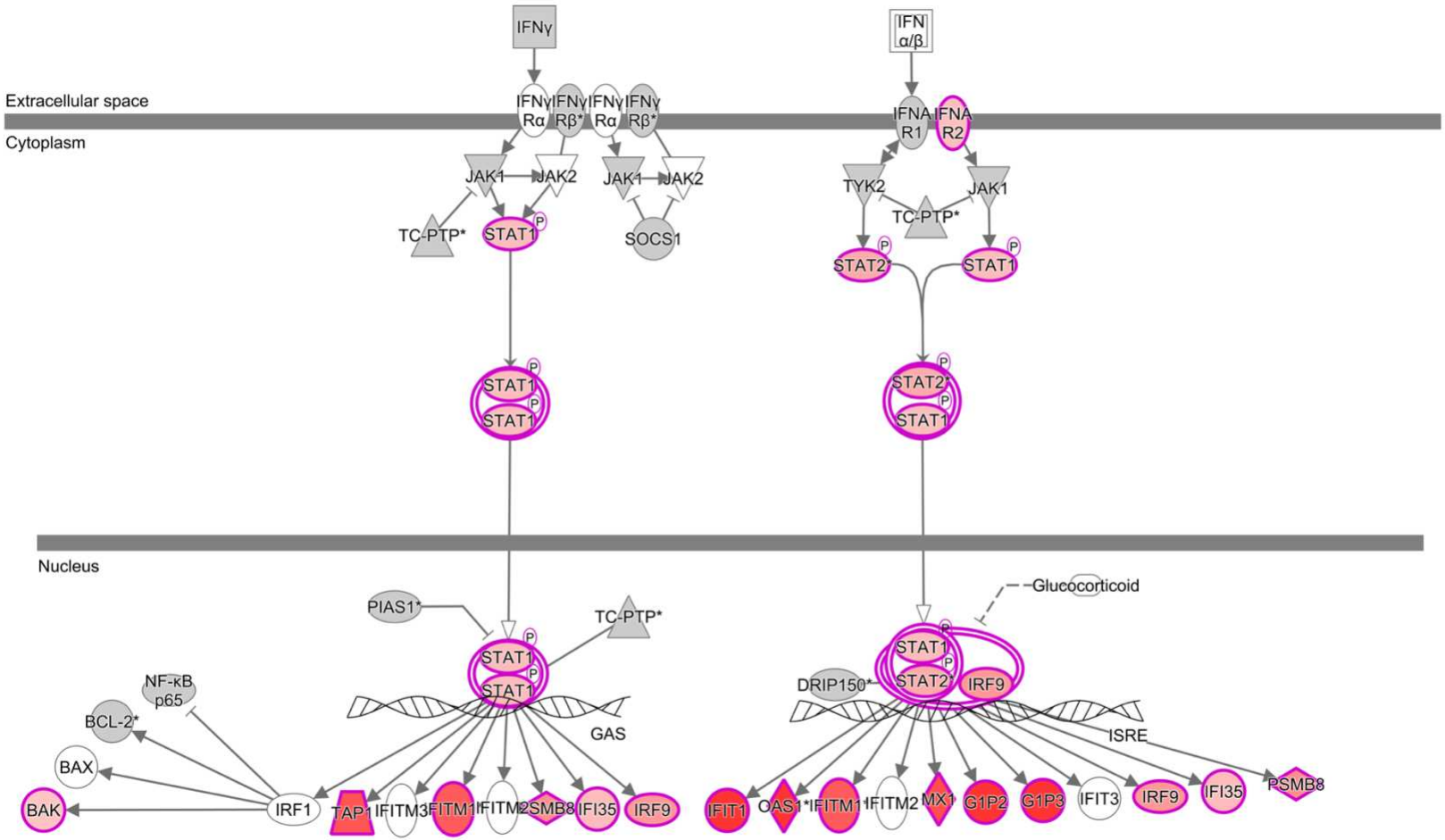

Figure 1: IPA identified IFN signaling as a top canonical pathway from the day 97 microarray data. Red/Pink = upregulated mRNAs in PI fetal spleens compared to controls.

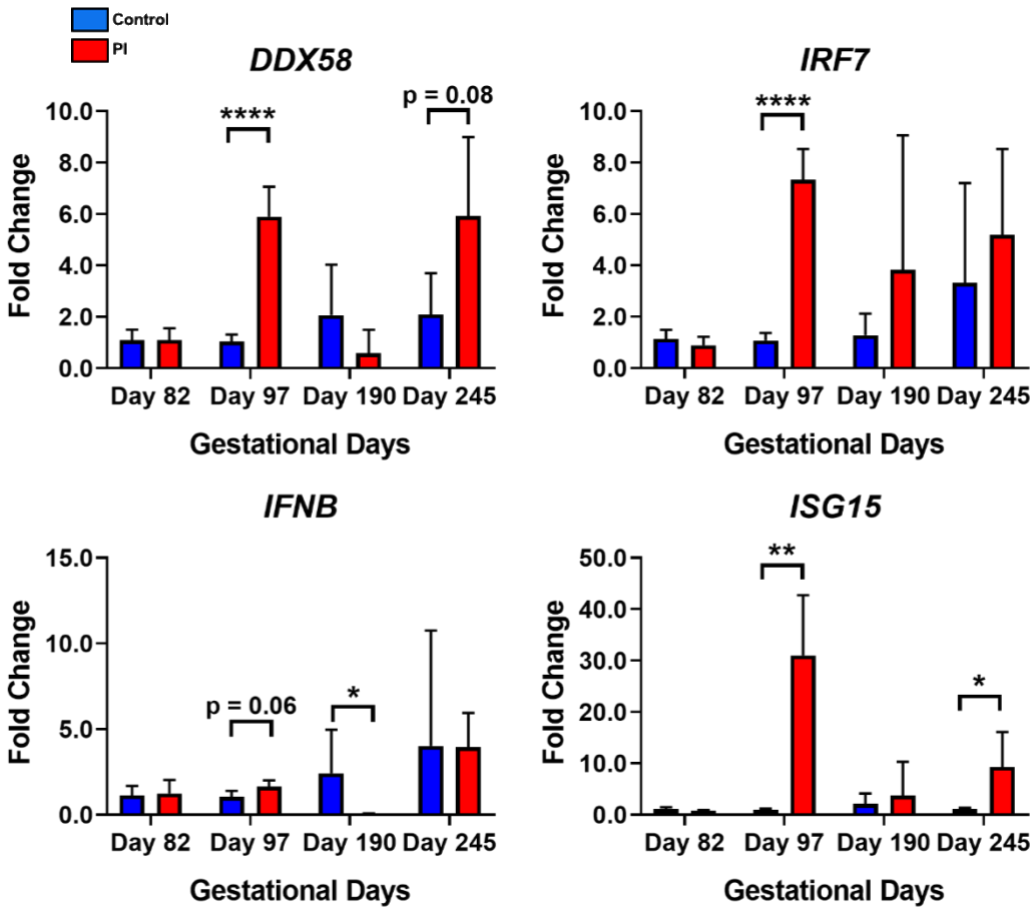

Figure 2: Type I IFN pathway genes associated with the innate branch of the immune system measured by RT-qPCR in PI (red) and control (blue) fetal spleens throughout gestation.

si

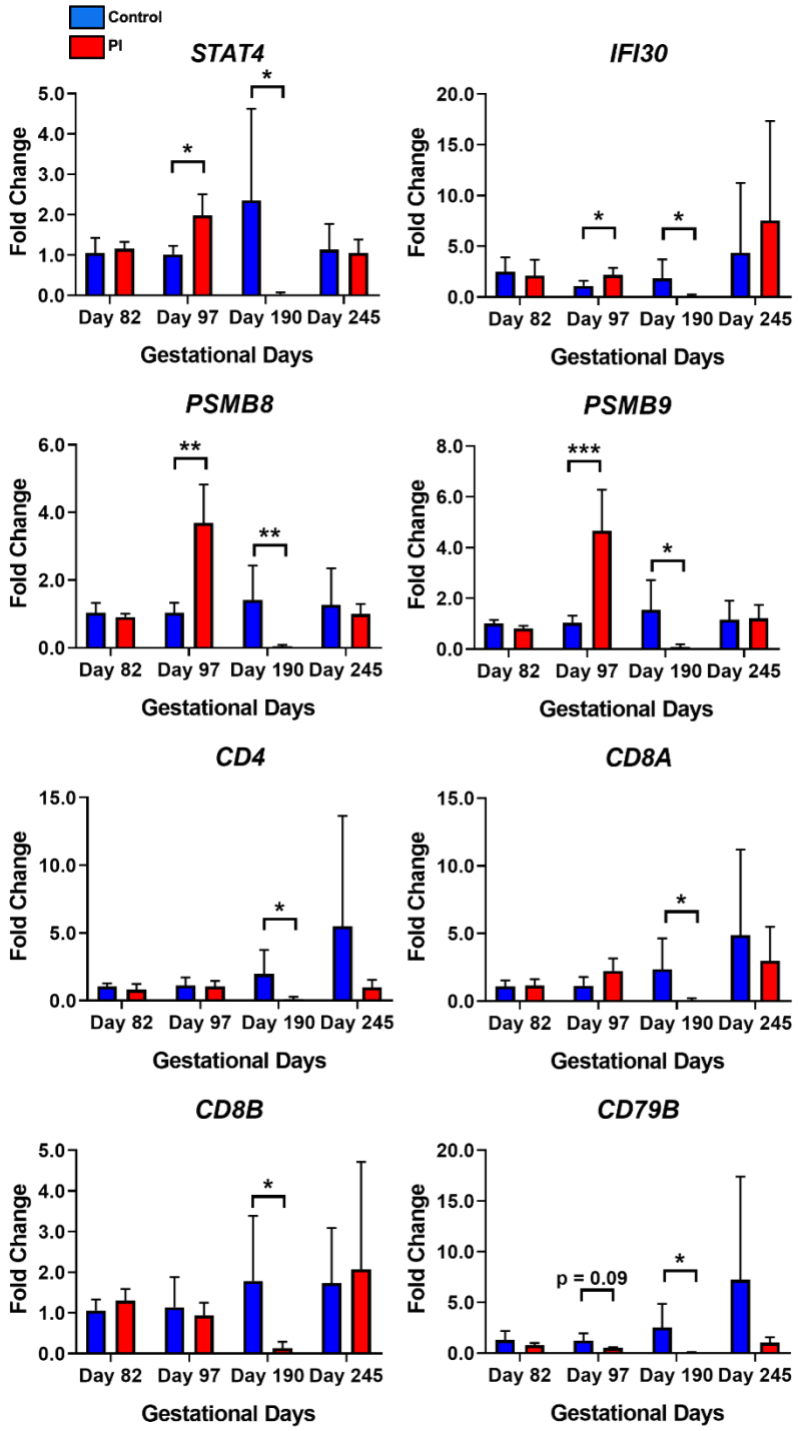

Figure 3: mRNA expression of antigen presentation and lymphocyte markers in Pi (red) and control (blue) fetal spleens throughout gestation, as measured by RT-qPCR.

Table 2: RT-qPCR results recorded as relative *expression (RE, $2^{-\Delta Ct}$) and fold change (FC, $2^{-\Delta\Delta Ct}$). C = Control, PI = Persistently Infecte*

Gene Target	Analysis	Day 82			Day 97			Day 190			Day 245		
		C Mean	PI Mean	P Value	C Mean	PI Mean	P Value	C Mean	PI Mean	P Value	C Mean	PI Mean	P Value
DDX58	RE	0.0169	0.0171	0.9755	0.0216	0.1225	0.0002	0.0059	0.0016	0.1208	0.0010	0.0028	0.0845
	FC	1.0890	1.0990	0.9766	1.0380	5.8920	0.0002	2.0740	0.5858	0.1215	2.0890	5.9310	0.0809
NFKB	RE	0.0370	0.0372	0.9852	0.0538	0.0449	0.4872	0.0143	0.0017	0.0137	0.0038	0.0019	0.5849
	FC	1.1100	1.0770	0.9304	1.1340	0.9440	0.5217	1.3890	0.1643	0.0144	6.3970	3.5760	0.6236
IRF7	RE	0.0028	0.0023	0.4614	0.0040	0.0271	0.0001	0.0013	0.0039	0.2586	0.0021	0.0035	0.3548
	FC	1.1410	0.8916	0.3786	1.0680	7.3280	0.0001	1.2770	3.8200	0.2675	3.3110	5.1790	0.5365
IFNB	RE	0.0034	0.0038	0.8231	0.0069	0.0107	0.0630	0.0041	0.0001	0.0484	0.0040	0.0033	0.8758
	FC	1.1290	1.2440	0.8278	1.0510	1.6380	0.0584	2.4200	0.0413	0.0457	4.0110	3.9600	0.9907
ISG15	RE	0.0087	0.0060	0.2395	0.0087	0.2655	0.0022	0.0070	0.0123	0.5828	0.0019	0.0170	0.0520
	FC	1.0650	0.7376	0.2421	1.0200	31.0000	0.0022	2.0950	3.7390	0.5717	1.0840	9.3220	0.0541
STAT4	RE	0.0471	0.0516	0.6923	0.0830	0.1599	0.0171	0.1130	0.0015	0.0308	0.0146	0.0138	0.8763
	FC	1.0510	1.1610	0.6612	1.0170	1.9860	0.0138	2.3540	0.0305	0.0313	1.1360	1.0490	0.8415
IFI30	RE	0.0003	0.0002	0.6857	0.0007	0.0014	0.0439	0.0009	0.0000	0.0441	0.0008	0.0013	0.6431
	FC	2.5000	2.0990	0.7372	1.0980	2.1710	0.0429	1.8480	0.0796	0.0430	4.3750	7.5290	0.6340
PSMB8	RE	0.0337	0.0295	0.4908	0.0656	0.2326	0.0049	0.0819	0.0022	0.0073	0.0107	0.0084	0.6906
	FC	1.0350	0.9072	0.5071	1.0320	3.6930	0.0040	1.4140	0.0371	0.0078	1.2720	0.9926	0.6872
PSMB9	RE	0.2151	0.1722	0.0949	0.4260	1.9550	0.0045	0.5453	0.0283	0.0121	0.0881	0.0923	0.9177
	FC	1.0070	0.8182	0.1039	1.0280	4.6670	0.0043	1.5400	0.0793	0.0126	1.1550	1.2090	0.9195
CD4	RE	0.0080	0.0061	0.3643	0.0206	0.0191	0.8290	0.0064	0.0003	0.0254	0.0005	0.0001	0.4026
	FC	1.0470	0.7992	0.3626	1.1220	1.0410	0.8292	1.9580	0.1075	0.0301	5.4760	0.9792	0.3952
CD8A	RE	0.0024	0.0026	0.8724	0.0102	0.0202	0.0979	0.0151	0.0005	0.0290	0.0028	0.0017	0.6717
	FC	1.0940	1.1620	0.8498	1.1320	2.2340	0.0981	2.3620	0.0810	0.0338	4.8810	2.9770	0.6488
CD8B	RE	0.0077	0.0094	0.3036	0.0181	0.0148	0.6280	0.0075	0.0005	0.0265	0.0039	0.0016	0.3819
	FC	1.0620	1.3060	0.2976	1.1390	0.9343	0.6289	1.7900	0.1313	0.0299	1.7370	2.0740	0.8314
CD79B	RE	0.0099	0.0061	0.3919	0.0233	0.0102	0.0963	0.0073	0.0002	0.0185	0.0006	0.0001	0.3542
	FC	1.3010	0.7958	0.3868	1.2230	0.5309	0.1068	2.5390	0.0567	0.0259	7.2260	1.0310	0.3506

Western Blot

Significant upregulation of ISG15 in day 97 PI fetal spleens was validated using western blot (Fig. 4). ISG15 protein has two forms, conjugated and free. Both free (control: mean -0.011, SD 0.012, SEM 0.006 | PI: mean 0.196, SD 0.078, SEM 0.039) and conjugated ISG15 (control: mean 3.534, SD 1.157, SEM 0.578 | PI: mean 17.81, SD 8.928, SEM 4.464) were significantly ($p < 0.05$) upregulated in PI spleens. By day 190 of gestation, half of the PI fetuses (3 out of 6) continued to have significantly upregulated conjugated ISG15 (control: mean 0.189, SD 0.094, SEM 0.036 | PI: mean 1.38, SD 1.447, SEM 0.547); however, this difference was diminished and not significant by day 245 of gestation (control: mean 0.305, SD 0.146, SEM 0.073 | PI: mean 1.982, SD 2.077, SEM 1.120) .

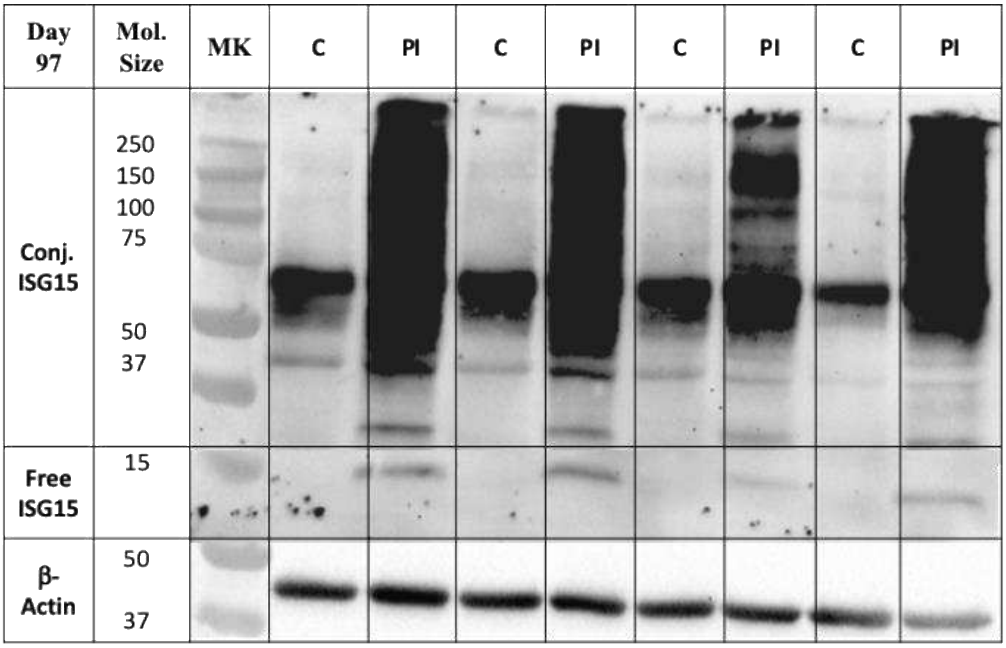

Figure 4: Western blot of ISG15 in day 97 fetal spleens. Control (C) and PI fetuses are shown.

CD79B protein (Fig. 5) was significantly downregulated in day 97 PI fetal spleens compared to controls (control: mean 0.088, SD 0.037, SEM 0.019 | PI: mean 0.035, SD 0.225, SEM 0.0112). However, CD79B did not differ in spleen on days 190 (control: mean 0.573, SD 0.255, SEM 0.096 | PI: mean 0.609, SD 0.226, SEM 0.092) and 245 of gestation (control: mean 0.861, SD 0.722, SEM 0.361 | PI: mean 0.405, SD 0.521, SEM 0.301). While other proteins were investigated, the limited cross reactivity of antibodies to those bovine proteins preclude reporting here.

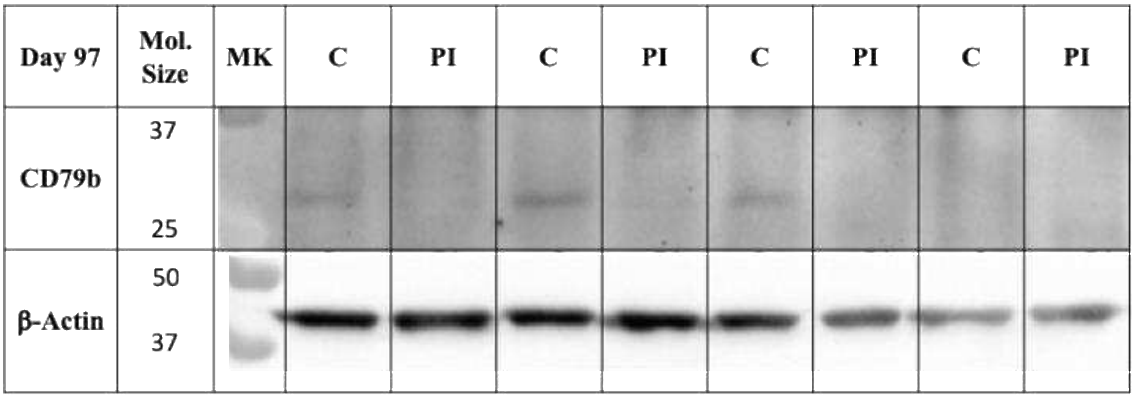

Figure 5: Western blot of CD79B in day 97 control (C) and PI fetal spleens. PI animals had significantly less CD79B protein when compared to controls.

Histology and Immunohistochemistry

Histological analysis of fetal spleens revealed that differences between PI and control animals did not begin until day 97 of gestation. At this time point, PI spleens exhibited attenuated periarteriolar sheath (PALS) development, as reflected in cell layers (width), and a slight increase in hematopoietic activity. By day 190 of gestation, a slight increase in lymphocytes and megakaryocyte numbers were observed in PI spleens;

however, these cells appeared to be degenerating. On day 245, PI fetal spleens had fewer lymphocytes in the PALS compared to controls.

The CD3-epsilon chain, part of the T-cell receptor complex, was utilized as a general T-cell marker for IHC analysis, as the expression of this chain is activation independent [120]. Although there was not a significant difference between control and PI animals at any stage of gestation in terms of overall $CD3^+$ cell numbers, it was observed that the PI animals had fewer T-cells clustering in the PALS of the splenic white pulp compared to control fetuses (Appendix Table 3, Fig. 6A), corroborating the histological assessment of a less well-developed PALS in the PI fetal spleens.

B cell receptor subunit CD79A was significantly decreased in day 190 PI spleens as determined by IHC analysis (control: ratio mean 0.1873, SEM 0.02257 | PI: ratio mean 0.08536, SEM 0.03388; $p<0.05$) (Appendix Table 3, Fig. 6B). B cell clustering in the B cell follicles was also observed to be decreased in PI animals compared to the control fetuses.

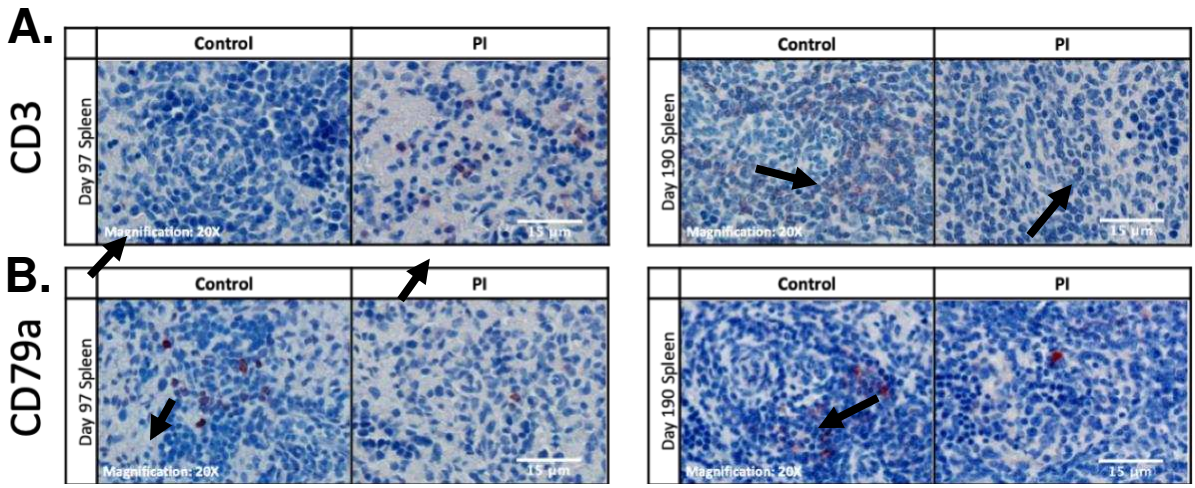

Figure 6: Immunohistochemistry of CD3 (A) and CD79A (B) in fetal spleens on days 97 and 190 of gestation. Number of CD3 positive cells (panel A, red) were not significantly different on either day between PI and controls. However, clustering of CD3 positive cells was different in PI fetal spleens on both days. In panel B, there was a significant decrease in CD79A B cells in day 190 fetal spleens ($p < 0.05$).

Discussion

The spleen is a critical lymphoid organ for initial viral recognition and immune response to blood-borne pathogens. The spleen is populated with lymphocytes and APCs, making it a prime organ for studying immune system modulation and development in the fetus [40, 121]. Upon recognition of viral antigens by extracellular toll like receptors (TLRs) or DDX58 receptors, IRF7 is phosphorylated and translocated to the nucleus for the induction of type I *IFN* transcription [122]. IFNs bind to receptors on neighboring cells, activating the Janus kinase (JAK)/ STAT pathway resulting in the transcription and translation of ISGs which regulate normal cell processes to inhibit viral replication [122]. Following activation of the innate pathway, IL-12 is released and stimulates STAT4, which in turn induces IFNG [123]. IFN-gamma, a type II IFN, stimulates major histocompatibility complex (MHC) I and II expression on antigen presenting cells (APC) via JAK1/JAK2/STAT1 signal transduction and phosphorylation of JAK [122, 123]. Activated APCs recognize and process viral antigens for presentation and activation of both $CD4^+$ helper T cells and $CD8^+$ cytotoxic T cells [40, 124]. CD8 T cells induce apoptosis of infected cells and further immune cell communication through the secretion of IFNG, tumor necrosis factor alpha (TNFA), and tumor necrosis factor beta (TNFB) for the activation of APCs [124, 125]. $CD4^+$ T cells release cytokines which activate B and T cells, as well as macrophages, to engage in antigen specific functions such as antibody production by B cells or destruction of infected cells by macrophages [40, 126].

Previous work indicated that the innate immune system, specifically type I *IFN*s, was upregulated in day 97 PI fetuses as well as in PI post-natal steers [127]. Therefore, it was originally hypothesized that the innate immune system, specifically type I *IFN*s, was

chronically upregulated in BVDV PI fetuses throughout gestation with an attenuation of the adaptive immune system, specifically the T and B cells.

PI animals continue to be the main reservoir of BVDV despite attempted management practices focused on controlling this devastating infection. The mechanism by which BVDV establishes persistence and immunotolerance in these fetuses is still largely unknown. Previously, we described that BVDV crosses the placenta and infects the fetus 7-14 days post maternal infection [84, 87]. This 7-14 day interval between maternal and fetal infection is reflected in the present studies, with innate and adaptive gene expression at the same levels as controls by day 82 of gestation, which is 7 days post maternal inoculation. Additionally, BVDV transcripts were not observed in the fetal spleen until day 97 (22 days post maternal inoculation). This delay in fetal infection with BVDV is expected as the virus replicates in the respiratory tract of the dam, causes viremia, then crosses the placenta for replication in fetal membranes, and finally reaches the fetus proper [82].

As expected from the results of previous studies, the innate immune system, specifically type I IFN signaling, was highly upregulated in PI fetuses on day 97 of gestation coinciding with the peak in fetal viremia [84, 86]. ISG15 mRNA and protein were highly upregulated in PI animals, which corroborates previous data suggesting that the type I IFN response is reactive to fetal BVDV infection [110, 128]. The microarray data revealed *STAT4* transcript upregulation, possibly contributing to downstream gene expression for antigen presentation. As a part of the innate immune response, interleukin 12 (IL12) induces STAT4 expression, while type I IFNs directly stimulate IFNG transcription and translation [123]. Together, STAT4 and IFNG are communication

branchpoints from the innate immune system to the adaptive, stimulating the expression of MHC class I and II on APCs. Previously, *IFNG* transcription was reported to be upregulated in the PI fetal spleen on day 97 [86]. The *STAT4* upregulation was validated in RT-qPCR and additionally, *IFI30*, *PSMB8*, and *PSMB9*, all inducers of MHC expression, were increased as well. The increased transcription of these genes suggests active presentation of BVDV antigens to T cells. However, the T cell marker mRNA, *CD4*, *CD8A* and *CD8B*, were not different from controls. *CD79B* mRNA, a B cell marker, tended to be downregulated ($p = 0.09$) at this time point, suggesting an absence of activation by T cells resulting in a delay of B cell maturation.

By day 190 of gestation, there was a drastic abrogation of the adaptive immune system and *IFNB* mRNA concentrations based on RT-qPCR. *IFNB* was the only gene in the innate immune system to be significantly downregulated compared to controls at this time point. One suggested explanation for this is that once the viral infection is established and the virus is actively replicating in the fetus, *IFNB* may be directly inhibited, similar to the direct inhibition of type I *IFN*s shown in *in vitro* studies [111]. Additionally, all genes associated with the adaptive immune system, including antigen presentation and lymphocyte markers, were significantly downregulated, suggesting a massive inhibition of the fetal immune system, which is consistent with establishment of immunotolerance or anergy to BVDV.

Histological observations found that megakaryocytes and lymphocytes were increased but degenerating in PIs. Previously, these cells were shown to be BVDV antigen positive and would have important consequences for platelet function and hemorrhages [109, 115, 129]. Interestingly, IHC data with CD3-theta as a T cell marker

did not show a difference in T cell populations between PI and control spleens. CD3-epsilon is one of the chains of T cell receptor complex and is present on all T cell populations, including CD4 and CD8 positive T cells. The lack of significant difference in T cell populations reflected in IHC data further demonstrates a lack of T cell activation in response to BVDV. The decrease in the B cell marker CD79A was interpreted to reflect presence of fewer B cells residing in the splenic tissue of PIs compared to controls. A decrease or inhibition of B cells to mature and potentially produce antibodies for BVDV clearance may contribute to the development of apparent immunotolerance. Interestingly, postnatal PI calves lack antibodies to BVDV and have lowered antibody reactivity to other viral infections, most likely due to this attenuation of B cells [130, 131].

Thirty-five days prior to parturition and 115 post maternal inoculation, day 245 data exhibited minimal changes in the PI immune system relative to controls. *ISG15* transcripts were significantly upregulated, while all other gene transcripts were not significantly different from controls. However, histologically, fewer lymphocytes were observed in the PALS of PI fetuses, likely due to an early senescence caused by viral infection. Parturition, at day 280 of gestation for cattle, is a stressful event, with several factors potentially affecting the neonates' immune responses [132]. The maternal fetal interface during parturition is extremely complex, requiring a balance of immune suppression and immune activation. Several mechanisms including dendritic cell mediated immune suppression of the fetus and IL10 mediated suppression keep the fetus from being reactive to the mother and vice versa [133-135]. It is speculated that the lack of difference between control and PI fetal immune systems is due to this suppression and that differences between these groups may recur postnatally.

Development of the fetal immune system is complex as T cells learn to distinguish self from non-self. Studies in mice and humans have revealed two distinct CD4 T cell populations in the developing fetus. Early in human gestation, ~16 weeks of gestation (112 days), the dominant CD4 T cell population is composed of tolerogenic T regulatory cells (Tregs) [136, 137]. As seen in humans and mice, Tregs promote fetal tolerance to self during early fetal development. About mid-gestation, 24 weeks of gestation, ~168 days, the T cell population shifts to tolerogenic T cells and the fetus become immunocompetent; whereas immunogenic CD4 T cells begin to emerge becoming the dominant CD4 T cell population by 40 weeks of gestation (full term, ~280 days) [136, 137]. Minimal work has been done on Tregs during bovine fetal development; however, it is reasonable to assume that as seen in humans, tolerogenic Tregs predominate in early gestation. Therefore, it is likely that BVDV infection prior to gestational day 120, occurs during the time in which Tregs dominate. The presence of virus during this time period instructs Tregs to accept BVDV antigens as self and thus allows the virus to persist. In the presented data, the innate and adaptive immune responses reacted initially to BVDV infection, but these immune responses may then have been curbed by Tregs. These Tregs may establish immunotolerance to BVDV between day 97 and 190 of gestation. Previously, it was shown that PI $CD4^+$ T cells were unable to respond *in vitro* to the homologous strain of BVDV with which the animal was initially infected; however, the CD4 T cells were able to react to heterologous strains of BVDV, suggesting that CD4 T cells are in fact the determining factor of immunotolerance to BVDV [138].

The inhibition of the adaptive immune system, as seen in the presented data and in other postnatal studies, may be indicative of permanent gene regulation caused by

persistent BVDV infection. Several viruses with the ability to cause fetal infection are known to cause epigenetic changes that last through post-natal lives [139]. Epigenetic changes of immune related genes due to the persistent presence of BVDV in the developing fetus is very likely and should be investigated further.

This study presents a timeline of fetal immune responses to BVDV at days 82, 97, 190, and 245 of gestation (Fig. 7). The results indicate that the key cellular mechanisms leading to immunotolerance to BVDV occur between days 97 and 190 of gestation (22 – 115 days post maternal inoculation) resulting in a PI fetus, which will shed the virus throughout its post-natal life. Regulatory T cells as well as epigenetic changes are proposed to be the mediators of immunotolerance to BVDV, recognizing viral antigens as self, inhibiting any immunogenic reaction to the antigens, and affecting the PI animals' abilities to fight infection postnatally.

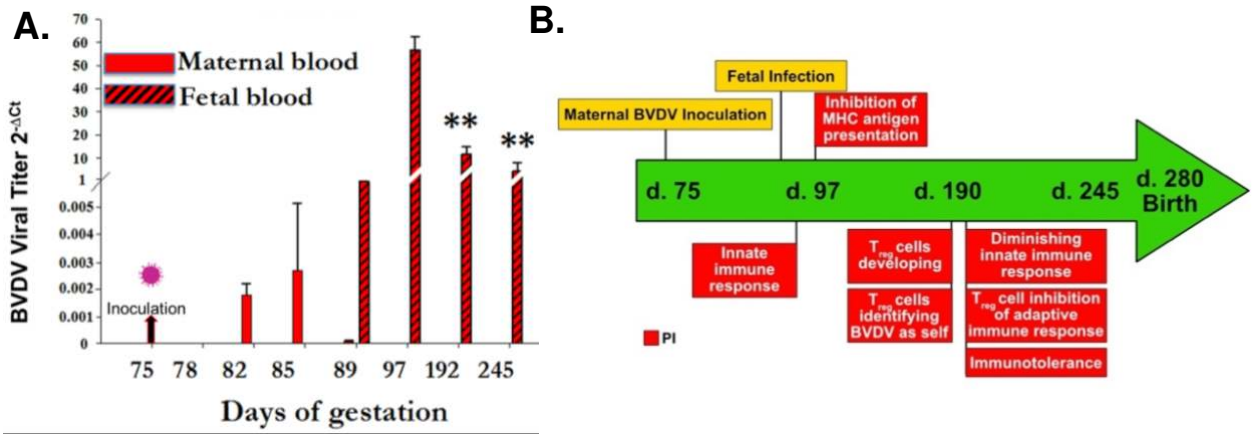

Figure 7: Maternal and fetal viremia (A) and proposed timeline of BVDV immunotolerance in PI fetuses (B). Panel A is adapted from [84]

Chapter 3: Epigenomic and proteomic changes in bovine viral diarrhea virus persistently infected fetal spleens: repercussions for the developing immune system, bone, brain, and heart.

Overview:

Maternal infection with bovine viral diarrhea virus (BVDV) during early gestation results in persistently infected (PI) immunotolerant calves that are the primary reservoirs of the virus. Pathologies observed in PI cattle include congenital defects of the brain, heart, and bone as well as marked defects in their immune systems. Previous studies demonstrated a decrease in innate and adaptive immune response genes in the PI fetal spleen and thymus 117 days post maternal inoculation, suggesting that PI fetal tolerance to BVDV infection may stem from an inability of T cells and B cells to respond appropriately to the infection. It was hypothesized that fetal BVDV infection alters T cell activation and signaling genes by epigenetic mechanisms. Splenic tissues were obtained from PI and control bovine fetuses collected on day 245 of gestation, 170 days post-maternal infection. DNA was purified for reduced representation bisulfite sequencing and protein was isolated for proteomics. Methylation sequencing files were analyzed using the methylKit R package, while proteomics analysis was performed using Scaffold. Within set parameters, 2,641 regions were differentially methylated: 1,951 hypermethylated and 691 hypomethylated regions were identified in PI fetuses compared to controls. Results revealed heavily methylated pathways associated with immune system, neural, cardiac, and bone development. The proteomic analysis revealed 12 differentially expressed proteins in PI vs control animals. Increased TMA7, PEPD, NUDC, SNRPF were associated with protein processing; whereas, THY1, HNRPC, CSRP1, VAPB, CSTB,

AKAP2, CNN2 associated with lymphocyte migration and development were decreased in PI fetal spleens vs controls. Decreased THY1 and VAPB protein concentrations were associated with hypermethylation of these genes. The epigenetic changes in these regulatory pathways may explain the immune dysfunctions, abnormal bone formation, brain and heart defects observed in PI animals.

Introduction

BVDV is a single stranded RNA virus in the family Flaviviridae and Pestivirus genus discovered in 1946 [1, 2, 6, 103, 140]. BVDV exists as two genotypes, BVDV1 and BVDV2 both having cytopathic (cp) and noncytopathic (ncp) biotypes [5, 6, 8, 103, 140]. The ncp biotype most commonly occurs in nature while cp biotypes arise from naturally occurring mutations of the ncp biotype in persistently infected (PI) animals [5, 17-20]. Most BVDV infections of healthy adult cattle result in subclinical to relatively mild disease depending on the strain of virus; however, severe pathologies occur in fetal infections following the vertical transmission from dam to fetus [96, 97, 141]. The outcome of BVDV fetal infection is determined by the time of infection relative to the development of the fetal bovine immune system [96, 97, 141]. If fetal BVDV infection occurs between gestational days 42 and 125, the fetus is unable to mount a competent immune response, becomes immunotolerant and persistently infected (PI), shedding the virus throughout its post-natal life [142, 143]. Fetal BVDV infections also cause a variety of congenital malformations including malformations of the brain such as cerebellar hypoplasia, hydranencephaly, hydrocephalus, bone malformations including brachygnathism, osteopetrosis, abnormal trabecular modeling, arthrogryposis, heart abnormalities, and thymic hypoplasia [90, 91,

96, 97, 99, 100]. Fetuses infected after day 150 of gestation are able to mount a more mature immune response to BVDV as evidenced by the presence of virus-specific antibodies and clearance of the virus prior to birth [96].

Our group previously developed an in vivo model of BVDV PI fetal infection by inoculating pregnant BVDV naïve heifers with BVDV on day 75 of gestation [109, 110]. Fetuses collected at several time points during gestation (days 82, 97, 190, and 245) revealed an approximate 2 week time period between maternal and fetal infection as determined by maternal and fetal viremia [84]. An innate interferon response in the PI fetus occurred early in the course of the infection; however, by day 190 both the innate and adaptive branches of the fetal immune system were dramatically attenuated [89, 144]. Pathological findings in the PI fetuses included bone abnormalities and BVDV antigen was present in neural tissues [75, 84, 86, 87, 91, 92, 98, 109-111]. It was reasoned that immune, neural and bone pathologies were due to the inhibition of interleukins and the presence of circulating interferons [87, 91, 98].

The present study aimed to determine if the inhibition of the immune system following the initial immune response and PI pathologies was due to epigenetic changes in the PI fetal DNA. It was hypothesized that spleens from PI fetuses would have increased methylation of genes and decreased concentrations of proteins associated with the adaptive immune response. Spleens from PI and control fetuses collected on gestational day 245 were examined because spleens are secondary lymphoid organs which survey the blood for pathogens; the day 245 time point was chosen for its proximity to parturition (~283 day gestation in the bovine) and would provide epigenetic data approximating what would be expected in postnatal animals. Reduced representation

bisulfite sequencing (RRBS) and liquid chromatography mass spectrometry (LC-MS) were performed on these samples to determine epigenetic changes to genes and effects of DNA methylation on protein expression. Differentially methylated regions and protein concentrations were found in PI fetuses compared to controls affecting pathways associated with compromised immune, neural, cardiac and bone development.

Methods

Animals, viral infections, and fetal collections

All animal experiments were approved by the Institutional Animal Care and Use Committee (provide approval number?) at Colorado State University and by the Colorado State University Biosafety Committee (BSL1 and BSL2 approval 19-037B for BVDV). Viral infections and fetal sample collections are described in previous studies [84, 86]. Briefly, a sample size of 3-4 animals per treatment group was determined to be sufficient to achieve a power of 1. Eight unvaccinated, BVDV naïve yearling Hereford heifers were purchased and confirmed to be seronegative for BVDV1 and 2 by virus neutralization assay and ear-notch BVDV antigen capture ELISA [84, 92]. The heifers were bred by artificial insemination and pregnancies were confirmed by ultrasound on days 35 and 70 post insemination. On day 75 of gestation, 4 randomly selected animals were intranasally inoculated with 2mL of sham MEM media to generate control fetuses while the other four animals were inoculated with 2mL ncp BVDV2 strain 96B2222 at 4.4 $\log_{10}$ $TCID_{50}$/mL to generate PI fetuses. Infected and control animals were confirmed infected or non-infected respectively by RT-qPCR and serum neutralization assay throughout gestation [84].

Seven fetuses were collected (4 control, 3 PI) by cesarean section on gestational day 245. Originally, 4 PI fetuses were generated; however, one fetus was aborted for reasons unrelated to BVDV. Control fetuses were collected prior to the collection of PI fetuses to avoid any contamination of their tissues. Standard surgical practices were used, and sterile surgical packs were replaced between each animal. Splenic tissue was sampled from the middle of the organ to ensure the inclusion of both red and white pulps. Samples were dissected into halves; one half was snap frozen in liquid nitrogen and stored at -80 for later DNA and protein extraction for this study.

Reduced Representation Bisulfite Sequencing

One mg of splenic tissue was homogenized and subjected to the Qiagen DNeasy Blood and Tissue Kit (Qiagen Hilden, Germany) according to manufacturer's instructions for DNA extraction. Extracted DNA (~300ng) was sent to Zymo Research (Irvine, CA) for genome wide classic reduced representation bisulfite sequencing (RRBS/methyl-seq). The following methods were provided by Zymo Research. Samples were digested with 30 unites of Mspl (NEB) and purified with DNA Clean &Concentrator-5 (Zymo Research). Fragments were ligated to pre-annealed adapters with cytosine replaced with 5'-methyl-cytosine according to Illumina's guidelines. Ligated fragments greater than 50 base pairs were recovered with the DNA Clean & Concentrator-5 (Zymo Research) then bisulfite treated with the EZ DNA Methylation-Lightning Kit (Zymo Research). Samples were subjected to PCR with Illumina indices and products were then purified with DNA Clean & Concentrator-5 (Zymo Research). Size and concentrations were confirmed with the Agilent 2200 TapeStation and libraries were sequenced on an Illumina platform.

Methylation Bioinformatics and Pathway Analysis

Raw BAM files from Zymo Research were analyzed in R using the methylKit R package and the CSU CVMRIT03 server. Differentially methylated regions (DMR) were determined significant by Fisher's Exact Test. DMRs were considered significant with $p<0.05$ and a 25% or greater difference in methylation patterns. Gene IDs were identified using the genomation R package. Quality control plots and gene ontology plots were made generated with clusterProfiler, pathview, and gage R packages. Bioinformatic code is available at https://github.com/hanahm1/methyl_seq.git. Raw files are available in the NCBI Geo repository. Pathway analysis for both methylation and protein data was performed using Ingenuity Pathway Analysis (IPA; Qiagen Hilden, Germany).

Protein Sample Preparation

One hundred mg of frozen splenic tissue from day 245 fetuses were subjected to protein extraction via RIPA Lysis and Extraction Buffer (Thermo Scientific Waltham, MA) and Halt Protease and Phosphatase Inhibitor Cocktail (10μl HALT/1 mL RIPA; Thermo Scientific Waltham, MA) according to manufacturer's instructions. Protein was quantified using a Pierce BCA Assay (Thermo Scientific Waltham, MA). Detergents were removed from the protein samples using the Pierce Detergent Removal Spin Columns (Thermo Scientific Waltham, MA). Cleaned samples were submitted to the CSU Analytical Resources Core Bioanalysis and Omics for protein quantification, trypsin digestion, and protein identification via liquid chromatography and mass spectrometry (LC-MS). The following methods were provided by the CSU Analytical Resources Core Bioanalysis and

Omics. Aliquots of samples were diluted 1:2 in 2M urea, 2% SDS and measured with the Pierce BCA Protein Assay (Thermo Scientific Waltham, MA). Fifty micrograms total protein was aliquoted and processed for in-solution trypsin digestion as previously described [145]. Absorbance was measured at 205nm on a NanoDrop (Thermo Scientific Waltham, MA) and total peptide concentration was subsequently calculated using an extinction coefficient of 31 [146].

Liquid Chromatography and Mass Spectrometry

The following methods were provided by the CSU Analytical Resources Core Bioanalysis and Omics. Reverse phase chromatography was performed using water with 0.1% formic acid (A) and acetonitrile with 0.1% formic acid (B). One μg of peptides was purified and concentrated using an on-line enrichment column (Waters Symmetry Trap C18 100Å, 5μm, 180 μm ID x 20mm column). Chromatographic separation was performed on a reverse phase nanospray column (Waters, Peptide BEH C18; 1.7μm, 75 μm ID x 150mm column, 45°C) using a 90 minute gradient: 5%-30% B over 85 minutes followed by 30%-45%B over 5 minutes at a flow rate of 350 nanoliters/min. Peptides were eluted directly into the mass spectrometer (Orbitrap Velos Pro, Thermo Scientific Waltham, MA) equipped with a Nanospray Flex ion source (Thermo Scientific) and spectra were collected over a m/z range of 400–2000 under positive mode ionization. Ions with charge state +2 or +3 were accepted for MS/MS using a dynamic exclusion limit of 2 MS/MS spectra of a given m/z value for 30 s (exclusion duration of 90 s). The instrument was operated in FT mode for MS detection (resolution of 60,000) and ion trap mode for MS/MS detection with a normalized collision energy set to 35%. Compound lists

of the resulting spectra were generated using Xcalibur 3.0 software (Thermo Scientific Waltham, MA) with a S/N threshold of 1.5 and 1 scan/group.

Proteomics Data Analysis and Instrument Quality Control

The following methods were provided by the CSU Analytical Resources Core Bioanalysis and Omics. Tandem mass spectra were extracted, charge state deconvoluted and deisotoped by ProteoWizard MsConvert (version 3.0). Spectra from all samples were searched using Mascot (Matrix Science, London, UK; version 2.6.0) against reverse concatenated Uniprot_Bovine_rev_102819 and cRAP_rev_100518 databases (UP000009136, downloaded 28Oct2019 & cRAP, downloaded 05Oct2018, 75997 total entries) assuming the digestion enzyme trypsin. Mascot was searched with a fragment ion mass tolerance of 0.80 Da and a parent ion tolerance of 20 PPM. Carboxymethylation of cysteine was specified in Mascot as a fixed modification. Deamidation of asparagine and glutamine and oxidation of methionine were specified in Mascot as variable modifications.

Search results from all samples were imported and combined using the probabilistic protein identification algorithms implemented in the Scaffold software (version 4.11.1, Proteome Software Inc., Portland, OR) [147, 148]. Peptide thresholds were set (0.1%FDR) such that a peptide FDR of 0.05% was achieved based on hits to the reverse database [149]. Protein identifications were accepted if they could be established at less than 1% FDR and contained at least two identified peptides. Protein probabilities were assigned by the Protein Prophet algorithm [150]. Proteins that

contained similar peptides and could not be differentiated based on MS/MS analysis alone were grouped to satisfy the principles of parsimony.

Relative quantitation was determined using spectral counting (SpC) [151]. A student's t-test was applied to determine protein species that were significantly different in abundance between groups (p-value < 0.05). Pseudo values were added (+1) prior to fold change calculations to eliminate zero values.

Instrument suitability was monitored through analysis of a commercially purchased BSA standard digest and automated monitoring using PanormaQC. Metrics (e.g., mass accuracy, peak area, retention time, etc.) are monitored and flagged as outliers if results are outside +/- 3 standard deviations of the guide set (i.e., optimal operation). Values for all metrics were within normal limits throughout the duration of the experiment indicating instrument stability and data robustness.

Results

Reduced Representation Bisulfite Sequencing

Classic RRBS indicated no significant changes in whole genome global methylation levels between control and PI animals. At the regional level, there were 2,641 differentially methylated regions (DMR) between control and PI animals. Of those DMRs, 1,951 regions were hypermethylated in PI animals compared to controls while 691 regions were hypomethylated in PIs compared to controls.

The pathways reported are predicted to be downregulated, due to hypermethylation of genes, unless otherwise stated. Several pathways associated with general biological signaling were shown to be significantly affected, as predicted by IPA.

In order of higher significance to lower significance, these pathways include but are not limited to: signaling by Rho family GTPases, human embryonic stem cell pluripotency, Wnt/b-Catenin signaling, protein kinase A signaling, PI3K/AKT signaling, calcium signaling (predicted upregulation), STAT3 signaling, mTOR signaling, phospholipase c signaling, and Wnt-Ca signaling. Pathways associated with immune development and activation include the role of macrophages, fibroblasts and endothelial cells in rheumatoid arthritis, CCR5 signaling in macrophages (predicted upregulation), IL-8 signaling, IL-15 production, regulation of IL-2 expression in activated and anergic T lymphocytes, IL-1 signaling, B cell activating factor signaling, CXCR4 signaling, PKCO signaling in T lymphocytes, leukocyte extravasation signaling, and CD27 signaling in lymphocytes (predicted upregulation). Pathways associated with neural development include axonal guidance signaling, synaptogenesis signaling pathway (predicted upregulation), CREB signaling in neurons, alpha adrenergic signaling, and synaptic long-term depression. Pathways associated with cardiac development include factors promoting cardiogenesis in vertebrates, role of NFAT in cardiac hypertrophy (predicted upregulation), and cardiac hypertrophy signaling. Pathways associated with bone development or bone disease include the role of osteoblasts, osteoclasts and chondrocytes in rheumatoid arthritis, osteoarthritis pathway, and actin cytoskeleton signaling. When considering both hypo- and hypermethylated regions of PI fetuses, the nuclear factor of activated T cells (NFAT) family and signaling pathway stood out. Within that signaling cascade, calcium channel ORAI, calmodulin 1 (CALM1), and NFATc2 were hypomethylated while co-stimulatory molecules CD247, VAV1, NFATc1, and NFATc4 were hypermethylated in PIs compared

to controls. Significantly different genes associated with these pathways can be found in appendix table 4.

Proteomics

Proteomic analysis from LC-MS identified 12 significantly different proteins, with a 1.5-fold cutoff, in PI fetuses vs controls. Increased proteins were translation machinery associated protein 7 (TMA7), peptidase d (PEPD), nuclear migration protein nudc (NUDC), tropomodulin 3 (TMOD3), and small nuclear ribonucleoprotein F (SNRPF). Proteins decreased in PI fetuses compared to controls include Thy-1 cell surface antigen (THY1), heterogenous nuclear ribonucleoprotein c (HNRPC), cysteine and glycine rich protein 1 (CSRP1), vesicle associated membrane protein B (VAPB), CSTB protein (CSTB), AKAP2 c domain containing protein (AKAP2), and calponin 2 (CNN2).

Discussion

Day 245 fetal spleen samples are an imperfect but unique sample set. Since the developing fetus has a constantly changing epigenome, the fetuses on day 245 provide epigenetic data most similar to what we would expect to see in postnatal animals (i.e., approximately 30 days further along in development). When discussing methylation data, it is important to understand its limitations without RNA expression data. Unfortunately, the data presented here do not contain RNA expression data due to degraded RNA from splenic tissue; however, this leaves opportunities for future studies. Additionally, the epigenetic changes found in PI fetal spleens were not completely reflected in protein abundance. Although another challenge in interpretation, changes in methylation are

rarely reflected by gene expression at one given time. Gene expression changes may have occurred prior to day 245 or may occur postnatally, as discussed below. Despite these limitations to interpretation, the results discussed below are still extremely valuable in understating the affects BVDV PI has on fetal development.

Fetal BVDV PI spleens contained 2,641 DMRs and differences in the expression of 12 proteins compared to controls. Hyper- and hypomethylated genes were found in pathways related to the immune system, osteoclastogenesis in bone, the developing neural system and heart in PI fetal spleens.

Fetal BVDV PI alters the expression of genes that influence lymphocyte development.

Previously, it had been hypothesized that the dramatic attenuation of BVDV PI fetal immune responses and specifically, the inactivation/lack of response from lymphocytes was due to fetal Treg cells identifying BVDV as self [144]. This immunotolerance was expected to affect lymphocyte development and reaction to pathogens. The data presented here suggest that epigenetic changes affecting genes responsible for bone development may also interfere with hematopoiesis and cell trafficking with subsequent effects on lymphocyte and immune system development. Methylated pathways associated with immune system development are summarized in Figure 8.

Interleukin 2 (IL2) is an important cytokine in the development and activation of T cells promoting both the activation and anergy of T cells as well as Treg development [152-155]. Genes within the IL2 pathways involved in the regulations of IL2 expression and PKC) signaling in T cells were heavily hypermethylated. For example, CD247 (also known as CD3 subunit zeta), a critical T cell receptor co-stimulatory molecule, was

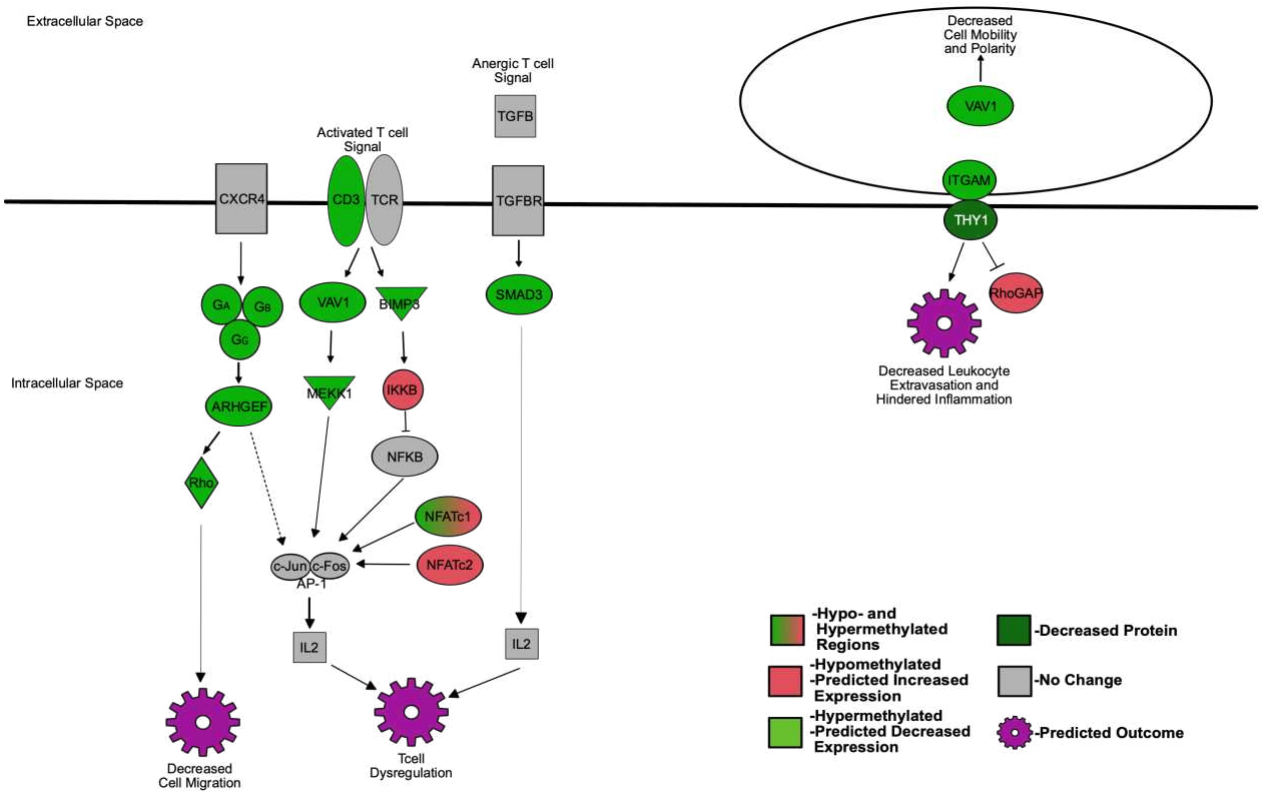

Figure 8: Summarized differentially methylated pathways and genes in PI fetal spleens associated with development of the fetal immune system. Green = hypermethylated, predicted decreased expression; Red. = hypomethylated, predicted increased expression; grey = not differentially methylated or not identified in RRBS

hypermethylated. Reduced expression of CD247 would reduce the release of IL2. IL2 is a potent stimulator of FOXP3 expression in Treg development, potentially causing an increase in Treg cell development through increased FOXP3 expression [154, 155]. Treg cells compete with T helper (Th) cells for available IL2 causing apoptosis of effector cells [152, 154]. IL2 knockout mice exhibit lymphoproliferation and lethal autoimmunity which is prevented by adoptive transfer of normal Treg cells [153, 156]. In a previous study, it was hypothesized that PI fetuses develop normal Treg cells prior to/during BVDV infection prior to the development of effector T cells, causing Treg cells to identify viral antigens as self [144]. With the current data, it is postulated that as the fetal spleen and thymus develop, genes in the CD4 Th cells' IL2 signaling pathway are hypermethylated (CD247, VAV, BMP3, and SMAD3), shifting the IL2 signaling towards the maintenance of Treg

cells while hindering Th cell development. Unfortunately, these genes were not reflected in the proteomic data.

Leukocyte extravasation is the movement of cells from the blood across blood vessel walls to infected tissues in response to chemokines and cytokines released as a part of the innate immune response. Recruitment of leukocytes requires gene products that stimulate leukocyte migration and adhesion to endothelial cells (EC). Several signaling genes within this pathway were hypermethylated in fetal PI spleens including vav guanine nucleotide exchange factor 1 (VAV1), integrin subunit alpha M (ITGAM), THY1, and others. The effects of hypermethylation of THY1 was reflected in decreased THY1 protein in PI fetal spleens compared to controls. THY1 is expressed in fibroblasts, neurons and hematopoietic stem cells and has several functions including mediating the binding of leukocytes to ECs and triggering neutrophil effector functions. THY1 knockout mice have decreased extravasated leukocytes and altered cytokines released at sites of inflammation [157]. TMOD, an increased protein in PI fetal spleens, has been shown to negatively regulate endothelial cell motility by capping pointed ends of actin structures possibly contributing to decreased leukocyte migration [158]. Despite TMOD not being differentially methylated, other mediators involved in the pathway may be affecting its expression.

C-X-C motif chemokine receptor 4 (CXCR4) was previously shown to be decreased for several months in maternal peripheral blood mononuclear cells (PBMCs) in the dams carrying PI fetuses and in post-natal PI animals compared to control animals [109]. Moreover, CXCR4 levels in herds with several PIs were decreased compared to herds without PI animals [159]. CXCR4 has several functions in regulating leukocyte

trafficking, lymph node organization, T cell priming, B cell development, bone marrow homeostasis, and is essential for normal cardiac development [160]. Although CXCR4 was not differentially methylated or expressed as a protein, its signaling pathways, including G proteins and Rho signaling, were both hypermethylated in the data from the current experiment [160]. Inhibition/hypermethylation of G protein and Rho signaling may give insight into the CXCR4 inhibition in PI animals, possibly contributing to dysfunctional leukocyte and lymphocyte development in PI animals. These genes were not reflected in the proteomics data, indicating that their differential expression may occur at another time point.

AKAP2 protein was decreased in fetal BVDV PI spleens compared to controls. AKAP family members anchor and compartmentalize PKA for regulation of cAMP signaling [161]. More recently, AKAP2 was identified as an upregulated protein in CD8 cells responding to IL35 stimulation, suggesting a role for AKAP2 in the differentiation of CD8 T cells [162]. AKAP2 was also increased in T cells from patients with systemic lupus erythematosus suggesting a role for AKAP2 in Treg cell functions [163]. The literature for AKAP2 is limited and the reason for its decrease is unknown; however, its decrease in BVDV PI fetal spleens suggest a role in immune dysfunction and in dysfunction of the PKA/cAMP signaling pathways.

CNN2 has been associated with the development of immune cells of the myeloid lineage. Peripheral blood neutrophils and monocytes were decreased in CNN2 interrupted mice, concurrently with increased proliferation and migration of neutrophils and monocytes, and increased macrophage phagocytic activity. In contrast, increased CNN2 was associated with the adhesion dependent maturation of macrophages. In this

study, CNN2 was decreased in BVDV PI fetal spleens, which could cause a decrease in mature macrophages while increasing the proliferation and migration of immature monocytes in PI animals. These effects could be due to direct effects on macrophage development, or due to osteopetrosis resulting in the migration of immature leukocytes from bone marrow to the spleen and increased extramedullary splenic hematopoiesis.

BVDV fetal infection alters osteoclastogenesis resulting in extramedullary splenic hematopoiesis

Three hundred and eighty-five million years ago, the vertebrate skeletal system and immune system evolved together as aquatic vertebrates became terrestrial [164]. The evolution of the acquired immune system and the skeletal system together has been theorized as the reason for the interplay between the two systems [164, 165]. Several of the molecules that affect bone development also affect immune development/activation in modern mammals [164, 166, 167]. In the early 2000s, the term “osteoimmunology” was coined to more comprehensively describe the importance of the two systems and their interactions [164, 166, 167]. In addition to providing support for locomotion and minerals for homeostasis, the bone is a primary lymphoid organ, in which hematopoietic stem cells, lymphocytes, monocytes, and macrophages develop and reside [168]. The bone marrow houses chondrocytes, osteocytes, osteoblasts, and osteoclasts critical for bone metabolism as well as the constant remodeling, i.e., built by osteoblasts and resorbed by osteoclasts [168]. The progenitors of osteoclasts are cells of the macrophages/monocytes lineage and their differentiation is mediated by macrophage colony stimulating factor (CSF1 or M-CSF), receptor activator of nuclear factor kappa B ligand (RANKL), and other cytokines [168]. Although mediated by CSF1 and RANKL, NFATc1 is considered the

master transcription factor for osteoclastogenesis [168-171]. Osteoclast bone resorption is also stimulated by the inflammatory interleukins, interleukin (IL)1 and IL6, secreted by antigen stimulated immune cells [168]. Osteopetrosis, also known as marble bone disease, is associated with several human genetic mutations, and characterized by brittle bones and reduced size of bone marrow cavity [164, 172, 173]. Postulated to be caused by a decrease in osteoclasts, the reduction in the size of the bone marrow cavity severely restricts hematopoiesis in this location forcing the movement of hematopoietic cells to lymph nodes, the spleen, and/or the liver. Extramedullary hematopoiesis results in severe anemia and impairs immune cell differentiation [164, 172, 173]. Previous studies reported osteopetrosis and abnormal bone development in BVDV PI animals and in Border disease virus infected lambs [90-92, 98, 99]. Three of 6 PI fetuses exhibited thickened femoral cortical bone and a significantly smaller medullary space compared to controls, and day 245 BVDV PI fetuses had transverse bands and lesions in the middle and distal zones of the tibia and femur, indicative of osteopetrosis and altered osteoclast differentiation/osteoclastogenesis [91, 92]. Decreased numbers of osteoclasts and osteoblasts were observed in the PI tibias, further evidence of abnormal osteoclastogenesis and bone development [91]. In a case study, post-natal PI calves were observed to have irregular bands and lesions in the femur and tibia [90]. The calves lacked osteoclasts and megakaryocytes in the bone marrow, which also exhibited smaller bone marrow spaces [90]. Additionally, the calves had lymphoid depletion in the spleen and lymph nodes [90]. Increased hematopoietic activity was observed in fetal PI spleens early in gestation, while the day 245 spleens exhibited fewer lymphocytes [144]. Another BVDV case study revealed dense bones with striped appearance in a two-day old calf

admitted for a fractured femur [99]. At 13 months of age, necropsy revealed lymph node hyperplasia, extramedullary hematopoiesis in the spleen, and BVDV infected osteoblasts, osteocytes and splenic blood leukocytes [99]. All three studies agree that the observed changes are the result of decreased osteoclasts and suggest different mechanisms for osteopetrosis including BVDV induced secretion of IL-1 inhibitor from monocytes, direct viral changes to bone marrow derived cells, and inhibition of osteoclastogenesis by type I interferons [164, 172, 173]. Similar bone lesions and pathologies are found in human neonates following transplacental infection with human cytomegalovirus (CMV) and rubella virus, characterized by irregular radiodense zones and pathologic fractures [98, 174-178]. Several pathways identified by IPA including signaling by Rho family GTPases, Wnt/b-Catenin signaling, protein kinase A signaling, PI3K/AKT signaling, calcium signaling, STAT3 signaling, phospholipase c signaling, and Wnt-Ca signaling pathways contained the same differentially methylated genes affecting osteoclastogenesis in PI fetal spleens compared to controls. Changes in signaling due to DNA methylation may explain the decreased number of osteoclasts observed in PI animals (summarized in figure 9) [164, 172, 173]. The inhibition of osteoclastogenesis would dramatically reduce calcium levels in the body, as bone resorption normally maintains extra- and intra-cellular calcium levels [179]. Hypomethylation of the calcium channels ORAI and PMCA, ion exchange channel NCX, and calmodulin (CALM) genes may be an attempt to increase intracellular calcium. Additionally, protein kinase C (PKC) and inhibitor of nuclear factor kappa B kinase subunit beta (IKBKB) may be hypomethylated to further amplify calcium signaling to compensate for the lack of extracellular calcium, although this is purely

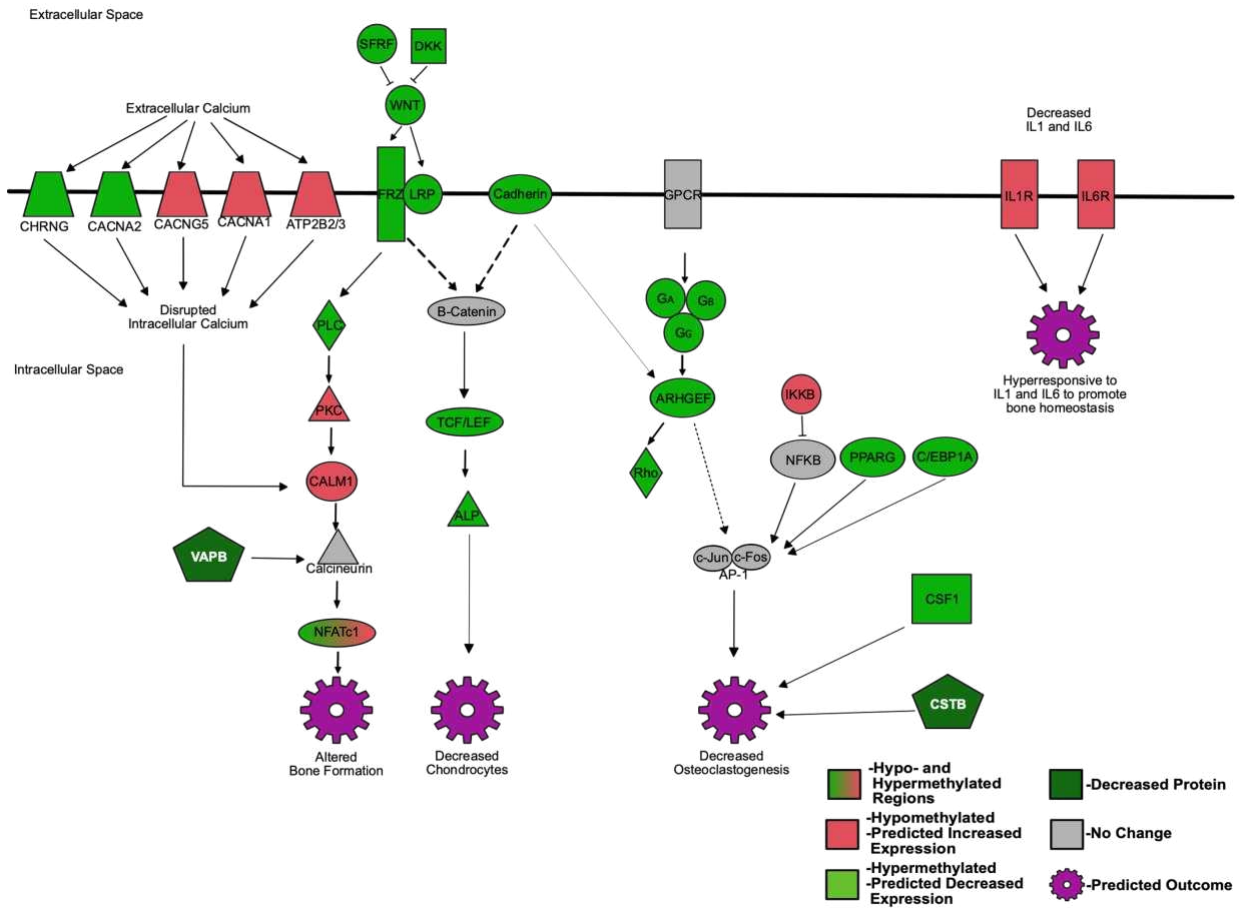

Figure 9: Summarized differentially methylated pathways in PI fetal spleens associated with bone development and osteoclast differentiation. Green = hypermethylated, predicted decreased expression; Red = hypomethylated, predicted increased expression; grey = not differentially methylated or not identified in RRBS.

speculative since calcium measurements were not performed in this study. Most genes in the signaling pathway of the Rho family GTPases are hypermethylated affecting activator protein transcriptional complex (AP1) formation/AP1 gene expression. The AP1 transcription complex includes the cFos and Jun family proteins. The cFos proteins are stimulated by not only rho family GTPases, but also nuclear factor kappa B. NFKB is expected to be inhibited due to hypomethylation of inhibitor of NFKB subunit beta and peroxisome proliferator activated receptor gamma (PPARG), and hypermethylation of PPARG coactivator 1 beta (PGCA1B), and CCAAT/enhancer binding protein alpha (C/EBP1A) [168, 180-183]. As a result of the increased methylation of rho family GTPase

pathway and cFos stimulants, the cFos and AP1 complex are thought to be decreased and thus, unable to stimulate osteoclastogenesis. In mouse studies, mice lacking cFos proteins developed osteopetrosis due to impaired osteoclastogenesis [168, 180, 184].

The Wnt signaling pathway is important for both osteoclast and osteoblast differentiation, and the role of Wnt signaling depends on which Wnt molecule binds to the Frizzled receptor (hypermethylated). Normally, Wnt2b expression is higher in mature osteoblasts compared to osteoblast progenitors, however, its direct role in osteoblast differentiation is unknown. Wnt2b was hypermethylated in our data, possibly inhibiting not only its signaling pathway, but also affecting osteoblast maturation [185]. Wnt7a was also hypermethylated in our data. Previous studies have shown Wnt7 conditional knockout causes a decrease in bone formation and chondrocyte differentiation [186].The methylation of this pathway is extremely intriguing as most of the genes are hypermethylated; however, inhibitors of the pathway are also hypermethylated. The predicted decreased expression of hypermethylated genes in the pathway is expected to cause altered bone development and hindered osteoblast and osteoclast maturation/differentiation, contributing to the osteopetrosis and decreased osteoclast numbers seen in these fetuses [91, 92]. Osteoblast derived dickkopf WNT signaling pathway inhibitor 1 (DKK1), a Wnt inhibitor, is also hypermethylated which may compensate for a decreased osteoclastogenesis. Phospholipase C signaling contains the same signals as the rho family GTPases pathway with direct effects on nuclear factor of activated T cells (NFATc1) expression. The hypermethylation of the G proteins and rho are expected to decrease the signal for calcium mediated gene expression.

The IPA identified pathways associated with osteoarthritis and bone development have overlapping genes and signaling pathways, with the Wnt signaling pathway being present in all bone related pathways. Colony stimulating factor 1(CSF1; also known as macrophage colony stimulating factor) is hypermethylated and a large inducer of osteoclastogenesis, macrophage differentiation, and osteoclast survival. CSF1 is produced by osteoblasts and activated T cells to induce differentiation of macrophages or dendritic cells into osteoclasts [187]. Therefore, hypermethylation of CSF1 would greatly inhibit osteoclastogenesis from monocytic cells. Mice lacking CSF1 exhibit severe osteopetrosis due to a decrease in osteoclastogenesis [188, 189]. Interestingly, IL1 and IL6 receptors, both inducers of osteoclastogenesis, are hypomethylated. IL6 is secreted by bone marrow stromal cells, osteoblasts, and macrophages to induce an inflammatory response as well as osteoclastogenesis through the STAT3 (hypermethylated) pathway [190, 191]. Due to the secretion of IL6 from bone marrow derived cells, the actual expression of IL6 may be hindered due to the osteopetrotic pathologies of BVDV PI animals lacking bone marrow and thus, bone marrow derived cells. In response to such a decrease, IL6R may be hypomethylated to amplify the signal for downstream targets if IL6 does happen to bind. Despite the attempted amplification, the hypermethylation of STAT3 would further hinder the IL6 signaling for osteoclastogenesis. However, IL6 is also known to be anti-osteoclastogenic but through the hypermethylation of STAT3, the signaling will be hindered no matter the reason [191]. IL1 is another proinflammatory cytokine that is pro-osteoclastogenic. One study has determined that BVDV PI animals have inhibited IL1 expression through the expression of an IL1 inhibitor from infected cells

[192]. This inhibition of IL1 may be an indirect cause of the hypomethylation of its receptor, for the same proposed reasons as the hypomethylation of IL6R discussed above.

NFATc1 has been identified as the master transcription factor for osteoclast differentiation [171]. In a healthy mammal, RANKL induces calcium oscillations in the bone marrow cells, activates calcineurin, then induces NFATc1 expression via TNF receptor associated factor (TRAF) 6 and cFos signaling [171]. NFATc1 autoamplifies and, with the assistance of the AP1 transcription complex, stimulates transcription of genes for osteoclastogenesis [171]. In the methylation data, NFATc1 was both hypo and hypermethylated. Although the interpretation of this data is difficult, differing methylation patterns on a gene have been associated with carcinogenesis [193]. One study suggests that in the case of differing methylation patterns on one gene, hypermethylation is associated with developmental process functions and regulation of biological processes, while hypomethylation is associated with a response to stimulus (inflammation, infection, etc.) [193]. Despite the lack of information on this specific phenomenon, it is clear that NFATc1 expression would be altered and would cause an imbalance in osteoclast differentiation signaling. Interestingly, an upstream regulator to NFATc1, calmodulin, was hypomethylated. Calmodulin is a regulator for all NFAT family members as it is involved with general calcium signaling. It's hypomethylation could be an attempt to stimulate other NFAT family members or amplify calcium signaling which was discussed above.

CSTB has several biological functions including chemotaxis, stimulation of cytokine secretion, release of nitric oxide, regulation of apoptosis, protection of neurons, cell cycle regulation, and bone resorption. CSTB was identified as a decreased protein in PI animals compared to controls. CSTB knockout mice mimic the progressive myoclonus

epilepsy of Unverricht-Lundborg type (EPM1) epileptic phenotype in humans, causing inflammation in the brain [194]. CSTB has been shown to have a protective role in osteoclast development and bone resorption, through the inhibition of cathepsin K, the main osteoclast proteolytic enzyme [195]. In addition to epileptic phenotypes, CSTB knockout mice showed a significant decrease in osteoclasts and increased bone mineral densities [196]. A direct inhibition of CSTB has been shown in mice infected with ectromelia virus and hypothesized to enhance viral replication [197]. It is possible the PI BVDV infection may be targeting CSTB in dendritic cells for increasing its own replication and contributing to the inhibition of osteoclastogenesis.

VAPB is a vesicle associated protein which can form dimers with itself or VAPA for vesicle transport. VAPB protein was decreased in PI animals compared to controls. VAPB has a role in osteoclastogenesis, by controlling the activation of phospholipase C (PLCG)-Ca-NFATc1 signaling pathway [198]. With decreased VAPB, NFATc1 decreases along with osteoclastogenesis [198]. The specific method by which VAPB regulated this pathway is still not known [198]. In humans, deficiency in VAPB results in amyotrophic lateral sclerosis (ALS) [199]. Through this association, it was found that VAPB is required for neural and cardiac pacemaker channels, with mice deficient in VAPB presenting with bradycardia [199]. Although BVDV PI animals have not exhibited any cardiac arrhythmias, it is possible that decreased VAPB could contribute to altered cardiac development discussed below.

Although this data was procured from the fetal spleen, it most likely reflects pathologies observed in the bone. Hematopoietic stem cells are produced in the bone prior to migration into peripheral lymphoid organs [164, 172, 173]. With hindered

hematopoiesis occurring in the bone, any hematopoietic stem cells derived from the bone is expected to migrate to the spleen [164, 172, 173]. Additionally, due to the altered bone resorption and significantly smaller bone marrow cavity, the hematopoietic function is shifted to the spleen, causing extramedullary splenic hematopoiesis. Hence, epigenetic changes and protein differences found in the PI fetal spleen are reflective of bone marrow changes [99]. Additionally, with extramedullary splenic hematopoiesis occurring in response to PI of BVDV, cells derived from splenic hematopoiesis are mobilized to peripheral organs such as the heart and brain, discussed below [94]. Alterations in the methylation patterns and protein abundance, seen in the PI fetal spleen, may have effects on said peripheral organs, through the mobilization and migration of hematopoietic cells, further contributing to BVDV PI pathologies.

Methylation patterns and protein expression in the PI fetal spleen are related to neural defects in PI fetuses.

BVDV directly infects fetal neuronal tissues and is associated with a variety of neural defects including cerebellar hypoplasia, hydranencephaly, hydrocephalus and retinal dysplasia [87, 200-202]. In PI cattle, BVDV antigen is present in up to 90% of neurons including dendrites and axons [202], and has been localized to neurons in the cerebral cortex, olfactory bulb, hippocampus, hypothalamus, corpus quadrigeminus, pons, medulla, cerebellum and spinal cord [201]. Infection of the fetal brain occurs rapidly following maternal infection as BVDV positive microglial cells, decreased oligodendrocyte precursor cells, reduced numbers of neuron specific enolase positive nerve cells, hypomyelination, and vascular lesions are observed as early as 22 days post maternal

inoculation [87, 200, 202]. Although well studied, the molecular mechanisms causing the defects are not well understood.

The most significantly methylated canonical pathway identified by IPA was the axonal guidance signaling pathway with 60 differentially methylated genes, with 43 genes hypermethylated (72%) including G protein receptors, transcriptional regulators, enzymes, growth factors, kinases, and others. The affected genes/pathway are predictive of alterations in actin filament reorganization, microtubule assembly, axon attraction, and adhesion. In addition, genes within the synaptogenesis pathway were differentially methylated with most regions being hypermethylated. These genes are involved in neuron adhesion, microtubule stabilization, and axonal guidance signaling. In addition to the epigenetic changes, proteins VAPB, THY1, and CSTB, which were significantly decreased in PI fetal spleens, are associated with altered neural development. CSTB mutations are associated with progressive myoclonus epilepsy of Unverricht-Lundborg type (EPM1) while VAPB genetic mutations have been associated with amyotrophic lateral sclerosis (ALS) in humans [194, 203]. A study of VAPB and the ALS phenotype and found decreased VAPB protein in cells from ALS patients and motor neurons from ALS animal models contributing to motor neuron degeneration [204-206]. THY1 is expressed on neurons and is an inhibitor of neurite outgrowth. While THY1 knockout mice do not have structural neural abnormalities, they exhibit alterations in spatial learning, a lack of social cues possibly reflecting abnormal neurite connections [207-209]. CSTB knockout mice exhibit alterations in GABAergic signaling possibly contributing to neuronal degeneration [203]. The decreased expression of these hypermethylated genes predict decreased neuron and axon growth, cell adhesion and reduced formation of synapses

which may explain some of the developmental defects of the fetal brain characteristic of BVDV PI fetal infections. The connection between DNA methylation and protein expression in fetal spleen and neural development is not known. The changes in DNA methylation of genes may be universal across fetal tissues including the brain, and/or alterations in the concentration of proteins in the fetal circulation may influence the development the fetal brain.

Genes affecting cardiac development are hypermethylated in the spleen of BVDV PI fetuses.

IPA identified several heavily methylated pathways associated with cardiac development, summarized in Figure 10. These pathways include the previously described pathways Wnt signaling, G proteins, and calcium signaling. Several hypermethylated genes in pathways promoting cardiogenesis in vertebrates contribute to a dysfunctional cell cycle of cardiomyocytes and cardiomyocyte differentiation, including transcription factors/ T cell factors 4 and 7 (TCF), t-box transcription factor 5 (TBX5), cyclin D1, and myocardin. In the pathway for the role of NFAT in cardiac hypertrophy, histone deacetylase 7 and NFATc4 were both hypermethylated. Mice with attenuated NFAT (specific experimental NFAT not identified) in late gestation showed a thinning of the myocardium [210]. The cardiac hypertrophy signaling pathway also identified the hypermethylated gene, myocyte enhancer factor 2D (MEF2D). Interestingly, VEGF was also hypermethylated. VEGF is needed in the developing fetus for the organization of the vascular system and its predicted decreased expression may alter said organization

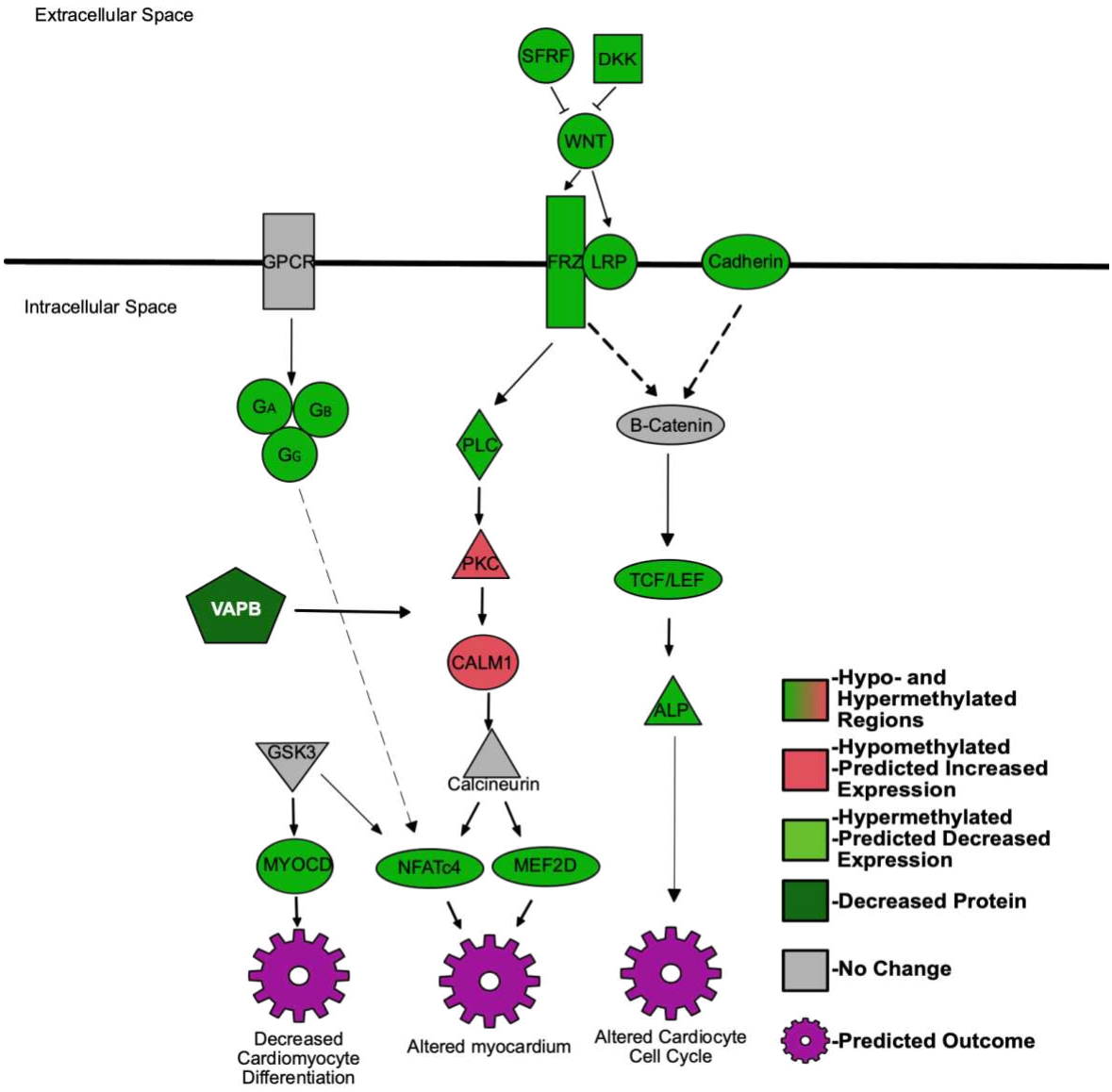

Figure 10: Summarized differentially methylated pathways and genes in PI fetal spleens associated with cardiac development. Green = hypermethylated, predicted decreased expression; Red = hypomethylated, predicted increased expression; grey = not differentially methylated or not identified by RRBS.

[211]. The methylation patterns of these pathways and genes suggest disruptions in cardiac development of the BVDV PI fetuses. Evidence for abnormal heart development in pre- and postnatal PI animals include enlarged/"flabby"[sic] hearts, cardiac lesions, occluded spindle cells, and cardiomyocyte loss/fibrosis [212, 213].

BVDV Replication and Immune Evasion

Several of the increased proteins in PI animals, compared to controls, have a tie to viral replication. Not much is known about TMA7; however, it has been shown to be increased in influenza infections [214]. In a STRING analysis, TMA7 interacts with NFATc2 interacting protein; however, the importance and function of this interaction is not known. PEPD has been shown to bind flaviviral NS5 to inhibit interferon receptor 1 and thus, type I interferon (IFN) signaling, as a way to evade the host immune response [215]. NUDC has a role in cell migration, hematopoiesis, spindle formation, and as a regulator of inflammation [216, 217]. Its roles are not well understood and its role in BVDV PI animals difficult to speculate.

BVDV viral proteins have been shown to inhibit and evade several immune functions in vitro, including IFN responses [75-80]. The authors suggested that BVDV only inhibits/evades a type I IFN response directed to itself, but does not inhibit a response to any other invading pathogen [75-80]. Although in vivo models have shown a robust type I IFN response in PI fetuses following maternal infection, one cannot discount a possibility of BVDV to inhibit IFN responses in vivo. Previous studies have shown a PI fetal IFN response at day 97 of gestation, followed by a drastic downregulation of both the innate and adaptive immune responses by day 190 of gestation, seen in mRNA expression data [89, 144]. Interestingly, when comparing a previous microarray from day 97 fetal spleens to our current day 245 methylation data, we found an inverse relationship between day 97 mRNA differential expression and day 245 methylation/protein [144]. Of particular interest are NFATc2 (decreased mRNA concentration on day 97, hypomethylated by day 245), CD247 (increased mRNA concentration on day 97, hypermethylated by day 245), VAV1 (increased day 97 mRNA concentration, hypermethylated by day 245), ITGAM

(increased in day 97 mRNA concentration, hypermethylated by day 245), and CSTB (increased mRNA concentrations on day 97, decreased protein by day 245) [144]. To our knowledge, time course studies with mRNA, methylation, and protein data has not been done previously, therefore we can only speculate on the reason for this inverse relationship, with several possible explanations. The first being that day 97 PI fetuses exhibited a peak of immune response, whether it was a direct response to the virus or stimulated by placental inflammation. In response to this drastic increase in the fetal immune response, the fetus may differentially methylate some of the stimulated immune genes between days 97 and 245, overcorrecting for the fetal immune response on day 97. The second explanation may be that as Treg cells identify BVDV as “self”, Treg cells shut down the stimulated genes in order to disallow further response to the virus, i.e., the fetus differentially methylates the stimulated or downregulated genes. The third explanation might be that the PI fetal immune response on day 97 is only a reaction to maternal and placental inflammation, which once maternal or placental inflammation is subdued, BVDV evades and possible downregulates the immature fetal immune response, as suggested by in vitro studies, causing differential methylation patterns later in gestation. All of these explanations are reflected in the downregulation of day 190 PI fetal spleen immune related mRNAs measured in previous studies [89, 144]. Said day 190 mRNAs were specific targets measured via RT-qPCR and unfortunately not assessed for methylation patterns; however, their differential expression may be a direct result of the extramedullary splenic hematopoiesis previously seen in other studies and suggested by the current study [99].

Maternal factors contributing to fetal programming and health as an adult is a concept described as the Developmental Origin of Adult Health and Disease; originally a hypothesis by Barker and Osmond (1986) based on the effects of maternal heart disease on fetal growth [218, 219]. Fetal development is sensitive to the maternal environment including maternal diet, body mass index, mental health (anxiety, stress, depression) and bacterial/helminth/viral infections, and inflammation. These factors not only affect fetal growth, but the epigenetic programming of genes [218, 220]. In humans, the transplacental transmission of pathogens such as *Toxoplasma gondii*, HIV, parvovirus, *Listeria monocytogenes, Treponema pallidum*, varicella zoster virus, rubella virus, CMV, and herpes simplex virus (HSV) 1 and 2, and Zika virus (ZIKV) cause significant detrimental effects on the fetus [221]. Although BVDV is a virus that affects ruminants and pigs, the ability of BVDV to cross the placenta and affect the development of multiple fetal organ systems presents a unique opportunity to dissect the cellular and immune mechanisms by which pathogens affect gene expression with consequences for fetal development. These mechanisms and principles may give insight into the effects of human maternal infection on fetal development.

Conclusions

Methylation of genes and the impact on protein expression may help explain the pathologies in multiple organ systems associated with early BVDV transplacental infections. We suggest that the inflammation and cytokines associated with the early fetal response to BVDV infection, along with Treg suppression of the immune system during immunotolerance, inhibited proper osteoclastogenesis and bone formation (summarized

in figure 11). In earlier studies, our group found an upregulation of IFNB, IFNG, and ISG15 in day 97 PI fetuses (21 days post maternal infection) [86, 144]. These interferons and ISG15 are known inhibitors of osteoclastogenesis [164, 222, 223]. The expression of these interferons early in fetal development may not only inhibit ongoing osteoclastogenesis, but also cause the inhibition of osteoclastogenesis through hypermethylation of most pathways affecting bone development and immune cell

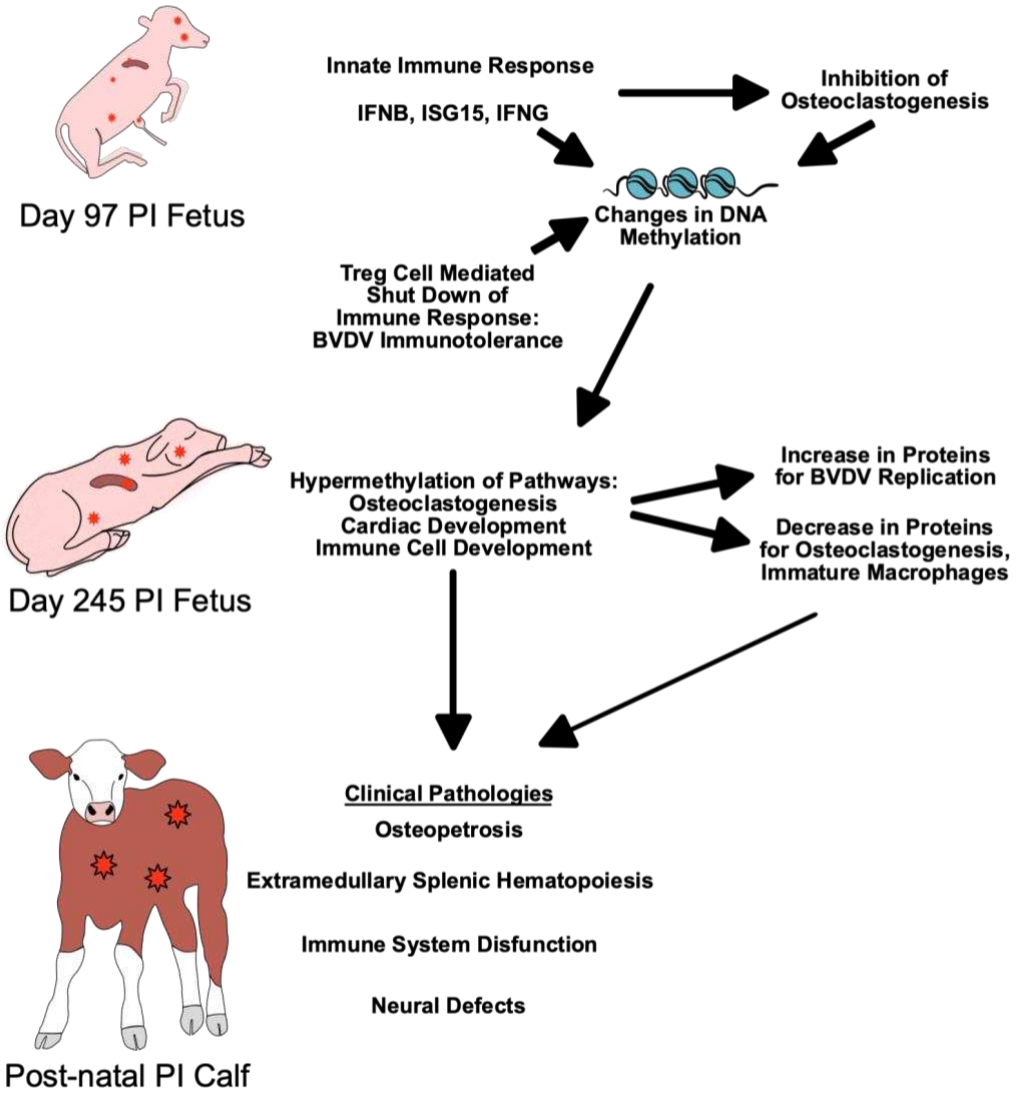

Figure 11: Hypothesized changes in prenatal PI calves in response to BVDV fetal infection and its effects on postnatal calf pathologies. Day 97 data from Georges et. al 2020 and Smirnova et al. 2012 [84].

development. By day 190 of gestation, Treg cells identified BVDV as self and suppressed the immune response to viral antigens; however, the epigenetic damage would have already been done. The results presented correlate with previously described pathologies observed in PI cattle postnatally, suggesting that the epigenetic changes caused by BVDV fetal infections have a large role in fetal development.

BVDV is an important economic problem for the cattle industries worldwide. While this research enhances our understanding of viral repercussions in PI animals, it also provides insight into potential epigenetic changes due to maternal and fetal viral infections in humans and other mammals. Maternal infection with ZIKV and other viruses cause severe defects of the fetal brain [224-226]. Osteopetrosis has been identified in infants positive for cytomegalovirus with abnormal amounts of leukocytes [227, 228]. Additionally, children from mothers infected with rubella virus or cytomegalovirus early in gestation had an increased risk of congenital heart defects [229]. While developmental defects of the brain, heart and limbs may be readily diagnosed during the neonatal period, immune system dysfunctions would likely escape detection in human infants. This study provides potential explanations for several pathologies described in BVDV PI cattle, identifies possible targets for therapeutic treatments, and provides a valuable model for the potential consequences of transplacental viral infections.

Chapter 4: Vertical transmission of BVDV leads to cyclical placental inflammation and intrauterine growth restriction in infected bovine fetuses.

Overview:

Molecular consequences and mechanisms underlying vertical transmission of viruses from mother to fetus has remained unidentified due to several study limitations. Bovine viral diarrhea virus (BVDV) possesses the ability to transmit across the placenta, causing fetal persistent infection (PI) if fetal infection occurs early in gestation, making it a unique model for transplacental infection studies. Both maternal placental tissues (caruncles) and fetal placental tissues (cotyledons) were collected at different time points following maternal BVDV inoculation at day 75 of gestation. Tissue samples were subjected to protein extraction, digestion, and liquid chromatography mass spectrometry (LC-MS) for proteomic analysis. Spectral counts were normalized and statistically analyzed in R. Pathway analysis was performed using Ingenuity Pathway Analysis (IPA). Within one week after inoculation, infected day 82 maternal caruncles had 3 increased proteins associated with a type I interferon (IFN) response. By day 89 infected caruncles had decreased proteins associated with nutrient exchange while infected fetal cotyledons exhibited an increase in type I and type II IFN responses as well as differential protein levels associated with nutrient exchange and angiogenesis. On day 97, infected caruncles once again had differential protein levels associated with nutrient exchange while infected cotyledons had a downregulation of proteins associated with cell survival/proliferation, immune signaling, and nutrient exchange. Both maternal and fetal tissues had an increase in inflammatory proteins on day 190 of gestation, paired with a decrease in general cell signaling (PI3K/AKT and EIF2). Finally, by day 245 of gestation,

only maternal caruncles exhibited a change in protein levels, with a decrease in mTOR signaling, actin cytoskeleton signaling, FAT10 signaling (IFNG induced), EIF2 signaling, and phagosome maturation. Overall, the data illustrates a cyclical pattern of IFN stimulation and inhibition, possibly as a protective mechanism of the placenta against inflammation or BVDV direct inhibition of antiviral responses. Additionally, a drastic dysregulation of nutrient exchange between maternal and fetal tissues, possibly a consequence of inflammation, could contribute to intrauterine growth restriction (IUGR) of the infected fetuses.

Introduction

Bovine viral diarrhea virus (BVDV) is an agriculturally significant disease, costing the cattle industry $1.5-2 billion annually [58, 59]. A single stranded RNA flavivirus in the Pestivirus genus, BVDV is classified as two types, BVDV1 and BVDV2, each type having both cytopathic and noncytopathic biotypes [5, 6, 8, 103, 140]. Interestingly, when BVDV infects pregnant females, the noncytopathic biotype of both BVDV 1 and BVDV2 have the ability to cross the placenta and infect the fetus, causing an array of fetal pathologies depending on the stage of gestation at which fetal infection occurs [96]. Fetal infection occurring prior to 30 days of gestation usually causes embryonic loss or fetal abortion [142]. Fetal infection occurring between days 42 and 125 of gestation causes a persistent infection (PI) in the fetus; due to the immaturity of the fetal immune system, the fetus becomes “immunotolerant” to the virus and will shed it throughout its postnatal lifetime [142]. If infection occurs after day 160 of gestation, the fetus becomes transiently infected and will clear the virus and seroconvert prior to parturition [96]. Animals PI with BVDV are

known as the primary reservoir of BVDV and can cause congenital malformations including cataracts, growth retardation, intrauterine growth restriction, cranial deformation, thymic hypoplasia, osteopetrosis, and many more [96]. However, congenital malformations are not always evident, making identification of PI animals difficult. Due to its prevalence, BVDV is heavily researched but many unknowns remain, including BVDV effects on placental growth and placental responses to infection during and after active infection.

The placental barrier is known to be protective of the fetus, inhibiting the transfer of pathogens while allowing proper exchange of nutrients from the dam to the fetus. Despite the protective role of the placenta, it is not perfect and can be affected by pathogens, maternal inflammation, maternal diet, and several other factors that affect fetal growth and development. The Developmental Origin of Adult Health and Disease is a concept introduced by Barker et. al., suggesting that maternal factors can affect fetal development and can have lifelong consequences on the progeny [219]. Pathogens are of particular interest, although the crossing of a pathogen from mother to fetus is relatively rare, it does occur in both humans and animals. BVDV maternal infection consequences on fetal development has mostly been studied in terms of in vitro cell culture or in vivo fetal development. In many cell culture models, BVDV has been shown to inhibit the production and effect of type I interferons (IFNs) [75, 111]. However, in the in vivo fetal models done by our group, BVDV has elicited robust activation of the fetal IFN response, in both PIs and TIs, early in fetal infection [84, 86, 89, 92, 109, 127, 144, 230]. But, by 115 days post maternal infection, PI fetuses exhibited decreased activity of both innate and adaptive branches of the immune response [89, 144]. This was hypothesized to be

due to regulatory T cell (Treg) inhibition of the fetal immune system as Treg cells began to identify BVDV as self [89, 144]. In addition to molecular immune system changes, pathological findings of PI fetuses included growth retardation and osteopetrosis, suggesting possible placental nutrient restriction and inflammation [91, 92, 98]. Despite the contradictions in in vitro and in vivo models, the effects of BVDV infection on the placenta and how those effects may contribute to pathological findings in BVDV fetuses is still not well understood.

Placental transfer of fetal waste or nutrients involves cargoes crossing several protective layers, making the transfer of pathogens from mother to fetus difficult. In ruminants, with a synepitheliochorial placenta, cargoes and pathogens must pass through 6 placental layers to get to the fetus [231]. In humans, with a hemochorial placenta, cargoes and pathogens must pass through only 3 tissue layers to reach the fetus [231]. The mechanisms of feto-maternal exchange can be passive (diffusion, osmosis, gradient/transport molecules/facilitated), active (requires energy), or vesicular (endocytosis/exocytosis) [232]. Of particular interest is clathrin mediated endocytosis (CME), which transfers cargoes across the placenta by invaginating transmembrane receptors and their bound ligands into clathrin coated pits [233]. Flaviviruses, such as West Nile virus, Zika virus, and dengue virus, are known to enter cells via CME [234, 235]. Additionally, BVDV viral entry has been found to be dependent upon CME following its binding to CD46 [236]. Although a promising explanation for the mechanism responsible for BVDV crossing the placenta, the study was done in vitro in bovine kidney cells (MDBK) [236]. The mechanisms of BVDV placental transfer and in vivo effects on the placenta are still not well known. It was hypothesized that maternal placental tissues,

caruncles, exhibited a quick inflammation/interferon response following infection while the fetal placental tissues (cotyledons) had a delayed but chronic inflammatory response to BVDV infection, affecting placental nutrient transfer and fetal growth. Through the use of liquid chromatography mass spectrometry (LC-MS), protein abundance and proteomics from infected and control animals were measured in both maternal caruncles and fetal cotyledons on days 82, 89, 97, 190, and 245 of gestation following maternal BVDV or sham inoculation on day 75 of gestation. Changes in proteins associated with nutrient exchange, inflammation, endocytosis, and stress were seen in both tissue types of infected animals throughout gestation, providing some insight into placental transfer of BVDV and effects of placental inflammation.

Methods

Animals, BVDV inoculation, and tissue collection

All animal work was approved by the Colorado State University (CSU) Institutional Animal Care and Use Committee and the CSU biosafety Committee (BSL1/2 approval 19-037B for BVDV). BVDV inoculation and fetal tissue collections are described in previous studies. A sample size of 3-4 was determined to be sufficient for a power of 1, as determined by Lenth's power calculator, therefore, a range of 3-7 animals were collected per collection day (specified below). Forty-four Hereford heifers (1 year of age) were purchased and confirmed BVDV naïve/seronegative by virus neutralization assays and ear-notch BVDV antigen capture ELISA. Heifers were bred by artificial insemination and confirmed pregnant by ultrasound. Pregnant heifers were randomly sorted into infection and control groups. Infection group heifers were intranasally inoculated with 2mL

ncp BVDV2 strain 96B2222 at 4.4 log_{10} $TCID_{50}$/mL on day 75 of gestation while control heifers were sham inoculated intranasally with media, also on day 75 of gestation. Infected and control groups were housed and fed separately, without contact, to avoid viral transmission. Control and infected heifers were confirmed as control or infected, respectively, by RT-qPCR and serum neutralization assays at multiple points during pregnancy. Control and infected (PI) fetuses were collected on days 82, 89, 97, 190, and 245. Caruncles (d82: Control n=4, PI=4; d89: Control n=4, PI=3; d97: Control n=4, PI n=4; d190: Control n=7, PI=6; d245 Control=4, PI=3) and cotyledons (d82: Control n=3, PI=4; d89: Control n=3, PI=3; d97: Control n=4, PI n=4; d190: Control n=7, PI=7; d245 Control=4, PI=3) were manually separated. Manual separation of caruncles and cotyledons may have some crossover of cells; therefore, tissues were confirmed mostly caruncle or cotyledon by measurement of alphafetoprotein (AFP) and chorionic somatomammotropin (CSH) protein abundance by LC-MS. Tissues that were unclear in either/both markers were not included in analysis, resulting in uneven sample numbers in some day groups.

Sample preparation for LC-MS

One-hundred mg of frozen placental tissue were aliquoted into 2mL tubes and submitted to the CSU Analytical Resources Core Bioanalysis and Omics for further preparation, digestion, and cleanup. The following methods were provided by the CSU Analytical Resources Core Bioanalysis and Omics: Samples were rinsed in 1mL of 1X PBS, then place in 1X sample volume 3.2mm stainless steel beads and 200µl of homogenization buffer (1X PBS and 1X HALT protease inhibitor cocktail (Thermo

Scientific Waltham, MA). Samples were homogenized in a Bullet Blender 5 Storm (Next Advance) at speed 12 for 5 minutes followed by incubation on ice, addition of 75ul homogenization buffer and a second homogenization at speed 12 for 3 minutes. Homogenates were then transferred to 1.5mL microcentrifuge tubes and SDS added to approximately 2% final concentration followed by cup horn sonication (amplitude 70, 10s pulse followed by 20s rest; 8 minutes total sonication). Lysates were then centrifuged at 10,000xg, 4ºC for 2 minutes. Supernatant aliquots were diluted 1:5 and 1:10 in 2M Urea, 2% SDS and subjected to a BCA Protein Assay (Pierce) following manufacturer's instructions. Absorbance at 550nm was measured on a BioRad 680 microplate reader and total protein abundance calculated based on a bovine serum albumin standard curve fit to a quadratic (Microplate Manager 5 software, BioRad). Samples were then processed using the EasyPep 96 MS Sample Prep Kit (ThermoFisher Scientific) following the manufacturer's instructions. Briefly, 50 μg total protein was aliquoted from each sample and raised to 100ul with lysis buffer. Reduction and alkylation solutions were sequentially added with gentle mixing followed by incubation at 50 ºC for 30 minutes. After cooling to room temperature, 10ug of a Trypsin/LysC mixture was added and samples were digested with shaking at 37 ºC for 4.5 hours. The enzymes were then deactivated with the Digestion Stop Solution and contaminants removed using mixed mode peptide clean up resin in 96well plate format. Peptide eluates were transferred to microcentrifuge tubes, fully dried in a vacuum evaporator and then resuspended in 5% acetonitrile/0.1% formic acid. Once resolubilized, absorbance at 205nm was measured on a NanoDrop (ThermoScientific) and total peptide abundance was subsequently calculated using an extinction coefficient of 31 [146].

Liquid chromatography mass spectrometry and proteomic analysis

The following methods were provided by the CSU proteomics core: Mass Spectrometry Analysis Reverse phase chromatography was performed using water with 0.1% formic acid (A) and acetonitrile with 0.1% formic acid (B). A total of 1µg of peptides were purified and concentrated using an on-line enrichment column (Waters Symmetry Trap C18 100Å, 5µm, 180 µm ID x 20mm column). Subsequent chromatographic separation was performed on a reverse phase nanospray column (Waters, Peptide BEH C18; 1.7µm, 75 µm ID x 150mm column, 45°C) using a 90 minute gradient: 5%-30% B over 85 minutes followed by 30%-45%B over 5 minutes at a flow rate of 350 nanoliters/min. Peptides were eluted directly into the mass spectrometer (Orbitrap Velos Pro, Thermo Scientific) equipped with a Nanospray Flex ion source (Thermo Scientific) and spectra were collected over a m/z range of 400–2000 under positive mode ionization. Ions with charge state +2 or +3 were accepted for MS/MS using a dynamic exclusion limit of 2 MS/MS spectra of a given m/z value for 30 s (exclusion duration of 90 s). The instrument was operated in FT mode for MS detection (resolution of 60,000) and ion trap mode for MS/MS detection with a normalized collision energy set to 35%. Compound lists of the resulting spectra were generated using Xcalibur 3.0 software (Thermo Scientific) with a S/N threshold of 1.5 and 1 scan/group.

Data Analysis

The following methods were provided by the CSU proteomics core: Tandem mass spectra were extracted, charge state deconvoluted and deisotoped by ProteoWizard

MsConvert (version 3.0). Spectra from all samples were searched using Mascot (Matrix Science, London, UK; version 2.6.0) against reverse concatenated Uniprot_Bovine_rev_030521 and cRAP_rev_100518 databases (UP000009136 downloaded 5 March 2021 and cRAP downloaded 5 October 2018; 75997 total entries) assuming the digestion enzyme trypsin. Mascot was searched with a fragment ion mass tolerance of 0.80 Da and a parent ion tolerance of 20 PPM. Carbamidomethylation of cysteine was specified in Mascot as a fixed modification. Oxidation of methionine was specified in Mascot as a variable modification.

Search results from all samples or tissue subsets were imported and combined using the probabilistic protein identification algorithms implemented in the Scaffold software (version 5.0.0, Proteome Software Inc., Portland, OR) [148, 149]. Peptide thresholds were set (0.1%FDR) such that a peptide FDR of 0.03-0.06% was achieved based on hits to the reverse database [150]. Protein identifications were accepted if they could be established at less than 1% FDR and contained at least 2 identified peptides. Protein probabilities were assigned by the Protein Prophet algorithm [151]. Proteins that contained similar peptides and could not be differentiated based on MS/MS analysis alone were grouped to satisfy the principles of parsimony.

Statistical and pathway analyses

Relative quantitation was determined using spectral counting (SpC) [7]. Normalized total spectral counts were exported from Scaffold (version 5.0.0, Proteome Software Inc., Portland, OR) and analyzed in R. Data were handled with packages dplyr, stringr, and tidyr [237-239]. Statistical analyses were performed using the DESeq2 R

package with a Benjamini-Hochberg multiple comparison correction [240]. Data were subset into tissues and days, DESeq2 comparisons were performed between infected and control groups within days. Additional comparisons include infected vs. control groups across all days (collection day was a factor), within tissues. Differences between tissues and between days were not studied at this time. Quality control graphs were generated with ggplot2 R package [238]. Results were subjected to pathway analysis by Ingenuity Pathway Analysis (Qiagen Hilden, Germany), with a p-value cutoff of $p<0.1$ and fold change cutoff of 1.5. Raw data files can be found at the NCBI Geo repository and R code can be found at https://github.com/hanahm1/placental_proteomics.git.

Results

Caruncle

Day 82 caruncle tissue had 4 differentially expressed proteins ($p < 0.1$) between infected animals and controls: interferon stimulated gene 15 (ISG15; 5.53 Log_2 Fold Change), DNA damage binding protein 1 (DDB1; -4.78 Log_2 Fold Change), Interferon Induced Transmembrane Protein 1 (IFITM1; 4.72 Log_2 Fold Change), and Isoform 2 of Interferon induced GTP binding protein MX1 (MX1; 3.95 Log_2 Fold Change). Three out of 4 of these proteins (ISG15, IFITM1, and MX1) are associated with an activation of the type I IFN response and inflammation, as identified by IPA.

Three proteins were differentially expressed in day 89 caruncle tissue, infected vs. controls: Gc-globulin (GC; -5.07 Log_2 Fold Change), heterogeneous nuclear ribonucleoprotein M (HNRNPM; -4.35 Log_2 Fold Change), and malate dehydrogenase

(MDH1; -5.14 Log_2 Fold Change). IPA identified MDH1 as associated with Aspartate degradation and the TCA cycle/Gluconeogenesis.

On day 97, 7 proteins were differentially expressed in infected vs. control caruncle tissue: glycine amidinotransferase mitochondrial (GATM; 5.49 Log_2 Fold Change), 60S ribosomal protein L21 (RPL21; 4.67 Log_2 Fold Change), major vault protein (MVP; 4.58 Log_2 Fold Change), aminopeptidase (NPEPPS; 4.61 Log_2 Fold Change), prothymosin alpha (PTMA; 4.36 Log_2 Fold Change), ras-related protein Rab-1B (RAB1B; 5.13 Log_2 Fold Change), and cytochrome P450 family 1 subfamily B member 1 (CYP1B1; 4.38 Log_2 Fold Change). IPA identified GATM as part of the Glycine Degradation pathway.

Day 190 caruncle tissue had 45 differentially expressed proteins ($p<0.1$) when infected tissues were compared to controls, which are summarized in appendix table 5. IPA identified 4 pathways associated with the significant proteins; tRNA charging (leucyl-tRNA synthetase (LARS1), glutamine-tRNA ligase (QARS1), threonine-tRNA ligase 1 (TARS1), tryptophan-tRNA ligase (WARS1)), methylglycoxal degradation III (dehydrogenase/reductase SDR family member 11 (DHRS11), prostaglandin reductase 2 (PTGR2)), EIF2 signaling (eukaryotic initiation factor 4A-1 (EIF4A1), eukaryotic initiation factor 4G-2 (EIF4G2), 60S ribosomal protein L11 (RPL11), WARS1), and IL15 production (non-specific protein tyrosine kinase (PTK2), signal transducer and activator of transcription (STAT1), twinfilin-1 (TWF1)).

Caruncle tissue collected on day 245 had a total of 142 differentially expressed proteins when infected tissues were compared to controls, summarized in appendix table 5. IPA identified several pathways associated with different protein abundance. Of particular interest are actin cytoskeleton signaling, FAT10 signaling, clathrin mediated

endocytosis, EIF2 signaling, and phagosome maturation. Significant proteins within these pathways are summarized in table 3.

Table 3: Significant pathways and proteins in infected caruncles vs. controls, as identified by IPA

Pathway	Protein	Log_2 Fold Change	P Value
Day 82			
Interferon Signaling	ISG15	5.53	< 0.0001
	IFITM1	4.72	0.05
	MX1	3.95	0.08
Day 89			
Aspartate Degradation II TCA Cycle II Gluconeogenesis	MDH1	-5.15	0.07
LXR/RXR Activation FXR/RXR Activation	GC	-5.07	0.05
Day 97			
Glycine Degradation	GATM	5.50	0.003
Day 190			
tRNA Charging	LARS1	-3.22	0.09
	QARS1	3.68	0.04
	TARS1	3.22	0.07
	WARS1	3.72	0.04
Methylglyoxal Degradation III	DHRS11	2.95	0.09
	PTGR2	-3.08	0.09
EIF2 Signaling	EIF4A1	-2.24	0.08
	EIF4G2	-3.52	0.05
	RPL11	-3.38	0.06
	WARS1	3.72	0.04
IL15 Production	PTK2	-3.46	0.06
	STAT1	4.03	0.03
	TWF1	3.17	0.08
Day 245			
Actin Cytoskeleton Signaling	ARPC1A	-4.19	0.04
	CYFIP1	-4.01	0.06
	FN1	-3.44	0.02
	IQGAP2	-3.787	0.09
	ITGA2	-2.61	0.09
	PTK2	-3.74	0.09
	RDX	-4.51	0.03
	GNG12	3.84	0.09
FAT10 Signaling	PSMD3	-4.92	0.01
	PSMC6	-4.31	0.02
	PSMD13	-4.23	0.06
	PSMD11	3.76	0.06
Clathrin Mediated Endocytosis Signaling	AP1B1	-4.52	0.03
	ARPC1A	-4.19	0.04
	MYO6	-4.05	0.07
	ALB	-3.92	0.008
	ARF6	-3.81	0.09
	AP3B1	-3.74	0.09
EIF2 Signaling	RPS17	-4.60	0.008
	EIF5B	-4.40	0.02
	EIF4G3	-4.08	0.06
	EIF1	-3.70	0.06
	WARS1	5.50	0.004

Phagosome Maturation	DYNC112	-3.79	0.09
	PRDX1	-2.93	0.06
	ATP6V1A	3.29	0.02
	CTSS	3.66	0.09

Cotyledon

Cotyledon tissues from day 82 of gestation did not have any significantly different proteins when PIs were compared to controls. On day 89, 39 proteins were significantly different between PIs and controls, summarized in appendix table 6. Of these significant proteins, those associated with the innate immune response and IFN signaling are of particular interest, including MX1 (4.90 Log_2 Fold Change) and ISG15 (4.50 Log_2 Fold Change). IPA identified the FAT10 signaling pathway (proteasome subunit alpha type 6 (PSMA6), proteasome subunit type 2 (PSMA2), glycolysis/gluconeogenesis (fructose bisphosphate aldolase (ALDOC)), ketolysis and ketogenesis (3 ketoacyl CoA thiolase (ACAA2), enoyl CoA hydratase (HADHA)), and glycogen degradation (alpha 1,4 glucan phosphorylase (PYGB)).

On day 97, 79 proteins exhibited significantly different abundances in infected vs. control cotyledons, summarized in appendix table 5. Pathways associated with these proteins, identified by IPA, include mTOR signaling, EIF2 signaling, FCγ receptor mediated phagocytosis in macrophages and monocytes, FAT10 signaling, protein ubiquitination, clathrin mediated endocytosis, IL8 signaling, leukocyte extravasation, ketolysis/ketogenesis, and many more. Proteins identified in these pathways can be found in table 4.

Thirty-three proteins had significantly different protein abundance in day 190 infected vs. control cotyledons, summarized in table 4. With these proteins, IPA identified

3 pathways of significance: PI3K and AKT signaling (ITGA3, PPP2R1A, SFN, YWHAH), HIPPO signaling/ P70S6K signaling (PPP2R1A, SFN, YWHAH), IFN signaling (IFITM1, ISG15), and calpain cell mechanics (ITGA3, CAPN1).

Table 4: Significant pathways and proteins in infected fetal cotyledons vs. controls, as identified by IPA.

Pathway	Protein	Log_2 Fold Change	P Value
Day 89			
Ketolysis Ketogenesis	ACAA2	4.35	0.05
	HADHA	4.86	0.01
FAT10 Signaling	PSMA6	4.28	0.07
	PSMD2	5.10	0.01
Interferon Signaling	ISG15	4.50	0.07
	MX1	4.90	0.05
Day 97			
mTOR Signaling	PPP2R1A	-4.30	0.03
	RAC1	-3.49	0.09
	RPS5	-4.13	0.05
	RPS7	-4.36	0.04
	RPS10	-5.10	< 0.001
	RPS26	-3.76	0.07
EIF2 Signaling	EIF5	-3.95	0.04
	RPL10A	-3.21	0.05
	RPS5	-4.13	0.05
	RPS7	-4.36	0.04
	RPS10	-5.10	< 0.001
	RPS26	-3.76	0.07
FCG Receptor Mediated Phagocytosis in Macrophages and Monocytes	ARPC3	-4.41	0.02
	RAB11B	-4.14	< 0.001
	RAC1	-3.49	0.09
	VASP	-4.19	0.05
FAT10 Signaling	PSMB5	-4.07	0.05
	PSMC2	-4.00	0.06
	PSMC3	-3.86	0.06
Clathrin Mediated Endocytosis Signaling	AP2M1	-3.64	0.06
	ARPC3	-4.41	0.02
	RAB11B	-4.14	< 0.001
	RAC1	-3.49	0.09
IL8 Signaling Leukocyte Extravasation	GNAI3	-4.93	0.02
	PAK2	-3.49	0.09
	RAC1	-3.49	0.09
	VASP	-4.19	0.05
Day 190			
PI3K/AKT Signaling HIPPO Signaling	ITGA3	-3.41	0.04
	PPP2R1A	-3.70	0.02
	SFN	-2.76	0.03
	YWHAH	-2.61	0.02
Interferon Signaling	IFITM1	3.67	0.04
	ISG15	3.61	0.05

No proteins were found to be significantly different in day 245 cotyledons when infected tissues were compared to controls.

Discussion

The ability to perform big data analyses have transformed scientific understanding of biology and biological processes. The data set discussed sheds light on the effects of BVDV transplacental transmission during gestation; however, limitations of this dataset should be acknowledged. Ideally, proteomic data should be followed by validation of proteins of interest by other protein quantification methods such as western blot or immunohistochemistry. Due to very small quantities of available tissue and the limitation of antibodies reactive to bovine proteins, validation was not possible. Additionally, proteins are not perfect molecules to measure, with regulatory factors such as miRNAs, or modifications affecting their biological activity, unable to be detected by LC-MS. Finally, the timepoints chosen may not be reflective of all of the expression patterns happening throughout gestation. With these limitations in mind, we have interpreted the data as follows.

Placental inflammation and hindered nutrient transport in early infection sets the stage for IUGR

BVDV vertical transmission has remained a mystery despite several in vivo studies. Maternal BVDV viremia occurs approximately 7 days post inoculation, while fetal BVDV viremia occurs between days 10 and 14 post maternal infection, indicating a 3-7 days delay for vertical transmission [84, 241]. The presented data show an increase in IFN signaling in the day 82 (7 days post maternal inoculation) infected maternal caruncles but not in the cotyledons, which is expected considering the 3-7 days delay between

maternal and fetal viremia. The proteins associated with IFN signaling (IFITM1, ISG15, and MX1) in the caruncles suggest an innate immune response against BVDV, potentially causing placental inflammation in attempt to inhibit BVDV replication and transmission to the fetus. Despite an attempt at a protective role, this placental inflammatory response to BVDV may have detrimental effects on placental function. For example, IFITM1, upregulated in day 82 infected caruncles, is known to inhibit syncytiotrophoblast formation, fusion, and function in human cell culture, contributing to placental abnormalities. Although this was observed in humans, ruminant placental structure contains binucleate cells that form syncytial plaques, functionally similar to the human syncytiotrophoblasts, which have been shown to be infected by BVDV in an in vivo sheep model [82, 242]. The bovine placenta is established between days 40 and 50 of gestation [243]. During placental establishment, binucleate cells migrate and bind to the uterine epithelium, forming a syncytial plaques, which are replaced by uterine epithelial cells on day 40, forming a minisyncytia at the placentomic region [243]. The increase in maternal/caruncular IFITM1 so early in gestation may elude to dysfunction at the minisyncytia in the placentomes [243]. In addition to IFITM1, ISG15 and MX1 protein abundances were also increased in day 82 infected caruncles. All three proteins are induced by IFNs and indicative of a type I IFN response. Although they can be protective against pathogens at the placenta, overexpression can cause many pathologies including inhibition of placental development (associated with ZIKV), microcephaly, and many other pregnancy complications associated with inflammation [244].

Placental inflammation has been associated with not only infectious agents but with maternal obesity, adverse pregnancy outcomes, and preeclampsia as well [244].

Placental inflammation and IFN signaling, whether in response to a pathogen or another environmental factor, has been known to cause placental insufficiency, placental vascular changes, and intrauterine growth restriction (IUGR) [244]. Although only 3 protein abundances were different in day 89 caruncles, all 3 proteins are associated with nutrient exchange. MDH1, needed for shuttling NADH into mitochondria, GC, which regulates placental function, fetal nutrient deliver, vascularization, and inflammation, and finally, HNRNPM, which has a role in glucose consumption, were all decreased in infected day 89 caruncles [245-248]. Together, this suggests severely hindered nutrient transport to the fetus, possibly due to the IFN response seen in day 82 tissues.

In contrast, the infected cotyledonary tissue at this time point, day 89, exhibited both a type I and type II IFN response, indicated by an increase in MX1, ISG15, PSMA6, and PSMA2. The induction of the innate immune response suggests that BVDV was successfully transmitted to the fetal membranes, which corroborates previous findings that fetal infection occurs 3-7 days post maternal viremia [84, 241]. CME pathway was also found to be increased, with 3 proteins being increased (ARPC3, CLTA, and RAC1) while 3 other proteins were decreased (APOA2, ORM1, TF). With the ability of BVDV and other flaviviruses possessing the ability to gain cellular entry via CME, this change in the CME pathway may be indicative of viral entry [236]. Metabolite associated proteins ALDOC, ACAA2, HADHA, and PYGB were all increased in infected caruncles. Although these proteins are not well studied in the placenta, they are indicative of nutrient exchange perturbations. However, the exact effects are not known and cannot be speculated at this time. Interestingly, there was also increased abundance of vasodilator stimulated phosphoprotein (VASP) in infected cotyledons at this timepoint. VASP has been identified

as a regulator of endothelial cell migration and is hypothesized to be stimulated by vascular endothelial growth factor (VEGF) and IL8 during placental vascularization and angiogenesis [249]. Although VASP protein is not a well-researched protein in placental stress models, it may be speculated that its expression would parallel the expression of VEGF. The decreased proteins in the maternal caruncles, suggesting decreased nutrient exchange, may cause the increase in VASP, as is seen in undernourished pregnant sheep with an increase in VEGF [250]. Following infection and inflammation in the caruncle, the ability to deliver nutrients to the fetus may be compromised, thus causing altered metabolite proteins and increase of VASP in the fetal cotyledon in attempt to overcome nutrient deficiency. However, at this point, BVDV has infected the fetal membrane causing an IFN response and inflammation, causing further stress and injury to the fetal cotyledons, which may also be contributing to the dysregulation of metabolite proteins.

Placental cellular stress responses inhibited; fetal protective mechanism, direct inhibition by BVDV, or viral immunotolerance?

By day 97 of gestation, maternal caruncles exhibited minimal differences in protein expressions between infected and noninfected groups. However, GATM was significantly higher in the infected caruncles. GATM, a rate limiting enzyme in creatine production, is a known imprinted placental gene often associated with placental dysfunction [251]. Despite this knowledge, GATM is still not well understood, with its differential expression, both over and under expression, being associated with IUGR [251-253].

Interestingly, day 97 infected fetal cotyledons exhibited a downregulation in several proteins and pathways associated with fetal growth. The mTOR signaling pathway is a

nutrient sensing placenta growth pathway, with signaling changes in response to maternal/fetal environment [254]. In infected fetal cotyledons, the mTOR pathway was downregulated (decrease in PPP2R1A, RAC1, RPS5, RPS7, RPS10, and RPS26), affecting the EIF2 signaling pathway. A decrease in mTOR signaling of the placenta is often seen with maternal malaria infection, contributing to impaired fetal growth and chronic disease [255]. Additionally, ZIKV non-structural proteins directly inhibit the AKT/mTOR pathway to allow for increased viral replication [256]. With similarities between ZIKV and BVDV transplacental transmission and in non-structural proteins, it is possible that BVDV non-structural proteins may have a similar direct inhibition of the mTOR pathway, or the inhibition seen in this data set is a stress response to inflammation. Either way, this inhibition affects several downstream pathways, one of which being EIF2 signaling, also downregulated in day 97 (EIF5, RPL10A, RPS5, RPS7, RPS10, and RPS26) infected cotyledons as well as days 190 (decreased EIF4A1, EIF4G2, PRL11; increased WARS1) and 245 caruncles (decreased EIF4B, EIF4G3, HMOX1, and RPS17). EIF2 signaling regulates protein translation in response to cellular stress [257, 258]. EIF2 was downregulated in placental tissues from ZIKV patients infected in the first trimester of pregnancy [257]. Additionally, a decrease in both mTOR and EIF2 signaling is associated with IUGR, due to reduced protein synthesis and cell proliferation in response to stress [259].

In addition to decreased mTOR and EIF2 signaling, the clathrin mediated endocytosis (CME) was also significantly deceased in day 97 infected cotyledons (decreased AP2M1, ARPC3, RAB11B, and RAC1) and day 245 infected caruncles (decreased ALB, AP1B1, AP3B1, ARF6, ARPC1A, and MYO6). As discussed earlier,

CME was identified as a potential site of cellular entry for BVDV [236]. CME is also known to function in uptake of maternal macrophage exosomes for placental transport and promotes the production of pro-inflammatory cytokines from placental tissues [260]. Inhibition of CME in response to viral infection is not well understood; however, it is possible that CME is inhibited as a protective mechanism of the placenta, protecting itself from BVDV vertical transmission or from stimulation of the inflammatory response. In fact, several of the proteins identified in the CME pathways are also shared with the viral entry via endocytosis (day 97 cotyledons: AP2M1, RAC1; day 245 caruncles: AP1B1, AP3B1, ITGA2) suggesting that the decrease in CME may also be inhibiting viral entry. Although CME placental inhibition effects on fetal growth has not been studied to our knowledge, this downregulation of CME is expected to limit maternal-fetal nutrient exchange through limitations of albumin, thyroid hormones, iron, and vitamin B2 across the placenta, affecting fetal growth [235].

In the day 190 infected fetal cotyledons, IPA identified 2 signaling pathways that were decreased. PI3K/AKT signaling (decreased ITGA3, PPP2R1A, SFN, and YWHAH) as well as HIPPO signaling (decreased PPP2R1A, SFN, and YWHAH) have overlapping genes and affect one another. The decrease in these pathways indicated a potential decrease in protein translation, contributing to the fetal IUGR and placental insufficiency [259].

Similar to day 97 cotyledons, day 245 caruncles exhibited an inhibition of the mTOR pathway and EIF2 signaling. Additionally, mTOR and EIF2 pathways contribute to the actin cytoskeleton signaling pathway, which had several decreased proteins in infected tissues compared to controls (decreased ARPC1A, CYF1P1, FN1, IQGAP2,

ITGA2, PTK2, and RDX; increased GNG12) [261]. GNG12 protein in the placenta is not well known nor its role in response to viral infection/nutrient restriction. Therefore, the reason for or effects of its increase cannot be speculated at this time. Disruption of the actin cytoskeleton signaling pathway has been associated with preeclampsia and life threatening hemolysis, elevated liver enzymes, and low platelet count (HELLP) syndrome in humans, reacting to placental stress including the release of anti-angiogenic factors, maternal endothelial cell dysfunction, and systemic inflammation [262].

Placental IFN and inflammatory response to BVDV is cyclical

The immune system reactions to placental infection exhibited an up and down pattern, with an increase occurring at one time frame, decreasing at another, then followed with another increase then decrease. Interestingly, this type of pattern was not seen in non-placental fetal or maternal tissues, seeming to be unique to the placenta [84, 89, 92, 127, 144].

In contrast to the expected increases in IFN signaling during BVDV transmission at day 82 for maternal and day 89 for fetal placental tissues, day 97 infected fetal cotyledons and day 245 maternal caruncles exhibited several downregulated immune pathways. These pathways include FCG receptor mediated phagocytosis in macrophages and monocytes, FAT10 signaling, IL8 signaling, and leukocyte extravasation. The downregulation of these pathways suggests inhibition of phagosome formation, immunoproteosome formation, inflammation, and leukocyte migration. This type of immune dysregulation may indicate a stress response of the placental cells to the virus, direct inhibition of inflammation by BVDV as suggested by in vitro studies, or a

mechanism of the placenta to limit fetal injury caused by inflammation. FCG receptor mediated phagocytosis is normally controlled by IFNG expression. When activated, the FCG receptor mediated phagocytosis works to stimulate phagocytosis of microbes and can lead to inflammatory tissue damage if not regulated properly [263]. Despite not being well understood in the placenta, it is possible that placental phagosome formation is altered due to the decrease in proteins associated with this pathway (day 97 cotyledons decreased ARPC3, RAB11B, RAC1, and VASP; day 245 caruncle decreased ARF6, ARPC1A, and HMOX1). Interestingly, day 245 maternal infected caruncles also had a decrease in proteins associated with phagosome maturation and antigen presentation (ATP6V1A, CTSS, CYNC112, and PRDX1), further supporting a hindered phagosome formation in these particular placental tissues.

FAT10 signaling, which was increased in day 89 infected cotyledons (increased PSMA6 and PSMA2), decreased in day 97 infected cotyledons (decreased PSMB5, PSMC2, and PSMC3), and decreased in day 245 infected caruncles (decreased PSMC6, PSMD3, PSMD11, and PSMD13), is associated with major histocompatibility complexes (MHC) for antigen presentation [264]. The FAT10 pathway is induced by IFNG to stimulate the adaptive immune response; however, it does inhibit type I IFNs in order to regulate inflammatory responses [264, 265]. The increase in FAT10 signaling proteins in day 89 cotyledons may be an indication of communication between the innate and adaptive immune responses as well as an inhibitor of type I IFNs. This inhibition of type I IFNs by FAT10 proteins could be a factor contributing to the cyclical nature of IFN responses in the placenta: when FAT10 signaling is increased, type I IFNs are inhibited,

but once FAT10 signaling goes down, type I IFNs are increased again. However, it is important to note that this type of pattern has not been reported in the literature.

IL8 and leukocyte extravasation signaling pathways were both decreased in day 97 infected cotyledons with the associated proteins being shared between the two pathways. Together, these proteins may be indicative of hindered cell migration and angiogenesis in the placenta [266, 267].

Aminoacyl-tRNA synthetases (ARS) are mostly known for their function in protein synthesis, catalyzing aminoacylation of transfer RNAs (tRNA) [268]. However, ARSs can also influence immune responses, immune cell migration, type I IFNs, and inflammation [268]. In day 190 infected caruncles, tRNA charging was an identified significantly altered pathway, including an increase in QARS1, TARS1, and WARS1 proteins and a decrease in LARS1 protein. Interestingly, WARS1 continued to be significantly increased in day 245 infected caruncles. WARS1 is stimulated by IFNG, causing activation of the p53 pathway and antiproliferative responses to cellular stress. Additionally, the increase in WARS1 and IFNG induces tryptophan metabolic reprogramming, in which tryptophan is depleted and contributes to negative regulation of effector T cells and hyperactivity of Treg cells [269]. In contrast, LARS1 is an intracellular leucine sensor, activating the mTOR and PI3K pathways, in the presence of leucine, for cell growth. During glucose deprivation, leucine binding sites on LARS1 are phosphorylated, inhibiting LARS1 activation of mTOR and PI3K, inducing a stress response to low energy. The decrease in LARS1 protein may be in response to limited availability of nutrients at the placenta, further exacerbating IUGR of the fetus. QARS1 has antiapoptotic function when in the presence of glutamine and dysregulated QARS1 has been associated with neural defects

[269, 270]. However, its role in the immune system or placenta is unknown. Finally, TARS has both angiogenic and immune activity, being produced in response to tumor necrosis factor alpha (TNFA) and affecting the expression of VEGF [271]. Interestingly, WARS1 is known to be antiangiogenic while TARS is proangiogenic but the direct implications of these two proteins being differentially increased together is not known [271]. Although differential tRNA charging has not been heavily studied in the placenta, it is expected that protein synthesis is altered with other possible effects such as altered cell proliferation, hindered T cell responses, and contribution to IUGR.

Increased IL15 expression has been associated with gestational diabetes mellitus and inflammation in the placenta. In day 190 infected caruncles, proteins associated with IL15 signaling were differentially expressed, with STAT1 and TWF1 being increased and PTK2 being decreased. IL15 itself was not identified in the dataset, however it's signaling pathway, including STAT1 and TWF1, is associated with placental inflammation and dysregulated trophoblast invasion [272]. Additionally PTK2 (also known as focal adhesion kinase) is a positively regulator of trophoblast proliferation, with its decrease being associated with reduced cell proliferation [273]. The type of alterations in an inflammatory pathway suggests not only the presence of inflammation in the day 190 infected caruncles, but also in placental cell proliferation.

Conclusions

Vertical transmission of viruses from mother to fetus continues to cause drastic losses in both humans and animals. To our knowledge, in vivo placental tissues collected over several time points during viral infection has not been previously studied. The above

discussed data is summarized in figure 1. An IFN response of tissues during the viral transmission was expected. However, the cyclical nature of the IFN response and inflammation was not and has not been described in the literature. The initial anti-viral response to BVDV transmission was unsuccessful in preventing fetal infection and instead, caused a series of protein perturbations affecting nutrient exchange between mother and fetus, cell survival/proliferation, angiogenesis, and ultimately, IUGR of the fetus. Growth restriction of PI animals have been previously reported [92]. Even more interesting is the persistence of inflammation in the maternal caruncles despite clearance of the virus and seroconversion. The maternal caruncles may be reacting to the persistent infection of the fetus and inflammation of the fetal cotyledons. The parallels seen with this data and human pathologies such as IUGR, ZIKV infection, gestational diabetes, and preeclampsia suggest that this work may not only give insight into BVDV vertical transmission but give insight into placental inflammation in response to general stress as well.

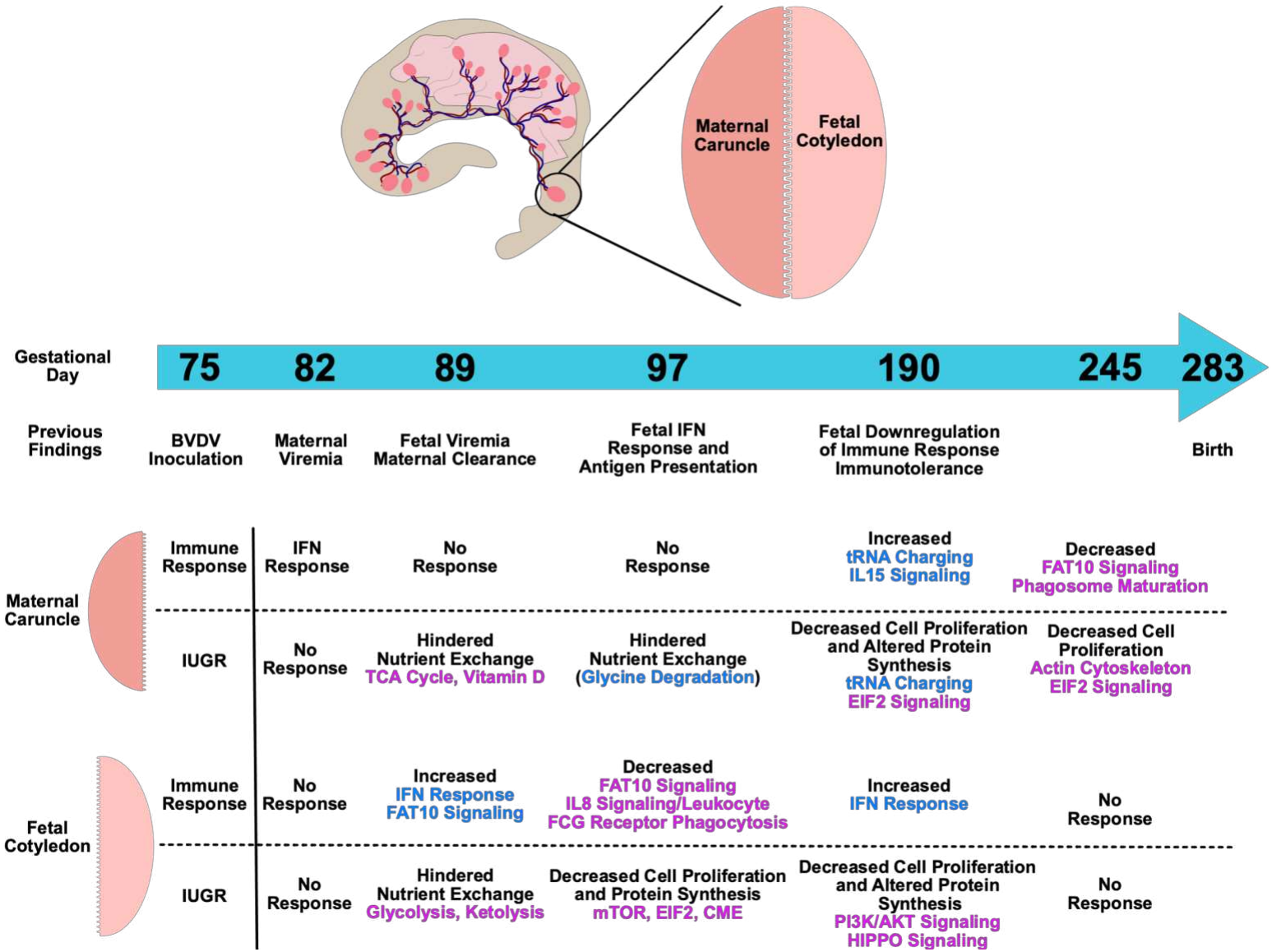

Figure 12: graphical representation of bovine placental tissues and summary of proteomic findings in infected placental tissues vs. controls. Pink text: IPA predicted decreased pathways in PIs. Blue text: IPA predicted increased pathways in PIs. Sources for previous findings include Smirnova 2012 [84], Georges 2020, and Knapek 2020 [89].

Chapter 5: Conclusions

Placental and fetal responses to the vertical transmission of any virus, in livestock or in humans, is still a mystery, with the molecular responses and effects on development over time being difficult to measure in vivo. The studies herein give unique insight into the consequences of viral transplacental infection, from both placental tissues and fetal splenic tissue.

Placental inflammation, with or without vertical transmission of a pathogen, can cause subsequent inflammation in the fetus, negatively affecting fetal growth and development. In humans, placental inflammation is an important cause of preterm birth with intrauterine infection being identified in 70% of preterm deliveries between 20 and 24 weeks and in 16% of preterm deliveries at 34 weeks [274, 275]. Several animal studies have shown that intrauterine infection/inflammation with bacteria or LPS can induce inflammatory responses in the chorioamnion, in the fetus, and alterations in fetal organ development [274]. The placental study discussed in chapter 4 revealed a robust inflammatory response in both the maternal and fetal tissues. Despite the IFN response being cyclical in both maternal and fetal placental tissues, an interesting observation was that inflammation was present in maternal caruncles following maternal clearance of BVDV, possibly in response to inflammation present in fetal tissues. The presence of placental inflammation at multiple time points following maternal inoculation of BVDV could be contributing to the fetal immune response. It is unclear if the fetal IFN/immune response seen in the spleen, thymus, or liver is in response to the virus itself, or responding to placental inflammation and maternal cytokines. As discussed in Chapter 1,

the in vitro studies of BVDV conclude that BVDV is able to inhibit/evade the IFN response but does not inhibit the IFN response to any other pathogens/signaling [75-77, 79, 85, 111]. The strong IFN response seen in day 97 PI fetuses could be stimulated by placental infection, by direct BVDV infection of the fetus, or a combination of the two. It is well established that this type of placental inflammation contributes to placental insufficiency and IUGR, seen in both the placental data discussed in chapter 4, in previous studies describing the pathologies of these fetuses and in the general literature [92, 244]. Although the placental proteomics data was highly informative, one large question remains unanswered: are the PI fetal pathologies due to general placental inflammation, direct response to BVDV infection, or both?

In earlier publications, an upregulation of the innate/IFN immune response in day 97 fetuses was suggested to be direct response to the virus [84, 86, 89, 91, 92, 110, 127]. However, with the placental data presented in chapter 3, the reason for an IFN response becomes a little more complicated. Several studies on placental inflammation in humans have concluded that placental inflammation, with or without vertical transmission of pathogens, can affect splenic and immune development. In cases of neonatal sepsis and chorioamnionitis, depletion of leukocytes in the fetal spleen is observed [276]. In a sheep study, intraamniotic LPS exposure caused a sustained immune response in the fetal spleen, including an increase in Treg cells [277]. In a recent mouse model, maternal infection with influenza A virus, without vertical transmission, caused some placental inflammation, fetal growth restriction, and hindered immune development in the fetal thymus [278]. Therefore, the innate immune response seen in day 97 fetal spleens may

be not only induced by the virus itself but could also be a direct result of placental inflammation.

The spleen is a critical secondary lymphoid organ, the white pulp surveying the blood for pathogens and being one of the first organs to mount an immune response against pathogens (reviewed in [279]). The white pulp of the spleen houses many mature immune cells and some naïve cells, ready to mount an immediate immune response (reviewed in [279]). The spleen was chosen as a target organ in the BVDV studies due to its important immune function, revealing potential hinderances in PI fetal immune development. Generally, it was found that the fetal immune response was inactive on day 82 of gestation, which is to be expected as the virus has not yet crossed the placenta. On day 97 of gestation, PI fetal spleens exhibited an IFN immune response as determined by microarray and RT-qPCR. Genes associated with antigen presentation were also upregulated at this time in PI fetal spleens compared to controls. Interestingly, lymphocytes remained unstimulated at this time point. By day 190, most of the target genes, including lymphocyte markers, measured by RT-qPCR were significantly downregulated, indicating an inhibition of sort. In order to understand the inhibition of the immune response later in gestation, methylation sequencing and proteomics were performed on day 245 spleens. Several genes and pathways were differentially methylated in PI fetal spleens compared to controls, most notably, pathways associated with bone, brain, and heart development, as well as immune cell migration. Proteomics at this time point did not reveal a substantial degree of significant differences, suggesting

that the methylation patterns may affect expression prior to day 245 of gestation or postnatally.

The methylation data from day 245 fetal spleens (chapter 3) were compared to the day 97 microarray data (chapter 2). Interestingly, an inverse relationship was found, where some genes identified as differentially expressed in the microarray, were methylated opposite of what one would think to reflect the expression seen in the microarray (ex: day 97 upregulation was hypermethylated by day 245, more detail can be found in chapter 3 discussion). Although surprising when comparing day 97 data RT-qPCR data to the day 245 methylation data, the day 245 methylation data likely more accurately represent the changes seen in the day 190 RT-qPCR data. The inhibition of the immune responses seen on day 190 (RT-qPCR, chapter 2) may be due to changes in methylation patterns, instigated by Treg cells identifying BVDV as self, as a response to the general IFN response, or as a protective mechanism of the PI fetus. Although the markers measured in the day 190 RT-qPCR data were not reflected in the methylation data, the methylation may have affected their expression through differential methylation of upstream regulators. Alternatively, the inhibition of the markers/general immune inhibition in PI fetal spleen may be a direct cause of the methylation seen in day 245 PI fetal spleens. Unfortunately, neither one of these hypotheses can be corroborated at this time but leaves opportunity for future studies.

The spleen and placental data presented provides valuable insight into pathologies seen with vertical transmission of pathogens. Specific to BVDV, we now have insight into the documented PI pathologies such as osteopetrosis, extramedullary splenic hematopoiesis, brain and heart malformations, neurological defects, and growth

retardation [90-92, 95-100]. With the presented data, the following is postulated: The placental inflammation discussed in chapter 4 contributes to placental insufficiency and IUGR of the PI fetus. Placental inflammation, along with BVDV itself, contributes to the initial IFN response in PI fetuses at day 97 of gestation. Type I IFNs are direct inhibitors of osteoclasts, affecting bone development and homeostasis, thus causing osteopetrosis like pathology and a shift to extramedullary splenic hematopoiesis. Extramedullary splenic hematopoiesis causes drastic changes in the immune system and migrating cells, where hematopoietic stem cells originate from the spleen and mobilize to other tissues, potentially contributing to the heart and brain malformations (in addition to effect of direct virus infection of those tissues). By day 190, the immune system is downregulated in PI fetal spleens, potentially by Treg cells, and along with changes in the above pathways, cause differential methylation of genes, as observed in day 245 PI fetal spleens. It is important to note that the timeline of inhibition and methylation is not known, methylation may have occurred prior to or after day 190.

BVDV continues to be an agriculturally relevant disease, costing the industry billions of dollars annually. Although this work is important to gain an understanding of BVDV, it has also shown parallels with human disease. In the last 30-40 years, the concept of maternal environment affect/contributing to fetal programming and health has developed into the Developmental Origin of Adult Health and Disease concept [219]. Factors such as maternal nutrition, body mass index, mental health, infections, and inflammation can affect fetal development [219]. This unique BVDV model offers a timeline of fetal development when challenged with maternal and fetal infection/inflammation, offering insight into consequences of viral infections on fetal

development. Viruses capable of vertical transmission in humans include Rubella virus, Parvovirus B19, Varicella Zoster virus, CMV, Zika virus, and Hepatitis E (reviewed in [280]). Fetal pathologies associated with vertical transmission of these viruses include cataracts, congenital heart disease, IUGR, hepatosplenomegaly, neurologic deficiencies, cognitive dysfunction, microcephaly, and more, all similar to pathologies observed in BVDV PI fetuses/animals (reviewed in [280]). The data presented gives not only specific molecular mechanisms behind BVDV PI but may also give insight into molecular consequences of general placental inflammation and maternal viral infections on fetal development.

Bibliography

1. Olafson P, MacCallum AD, Fox FH. An apparently new transmissible disease of cattle. The Cornell veterinarian 1946; 36:205-213.
2. Ridpath JF. Bovine Viral Diarrhea Virus: Global Status. Veterinary Clinics of North America: Food Animal Practice 2010; 26:105-121.
3. Childs T. X disease of Cattle—Saskatchewan. Canadian journal of comparative medicine and veterinary science 1946; 10:316.
4. Goens D. The evolution of bovine viral diarrhea: a review. The Canadian Veterinary Journal 2002; 43:946-954.
5. Underdahl N, Grace O, Hoerlein A. Cultivation in tissue-culture of cytopathogenic agent from bovine mucosal disease. Proceedings of the Society for Experimental Biology and Medicine 1957; 94:795-797.
6. Kalaycioglu AT. Bovine viral diarrhoea virus (BVDV) diversity and vaccination. A review. Veterinary Quarterly 2007; 29:60-67.
7. Simmonds P, Becher P, Bukh J, Gould EA, Meyers G, Monath T, Muerhoff S, Pletnev A, Rico-Hesse R, Smith DB, Stapleton JT, Ictv Report C. ICTV Virus Taxonomy Profile: Flaviviridae. The Journal of general virology 2017; 98:2-3.
8. Ridpath J, Bolin S, Dubovi E. Segregation of bovine viral diarrhea virus into genotypes. Virology 1994; 205:66-74.
9. Mosena ACS, Falkenberg SM, Ma H, Casas E, Dassanayake RP, Walz PH, Canal CW, Neill JD. Multivariate analysis as a method to evaluate antigenic relationships between BVDV vaccine and field strains. Vaccine 2020; 38:5764-5772.
10. Poole TL, Wang C, Popp RA, Potgieter LND, Siddiqui A, Collett MS. Pestivirus translation initiation occurs by internal ribosome entry. Virology 1995; 206:750-754.
11. Smith DB, Meyers G, Bukh J, Gould EA, Monath T, Scott Muerhoff A, Pletnev A, Rico-Hesse R, Stapleton JT, Simmonds P, Becher P. Proposed revision to the taxonomy of the genus Pestivirus, family Flaviviridae. The Journal of general virology 2017; 98:2106-2112.
12. Ridpath JF. BVDV genotypes and biotypes: practical implications for diagnosis and control. Biologicals: journal of the International Association of Biological Standardization 2003; 31:127-131.
13. Yeşilbağ K, Alpay G, Becher P. Variability and Global Distribution of Subgenotypes of Bovine Viral Diarrhea Virus. Viruses 2017; 9:128.
14. Workman AM, Heaton MP, Harhay GP, Smith TP, Grotelueschen DM, Sjeklocha D, Brodersen B, Petersen JL, Chitko-McKown CG. Resolving Bovine viral diarrhea virus subtypes from persistently infected US beef calves with complete genome sequence. Journal of Veterinary Diagnostic Investigation 2016; 28:519-528.
15. Fulton RW, Whitley EM, Johnson BJ, Ridpath JF, Kapil S, Burge LJ, Cook BJ, Confer AW. Prevalence of bovine viral diarrhea virus (BVDV) in persistently

infected cattle and BVDV subtypes in affected cattle in beef herds in south central United States. Canadian Journal of Veterinary Research 2009; 73:283.
16. Giangaspero M, Harasawa R, Weber L, Belloli A. Taxonomic and epidemiological aspects of the bovine viral diarrhoea virus 2 species through the observation of the secondary structures in the 5'genomic untranslated region. Vet Ital 2008; 44:319-345.
17. Donis RO. Molecular Biology of Bovine Viral Diarrhea Virus and its Interactions with the Host. Veterinary Clinics of North America: Food Animal Practice 1995; 11:393-423.
18. Kupfermann H, Thiel HJ, Dubovi EJ, Meyers G. Bovine viral diarrhea virus: characterization of a cytopathogenic defective interfering particle with two internal deletions. Journal of Virology 1996; 70:8175.
19. Fritzemeier J, Haas L, Liebler E, Moennig V, Greiser-Wilke I. The development of early vs. late onset mucosal disease is a consequence of two different pathogenic mechanisms. Archives of virology 1997; 142:1335-1350.
20. Tautz N, Thiel H-J. Cytopathogenicity of pestiviruses: cleavage of bovine viral diarrhea virus NS2-3 has to occur at a defined position to allow viral replication. Archives of virology 2003; 148:1405-1412.
21. Riedel C, Chen H-W, Reichart U, Lamp B, Laketa V, Rümenapf T. Real Time Analysis of Bovine Viral Diarrhea Virus (BVDV) Infection and Its Dependence on Bovine CD46. Viruses 2020; 12:116.
22. Maurer K, Krey T, Moennig V, Thiel H-J, Rümenapf T. CD46 Is a Cellular Receptor for Bovine Viral Diarrhea Virus. Journal of Virology 2004; 78:1792.
23. Krey T, Himmelreich A, Heimann M, Menge C, Thiel H-J, Maurer K, Rümenapf T. Function of Bovine CD46 as a Cellular Receptor for Bovine Viral Diarrhea Virus Is Determined by Complement Control Protein 1. Journal of Virology 2006; 80:3912.
24. Szillat KP, Koethe S, Wernike K, Höper D, Beer M. A CRISPR/Cas9 Generated Bovine CD46-knockout Cell Line—A Tool to Elucidate the Adaptability of Bovine Viral Diarrhea Viruses (BVDV). Viruses 2020; 12:859.
25. Merwaiss F, Czibener C, Alvarez DE. Cell-to-Cell Transmission Is the Main Mechanism Supporting Bovine Viral Diarrhea Virus Spread in Cell Culture. Journal of Virology 2019; 93:e01776-01718.
26. Lackner T, Müller A, Pankraz A, Becher P, Thiel H-J, Gorbalenya A, Tautz N. Temporal modulation of an autoprotease is crucial for replication and pathogenicity of an RNA virus. Journal of virology 2004; 78:10765-10775.
27. Lackner T, Müller A, König M, Thiel H-J, Tautz N. Persistence of bovine viral diarrhea virus is determined by a cellular cofactor of a viral autoprotease. Journal of virology 2005; 79:9746-9755.
28. Lattwein E, Klemens O, Schwindt S, Becher P, Tautz N. Pestivirus virion morphogenesis in the absence of uncleaved nonstructural protein 2-3. Journal of virology 2012; 86:427-437.
29. Agapov EV, Murray CL, Frolov I, Qu L, Myers TM, Rice CM. Uncleaved NS2-3 Is Required for Production of Infectious Bovine Viral Diarrhea Virus. Journal of Virology 2004; 78:2414-2425.

30. Brownlie J, Clarke M, Howard C. Experimental infection of cattle in early pregnancy with a cytopathic strain of bovine virus diarrhoea virus. Research in veterinary science 1989; 46:307-311.
31. Tautz N, Kaiser A, Thiel H-J. NS3 Serine Protease of Bovine Viral Diarrhea Virus: Characterization of Active Site Residues, NS4A Cofactor Domain, and Protease–Cofactor Interactions. Virology 2000; 273:351-363.
32. Liang D, Chen L, Ansari IH, Gil LHVG, Topliff CL, Kelling CL, Donis RO. A replicon trans-packaging system reveals the requirement of nonstructural proteins for the assembly of bovine viral diarrhea virus (BVDV) virion. Virology 2009; 387:331-340.
33. Mohamed YM, Bangphoomi N, Yamane D, Suda Y, Kato K, Horimoto T, Akashi H. Physical interaction between bovine viral diarrhea virus nonstructural protein 4A and adenosine deaminase acting on RNA (ADAR). Archives of virology 2014; 159:1735-1741.
34. Weiskircher E, Aligo J, Ning G, Konan KV. Bovine viral diarrhea virus NS4B protein is an integral membrane protein associated with Golgi markers and rearranged host membranes. Virology journal 2009; 6:1-15.
35. Suda Y, Murakami S, Horimoto T. Bovine viral diarrhea virus non-structural protein NS4B induces autophagosomes in bovine kidney cells. Archives of virology 2019; 164:255-260.
36. Zahoor MA, Yamane D, Mohamed YM, Suda Y, Kobayashi K, Kato K, Tohya Y, Akashi H. Bovine viral diarrhea virus non-structural protein 5A interacts with NIK- and IKKβ-binding protein. Journal of General Virology 2010; 91:1939-1948.
37. Isken O, Langerwisch U, Schönherr R, Lamp B, Schröder K, Duden R, Rümenapf TH, Tautz N. Functional characterization of bovine viral diarrhea virus nonstructural protein 5A by reverse genetic analysis and live cell imaging. Journal of virology 2014; 88:82-98.
38. Zhong W, Gutshall LL, Del Vecchio AM. Identification and characterization of an RNA-dependent RNA polymerase activity within the nonstructural protein 5B region of bovine viral diarrhea virus. Journal of Virology 1998; 72:9365-9369.
39. Ansari IH, Chen L-M, Liang D, Gil LH, Zhong W, Donis RO. Involvement of a bovine viral diarrhea virus NS5B locus in virion assembly. Journal of virology 2004; 78:9612-9623.
40. Janeway CA, Travers P, Walport M, Shlomchik M. Immunobiology: the immune system in health and disease. Current Biology London; 1996.
41. Amarante-Mendes GP, Adjemian S, Branco LM, Zanetti LC, Weinlich R, Bortoluci KR. Pattern Recognition Receptors and the Host Cell Death Molecular Machinery. Frontiers in Immunology 2018; 9.
42. Akira S, Uematsu S, Takeuchi O. Pathogen recognition and innate immunity. Cell 2006; 124:783-801.
43. Takeuchi O, Akira S. Pattern recognition receptors and inflammation. Cell 2010; 140:805-820.
44. Honda K, Takaoka A, Taniguchi T. Type I inteferon gene induction by the interferon regulatory factor family of transcription factors. Immunity 2006; 25:349-360.

45. McNab F, Mayer-Barber K, Sher A, Wack A, O'Garra A. Type I interferons in infectious disease. Nat Rev Immunol 2015; 15:87-103.
46. Stetson DB, Medzhitov R. Type I interferons in host defense. Immunity 2006; 25:373-381.
47. Nguyen KB, Watford WT, Salomon R, Hofmann SR, Pien GC, Morinobu A, Gadina M, O'Shea JJ, Biron CA. Critical role for STAT4 activation by type 1 interferons in the interferon-γ response to viral infection. Science 2002; 297:2063-2066.
48. Heink S, Ludwig D, Kloetzel P-M, Krüger E. IFN-γ-induced immune adaptation of the proteasome system is an accelerated and transient response. Proceedings of the National Academy of Sciences 2005; 102:9241-9246.
49. Monaco JJ. A molecular model of MHC class-I-restricted antigen processing. Immunology today 1992; 13:173-179.
50. Frucht DM, Fukao T, Bogdan C, Schindler H, O'Shea JJ, Koyasu S. IFN-γ production by antigen-presenting cells: mechanisms emerge. Trends in immunology 2001; 22:556-560.
51. Hastings KT, Lackman RL, Cresswell P. Functional requirements for the lysosomal thiol reductase GILT in MHC class II-restricted antigen processing. The Journal of Immunology 2006; 177:8569-8577.
52. Janeway Jr CA, Travers P, Walport M, Shlomchik MJ. B-cell activation by armed helper T cells. In: Immunobiology: The Immune System in Health and Disease. 5th edition: Garland Science; 2001.
53. Richter V, Lebl K, Baumgartner W, Obritzhauser W, Käsbohrer A, Pinior B. A systematic worldwide review of the direct monetary losses in cattle due to bovine viral diarrhoea virus infection. The Veterinary Journal 2017; 220:80-87.
54. Houe H. Epidemiological features and economical importance of bovine virus diarrhoea virus (BVDV) infections. Veterinary Microbiology 1999; 64:89-107.
55. McGowan MR, Kirkland PD, Rodwell BJ, Kerr DR, Carroll CL. A field investigation of the effects of bovine viral diarrhea virus infection around the time of insemination on the reproductive performance of cattle. Theriogenology 1993; 39:443-449.
56. Houe H. Economic impact of BVDV infection in dairies. Biologicals 2003; 31:137-143.
57. USDA-APHIS. I: Reference of dairy cattle health and management practices in the United States. US Department of Agriculture, National Animal Health Monitoring System 2007.
58. Riley JM, Peel DS, Raper KC, Hurt C. Invited Review: Economic consequences of beef cow-calf disease mismanagement: Bovine viral diarrhea virus. Applied Animal Science 2019; 35:606-614.
59. Ishmael W. How much money have you lost to BVD? In: Beef Editor's Blog, vol. 2021. Beef Magazine: Penton Media; 2016.
60. Hessman BE, Fulton RW, Sjeklocha DB, Murphy TA, Ridpath JF, Payton ME. Evaluation of economic effects and the health and performance of the general cattle population after exposure to cattle persistently infected with bovine viral diarrhea virus in a starter feedlot. American Journal of Veterinary Research 2009; 70:73-85.

61. Larson R, Pierce V, Grotelueschen D, Wittum T. Economic evaluation of beef cowherd screening for cattle persistently-infected with bovine viral diarrhea virus. The Bovine Practitioner 2002:106-112.
62. Loneragan GH, Thomson DU, Montgomery DL, Mason GL, Larson RL. Prevalence, outcome, and health consequences associated with persistent infection with bovine viral diarrhea virus in feedlot cattle. Journal of the American Veterinary Medical Association 2005; 226:595-601.
63. Drouillard JS. Current situation and future trends for beef production in the United States of America—A review. Asian-Australasian Journal of Animal Sciences 2018; 31:1007.
64. Van Campen H. Epidemiology and control of BVD in the U.S. Veterinary Microbiology 2010; 142:94-98.
65. Ridpath JF. Immunology of BVDV vaccines. Biologicals 2013; 41:14-19.
66. Lindberg A, Houe H. Characteristics in the epidemiology of bovine viral diarrhea virus (BVDV) of relevance to control. Preventive veterinary medicine 2005; 72:55-73.
67. Houe H, Lindberg A, Moennig V. Test Strategies in Bovine Viral Diarrhea Virus Control and Eradication Campaigns in Europe. Journal of Veterinary Diagnostic Investigation 2006; 18:427-436.
68. Deregt D. Introduction and History. In: Bovine Viral Diarrhea Virus; 2005: 3-33.
69. Newcomer BW, Chamorro MF, Walz PH. Vaccination of cattle against bovine viral diarrhea virus. Veterinary Microbiology 2017; 206:78-83.
70. Griebel PJ. BVDV vaccination in North America: risks versus benefits. Animal health research reviews 2015; 16:27.
71. Ridpath JF. Practical significance of heterogeneity among BVDV strains: Impact of biotype and genotype on U.S. control programs. Preventive Veterinary Medicine 2005; 72:17-30.
72. Woolums AR, Berghaus RD, Berghaus LJ, Ellis RW, Pence ME, Saliki JT, Hurley KA, Galland KL, Burdett WW, Nordstrom ST. Effect of calf age and administration route of initial multivalent modified-live virus vaccine on humoral and cell-mediated immune responses following subsequent administration of a booster vaccination at weaning in beef calves. American journal of veterinary research 2013; 74:343-354.
73. Van Campen H, Huzurbazar S. And now, the Bad News. In: American Association of Bovine Practitioners Proceedings of the Annual Conference; 2000: 145-145.
74. Newcomer BW, Walz PH, Givens MD, Wilson AE. Efficacy of bovine viral diarrhea virus vaccination to prevent reproductive disease: a meta-analysis. Theriogenology 2015; 83:360-365. e361.
75. Schweizer M, Peterhans E. Noncytopathic bovine viral diarrhea virus inhibits double-stranded RNA-induced apoptosis and interferon synthesis. Journal of Virology 2001; 75:4692-4698.
76. Baigent SJ, Zhang G, Fray MD, Flick-Smith H, Goodbourn S, McCauley JW. Inhibition of Beta Interferon Transcription by Noncytopathogenic Bovine Viral Diarrhea Virus Is through an Interferon Regulatory Factor 3-Dependent Mechanism. Journal of Virology 2002; 76:8979-8988.

77. Schweizer M, Mätzener P, Pfaffen G, Stalder H, Peterhans E. “Self” and “nonself” manipulation of interferon defense during persistent infection: bovine viral diarrhea virus resists alpha/beta interferon without blocking antiviral activity against unrelated viruses replicating in its host cells. Journal of Virology 2006; 80:6926.
78. Hilton L, Moganeradj K, Zhang G, Chen Y-H, Randall RE, McCauley JW, Goodbourn S. The NPro Product of Bovine Viral Diarrhea Virus Inhibits DNA Binding by Interferon Regulatory Factor 3 and Targets It for Proteasomal Degradation. Journal of Virology 2006; 80:11723-11732.
79. Magkouras I, Mätzener P, Rümenapf T, Peterhans E, Schweizer M. RNase-dependent inhibition of extracellular, but not intracellular, dsRNA-induced interferon synthesis by Erns of pestiviruses. Journal of general virology 2008; 89:2501-2506.
80. Darweesh MF, Rajput MK, Braun LJ, Rohila JS, Chase CC. BVDV Npro protein mediates the BVDV induced immunosuppression through interaction with cellular S100A9 protein. Microbial pathogenesis 2018; 121:341-349.
81. Brackenbury L, Carr B, Stamataki Z, Prentice H, Lefevre E, Howard C, Charleston B. Identification of a cell population that produces alpha/beta interferon in vitro and in vivo in response to noncytopathic bovine viral diarrhea virus. Journal of virology 2005; 79:7738.
82. Swasdipan S, McGowan M, Phillips N, Bielefeldt-Ohmann H. Pathogenesis of transplacental virus infection: pestivirus replication in the placenta and fetus following respiratory infection. Microbial Pathogenesis 2002; 32:49-60.
83. Tsuboi T, Osawa T, Kimura K, Kubo M, Haritani M. Experimental infection of early pregnant cows with bovine viral diarrhea virus: Transmission of virus to the reproductive tract and conceptus. Research in veterinary science 2011; 90:174-178.
84. Smirnova NP, Webb BT, Bielefeldt-Ohmann H, Van Campen H, Antoniazzi AQ, Morarie SE, Hansen TR. Development of fetal and placental innate immune responses during establishment of persistent infection with bovine viral diarrhea virus. Virus Research 2012; 167:329-336.
85. Charleston B, Fray MD, Baigent S, Carr BV, Morrison WI. Establishment of persistent infection with non-cytopathic bovine viral diarrhoea virus in cattle is associated with a failure to induce type I interferon. Journal of General Virology 2001; 82:1893-1897.
86. Smirnova NP, Webb BT, McGill JL, Schaut RG, Bielefeldt-Ohmann H, Van Campen H, Sacco RE, Hansen TR. Induction of interferon-gamma and downstream pathways during establishment of fetal persistent infection with bovine viral diarrhea virus. Virus Research 2014; 183:95-106.
87. Bielefeldt-Ohmann H, Smirnova NP, Tolnay AE, Webb BT, Antoniazzi AQ, van Campen H, Hansen TR. Neuro-invasion by a ‘Trojan Horse’strategy and vasculopathy during intrauterine flavivirus infection. International journal of experimental pathology 2012; 93:24-33.
88. Morarie-Kane SE, Smirnova NP, Hansen TR, Mediger J, Braun L, Chase C. Fetal Hepatic Response to Bovine Viral Diarrhea Virus Infection in Utero. Pathogens 2018; 7:54.

89. Knapek KJ, Georges HM, Van Campen H, Bishop JV, Bielefeldt-Ohmann H, Smirnova NP, Hansen TR. Fetal lymphoid organ immune responses to transient and persistent infection with bovine viral diarrhea virus. Viruses 2020; 12:816.
90. Scruggs DW, Fleming SA, Maslin WR, Wayne GA. Osteopetrosis, anemia, thrombocytopenia, and marrow necrosis in beef calves naturally infected with bovine virus diarrhea virus. Journal of Veterinary Diagnostic Investigation 1995; 7:555-559.
91. Webb BT, Norrdin RW, Smirnova NP, Van Campen H, Weiner CM, Antoniazzi AQ, Bielefeldt-Ohmann H, Hansen TR. Bovine viral diarrhea virus cyclically impairs long bone trabecular modeling in experimental persistently infected fetuses. Vet Pathol 2012; 49:930-940.
92. Smirnova NP, Bielefeldt-Ohmann H, Van Campen H, Austin KJ, Han H, Montgomery DL, Shoemaker ML, van Olphen AL, Hansen TR. Acute non-cytopathic bovine viral diarrhea virus infection induces pronounced type I interferon response in pregnant cows and fetuses. Virus Research 2008; 132:49-58.
93. Kim CH. Homeostatic and pathogenic extramedullary hematopoiesis. Journal of blood medicine 2010; 1:13.
94. Yang X, Chen D, Long H, Zhu B. The mechanisms of pathological extramedullary hematopoiesis in diseases. Cellular and Molecular Life Sciences 2020; 77:2723-2738.
95. Lanyon SR, Hill FI, Reichel MP, Brownlie J. Bovine viral diarrhoea: pathogenesis and diagnosis. The Veterinary Journal 2014; 199:201-209.
96. Baker JC. The Clinical Manifestations of Bovine Viral Diarrhea Infection. Veterinary Clinics of North America: Food Animal Practice 1995; 11:425-445.
97. Bielefeldt-Ohmann H. The Pathologies of Bovine Viral Diarrhea Virus Infection: A Window on the Pathogenesis. Veterinary Clinics of North America: Food Animal Practice 1995; 11:447-476.
98. Webb BT, McGilvray KC, Smirnova NP, Hansen TR, Norrdin RW. Effects of in utero pestivirus infection on bovine fetal bone geometry, biomechanical properties and composition. The Veterinary Journal 2013; 198:376-381.
99. Nuss K, Spiess A, Hilbe M, Sterr K, Reiser M, Matis U. Transient benign osteopetrosis in a calf persistently infected with bovine virus diarrhoea virus. Vet Comp Orthop Traumatol 2005; 18:100-104.
100. Done J, Terlecki S, Richardson C, Harkness J, Sands JJ, Patterson D, Sweasey D, Shaw I, Winkler C, Duffell S. Bovine virus diarrhoea-mucosal disease virus: pathogenicity for the fetal calf following maternal infection. The Veterinary Record 1980; 106:473-479.
101. Chase CCL. The impact of BVDV infection on adaptive immunity. Biologicals 2013; 41:52-60.
102. Lee K, Gillespie J. Propagation of virus diarrhea virus of cattle in tissue culture. American journal of veterinary research 1957; 18:952.
103. Collett MS, Moennig V, Horzinek MC. Recent Advances in Pestivirus Research. Journal of General Virology 1989; 70:253-266.
104. Givens MD, Marley MSD, Jones CA, Ensley DT, Galik PK, Zhang Y, Riddell KP, Joiner KS, Brodersen BW, Rodning SP. Protective effects against abortion and

fetal infection following exposure to bovine viral diarrhea virus and bovine herpesvirus 1 during pregnancy in beef heifers that received two doses of a multivalent modified-live virus vaccine prior to breeding. Journal of the American Veterinary Medical Association 2012; 241:484-495.
105. Yeruham I, Michael M, Perl S. An Unusual Congenital Malformation in a Calf with Serological Evidence of Foetal Bovine Viral Diarrhoea Virus Infection. Acta Veterinaria Scandinavica 2001; 42:425.
106. Ridpath J. Preventive strategy for BVDV infection in North America. Japanese Journal of Veterinary Research 2012; 60:S41-S49.
107. Scharnböck B, Roch F-F, Richter V, Funke C, Firth CL, Obritzhauser W, Baumgartner W, Käsbohrer A, Pinior B. A meta-analysis of bovine viral diarrhoea virus (BVDV) prevalences in the global cattle population. Scientific reports 2018; 8:1-15.
108. Chirase NK, Greene LW. Dietary zinc and manganese sources administered from the fetal stage onwards affect immune response of transit stressed and virus infected offspring steer calves. Animal Feed Science and Technology 2001; 93:217-228.
109. Shoemaker ML, Smirnova NP, Bielefeldt-Ohmann H, Austin KJ, Olphen Av, Clapper JA, Hansen TR. Differential Expression of the Type I Interferon Pathway during Persistent and Transient Bovine Viral Diarrhea Virus Infection. Journal of Interferon & Cytokine Research 2009; 29:23-36.
110. Hansen TR, Smirnova NP, Van Campen H, Shoemaker ML, Ptitsyn AA, Bielefeldt-Ohmann H. Maternal and fetal response to fetal persistent infection with bovine viral diarrhea virus. American Journal of Reproductive Immunology 2010; 64:295-306.
111. Peterhans E, Jungi TW, Schweizer M. BVDV and innate immunity. Biologicals 2003; 31:107-112.
112. Van Campen H, Vorpahl P, Huzurbazar S, Edwards J, Cavender J. A case report: evidence for type 2 bovine viral diarrhea virus (BVDV)-associated disease in beef herds vaccinated with a modified-live type 1 BVDV vaccine. Journal of Veterinary Diagnostic Investigation 2000; 12:263-265.
113. Bustin SA, Benes V, Garson JA, Hellemans J, Huggett J, Kubista M, Mueller R, Nolan T, Pfaffl MW, Shipley GL, Vandesompele J, Wittwer CT. The MIQE Guidelines: minimum information for publication of quantitative real-time PCR experiments. Clinical Chemistry 2009; 55:611.
114. Bielefeldt-Ohmann H. In Situ Characterization of Mononuclear Leukocytes in Skin and Digestive Tract of Persistently Bovine Viral Diarrhea Virus-infected Clinically Healthy Calves and Calves with Mucosal Disease. Veterinary Pathology 1988; 25:304-309.
115. Bielefeldt-Ohmann H, Rønsholt L, Bloch B. Demonstration of bovine viral diarrhoea virus in peripheral blood mononuclear cells of persistently infected, clinically normal cattle. Journal of general virology 1987; 68:1971-1982.
116. Gautier L, Cope L, Bolstad BM, Irizarry RA. affy—analysis of Affymetrix GeneChip data at the probe level. Bioinformatics 2004; 20:307-315.

117. Wu Z, Irizarry RA, Gentleman R, Martinez-Murillo F, Spencer F. A model-based background adjustment for oligonucleotide expression arrays. Journal of the American statistical Association 2004; 99:909-917.
118. Ritchie ME, Phipson B, Wu D, Hu Y, Law CW, Shi W, Smyth GK. limma powers differential expression analyses for RNA-sequencing and microarray studies. Nucleic acids research 2015; 43:e47-e47.
119. Georges HM. ImageJ_Analysis. In: GitHub; 2019.
120. Clevers H, Alarcon B, Wileman T, Terhorst C. The T Cell Receptor/CD3 Complex: A Dynamic Protein Ensemble. Annual Review of Immunology 1988; 6:629-662.
121. Mebius RE, Kraal G. Structure and function of the spleen. Nature Reviews Immunology 2005; 5:606-616.
122. Platanias LC. Mechanisms of type-I-and type-II-interferon-mediated signalling. Nature Reviews Immunology 2005; 5:375-386.
123. Suarez-Ramirez JE, Tarrio ML, Kim K, Demers DA, Biron CA. CD8 T cells in innate immune responses: using STAT4-dependent but antigen-independent pathways to gamma interferon during viral infection. MBio 2014; 5:e01978-01914.
124. Guermonprez P, Valladeau J, Zitvogel L, Théry C, Amigorena S. Antigen Presentation and T Cell Stimulation by Dendritic Cells. Annual Review of Immunology 2002; 20:621-667.
125. Janeway Jr CA, Travers P, Walport M, Shlomchik MJ. T cell-mediated cytotoxicity. In: Immunobiology: The Immune System in Health and Disease. 5th edition: Garland Science; 2001.
126. Janeway Jr CA, Travers P, Walport M, Shlomchik MJ. General properties of armed effector T cells. In: Immunobiology: The Immune System in Health and Disease. 5th edition: Garland Science; 2001.
127. Hansen TR, Smirnova NP, Webb BT, Bielefeldt-Ohmann H, Sacco RE, Van Campen H. Innate and adaptive immune responses to in utero infection with bovine viral diarrhea virus. Animal Health Research Reviews 2015; 16:15-26.
128. Brackenbury L, Carr B, Charleston B. Aspects of the innate and adaptive immune responses to acute infections with BVDV. Veterinary microbiology 2003; 96:337-344.
129. Shin T, Acland H. Tissue distribution of bovine viral diarrhea virus antigens in persistently infected cattle. Journal of veterinary science 2001; 2:81-84.
130. Givens MD, Marley MS. Immunology of chronic BVDV infections. Biologicals 2013; 41:26-30.
131. Fulton RW, Step DL, Ridpath JF, Saliki JT, Confer AW, Johnson BJ, Briggs RE, Hawley RV, Burge LJ, Payton ME. Response of calves persistently infected with noncytopathic bovine viral diarrhea virus (BVDV) subtype 1b after vaccination with heterologous BVDV strains in modified live virus vaccines and Mannheimia haemolytica bacterin-toxoid. Vaccine 2003; 21:2980-2985.
132. Tribe RM, Taylor PD, Kelly NM, Rees D, Sandall J, Kennedy HP. Parturition and the perinatal period: can mode of delivery impact on the future health of the neonate? J Physiol 2018; 596:5709-5722.

133. McGovern N, Shin A, Low G, Low D, Duan K, Yao LJ, Msallam R, Low I, Shadan NB, Sumatoh HR. Human fetal dendritic cells promote prenatal T-cell immune suppression through arginase-2. Nature 2017; 546:662.
134. Risalde M, Molina V, Sanchez-Cordon P, Pedrera M, Panadero R, Romero-Palomo F, Gomez-Villamandos J. Response of proinflammatory and anti-inflammatory cytokines in calves with subclinical bovine viral diarrhea challenged with bovine herpesvirus-1. Veterinary immunology and immunopathology 2011; 144:135-143.
135. Thaxton JE, Sharma S. Interleukin-10: a multi-faceted agent of pregnancy. American Journal of Reproductive Immunology 2010; 63:482-491.
136. Burt TD. Fetal regulatory T cells and peripheral immune tolerance in utero: implications for development and disease. American Journal of Reproductive Immunology 2013; 69:346-358.
137. Mold JE, Venkatasubrahmanyam S, Burt TD, Michaëlsson J, Rivera JM, Galkina SA, Weinberg K, Stoddart CA, McCune JM. Fetal and adult hematopoietic stem cells give rise to distinct T cell lineages in humans. Science 2010; 330:1695-1699.
138. Collen T, Douglas AJ, Paton DJ, Zhang G, Morrison WI. Single amino acid differences are sufficient for CD4+ T-cell recognition of a heterologous virus by cattle persistently infected with bovine viral diarrhea virus. Virology 2000; 276:70-82.
139. Paschos K, Allday MJ. Epigenetic reprogramming of host genes in viral and microbial pathogenesis. Trends in microbiology 2010; 18:439-447.
140. Lee KM, Gillespie JH. Propagation of virus diarrhea virus of cattle in tissue culture. Am J Vet Res 1957; 18:952-953.
141. Moennig V, Liess B. Pathogenesis of Intrauterine Infections With Bovine Viral Diarrhea Virus. Veterinary Clinics of North America: Food Animal Practice 1995; 11:477-487.
142. McClurkin AW, Littledike ET, Cutlip RC, Frank GH, Coria MF, Bolin SR. Production of cattle immunotolerant to bovine viral diarrhea virus. Canadian journal of comparative medicine : Revue canadienne de medecine comparee 1984; 48:156-161.
143. Brownlie J, Clarke M, Howard C. Experimental production of fatal mucosal disease in cattle. The Veterinary Record 1984; 114:535-536.
144. Georges HM, Knapek KJ, Bielefeldt-Ohmann H, Van Campen H, Hansen TR. Attenuated lymphocyte activation leads to the development of immunotolerance in bovine fetuses persistently infected with BVDV. Biology of Reproduction 2020.
145. Schauer KL, Freund DM, Prenni JE, Curthoys NP. Proteomic profiling and pathway analysis of the response of rat renal proximal convoluted tubules to metabolic acidosis. Am J Physiol Renal Physiol 2013; 305:F628-640.
146. Scopes RK. Measurement of protein by spectrophotometry at 205 nm. Analytical Biochemistry 1974; 59:277-282.
147. Keller A, Nesvizhskii AI, Kolker E, Aebersold R. Empirical statistical model to estimate the accuracy of peptide identifications made by MS/MS and database search. Anal Chem 2002; 74:5383-5392.

148. Searle BC, Turner M, Nesvizhskii AI. Improving sensitivity by probabilistically combining results from multiple MS/MS search methodologies. J Proteome Res 2008; 7:245-253.
149. Käll L, Storey JD, MacCoss MJ, Noble WS. Assigning significance to peptides identified by tandem mass spectrometry using decoy databases. J Proteome Res 2008; 7:29-34.
150. Nesvizhskii AI, Keller A, Kolker E, Aebersold R. A statistical model for identifying proteins by tandem mass spectrometry. Anal Chem 2003; 75:4646-4658.
151. Liu H, Sadygov RG, Yates JR, 3rd. A model for random sampling and estimation of relative protein abundance in shotgun proteomics. Anal Chem 2004; 76:4193-4201.
152. Busse D, de la Rosa M, Hobiger K, Thurley K, Flossdorf M, Scheffold A, Höfer T. Competing feedback loops shape IL-2 signaling between helper and regulatory T lymphocytes in cellular microenvironments. Proc Natl Acad Sci U S A 2010; 107:3058-3063.
153. Sadlack B, Löhler J, Schorle H, Klebb G, Haber H, Sickel E, Noelle RJ, Horak I. Generalized autoimmune disease in interleukin-2-deficient mice is triggered by an uncontrolled activation and proliferation of CD4+ T cells. European Journal of Immunology 1995; 25:3053-3059.
154. Liao W, Lin J-X, Leonard WJ. Interleukin-2 at the crossroads of effector responses, tolerance, and immunotherapy. Immunity 2013; 38:13-25.
155. Cheng G, Yu A, Malek TR. T-cell tolerance and the multi-functional role of IL-2R signaling in T-regulatory cells. Immunological Reviews 2011; 241:63-76.
156. Malek TR, Yu A, Vincek V, Scibelli P, Kong L. CD4 Regulatory T Cells Prevent Lethal Autoimmunity in IL-2Rβ-Deficient Mice: Implications for the Nonredundant Function of IL-2. Immunity 2002; 17:167-178.
157. Schubert K, Polte T, Bönisch U, Schader S, Holtappels R, Hildebrandt G, Lehmann J, Simon JC, Anderegg U, Saalbach A. Thy-1 (CD90) regulates the extravasation of leukocytes during inflammation. European Journal of Immunology 2011; 41:645-656.
158. Fischer RS, Fritz-Six KL, Fowler VM. Pointed-end capping by tropomodulin3 negatively regulates endothelial cell motility. Journal of Cell Biology 2003; 161:371-380.
159. Helal MA, Hoshino Y, Takagi S, Tajima M. C-X-C chemokine receptor type 4 and cytokine expressions in cows of a dairy herd with high prevalence of calves persistently infected with bovine viral diarrhea virus. Jpn J Vet Res 2013; 61:109-116.
160. Pozzobon T, Goldoni G, Viola A, Molon B. CXCR4 signaling in health and disease. Immunology Letters 2016; 177:6-15.
161. Huang LJ-s, Durick K, Weiner JA, Chun J, Taylor SS. D-AKAP2, a novel protein kinase A anchoring protein with a putative RGS domain. Proceedings of the National Academy of Sciences 1997; 94:11184-11189.
162. Li X, Dong Y, Tu K, Wang W. Proteomics analysis reveals the interleukin-35-dependent regulatory mechanisms affecting CD8+ T-cell functions. Cellular Immunology 2020; 348:104022.

163. Olferiev M, Jacek E, Kirou KA, Crow MK. Novel molecular signatures in mononuclear cell populations from patients with systemic lupus erythematosus. Clinical Immunology 2016; 172:34-43.
164. Tsukasaki M, Takayanagi H. Osteoimmunology: evolving concepts in bone–immune interactions in health and disease. Nature Reviews Immunology 2019; 19:626-642.
165. You X, Bian C, Zan Q, Xu X, Liu X, Chen J, Wang J, Qiu Y, Li W, Zhang X, Sun Y, Chen S, et al. Mudskipper genomes provide insights into the terrestrial adaptation of amphibious fishes. Nature Communications 2014; 5:5594.
166. Arron JR, Choi Y. Bone versus immune system. Nature 2000; 408:535-536.
167. Takayanagi H, Ogasawara K, Hida S, Chiba T, Murata S, Sato K, Takaoka A, Yokochi T, Oda H, Tanaka K, Nakamura K, Taniguchi T. T-cell-mediated regulation of osteoclastogenesis by signalling cross-talk between RANKL and IFN-γ. Nature 2000; 408:600-605.
168. Okamoto K, Nakashima T, Shinohara M, Negishi-Koga T, Komatsu N, Terashima A, Sawa S, Nitta T, Takayanagi H. Osteoimmunology: The Conceptual Framework Unifying the Immune and Skeletal Systems. Physiol Rev 2017; 97:1295-1349.
169. Asagiri M, Sato K, Usami T, Ochi S, Nishina H, Yoshida H, Morita I, Wagner EF, Mak TW, Serfling E, Takayanagi H. Autoamplification of NFATc1 expression determines its essential role in bone homeostasis. The Journal of experimental medicine 2005; 202:1261-1269.
170. Takayanagi H. Osteoimmunology and the effects of the immune system on bone. Nat Rev Rheumatol 2009; 5:667-676.
171. Takayanagi H, Kim S, Koga T, Nishina H, Isshiki M, Yoshida H, Saiura A, Isobe M, Yokochi T, Inoue J-i. Induction and activation of the transcription factor NFATc1 (NFAT2) integrate RANKL signaling in terminal differentiation of osteoclasts. Developmental cell 2002; 3:889-901.
172. Gerritsen EJ, Vossen JM, van Loo IH, Hermans J, Helfrich MH, Griscelli C, Fischer A. Autosomal recessive osteopetrosis: variability of findings at diagnosis and during the natural course. Pediatrics 1994; 93:247-253.
173. Tolar J, Teitelbaum SL, Orchard PJ. Osteopetrosis. New England Journal of Medicine 2004; 351:2839-2849.
174. Williams HJ, Carey LS. Rubella embryopathy: roentgenologic features. American Journal of Roentgenology 1966; 97:92-99.
175. Graham CB, Thal A, Wassum CS. Rubella-like bone changes in congenital cytomegalic inclusion disease. Radiology 1970; 94:39-43.
176. Kopelman AE, Halsted CC, Minnefor AB. Osteomalacia and spontaneous fractures in twins with congenital cytomegalic inclusion disease. The Journal of pediatrics 1972; 81:101-105.
177. Sacks R, Habermann E. Pathological fracture in congenital rubella. A case report. JBJS 1977; 59:557-559.
178. Smith RK, Specht EE. Osseous lesions and pathologic fractures in congenital cytomegalic inclusion disease: report of a case. Clinical orthopaedics and related research 1979:280-283.

179. Li Z, Kong K, Qi W. Osteoclast and its roles in calcium metabolism and bone development and remodeling. Biochemical and Biophysical Research Communications 2006; 343:345-350.
180. Grigoriadis AE, Wang ZQ, Cecchini MG, Hofstetter W, Felix R, Fleisch HA, Wagner EF. c-Fos: a key regulator of osteoclast-macrophage lineage determination and bone remodeling. Science 1994; 266:443-448.
181. Yamashita T, Yao Z, Li F, Zhang Q, Badell IR, Schwarz EM, Takeshita S, Wagner EF, Noda M, Matsuo K, Xing L, Boyce BF. NF-kappaB p50 and p52 regulate receptor activator of NF-kappaB ligand (RANKL) and tumor necrosis factor-induced osteoclast precursor differentiation by activating c-Fos and NFATc1. J Biol Chem 2007; 282:18245-18253.
182. Wei W, Wang X, Yang M, Smith LC, Dechow PC, Sonoda J, Evans RM, Wan Y. PGC1beta mediates PPARgamma activation of osteoclastogenesis and rosiglitazone-induced bone loss. Cell Metab 2010; 11:503-516.
183. Chen W, Zhu G, Hao L, Wu M, Ci H, Li Y-P. C/EBPα regulates osteoclast lineage commitment. Proceedings of the National Academy of Sciences 2013; 110:7294-7299.
184. Wang ZQ, Ovitt C, Grigoriadis AE, Möhle-Steinlein U, Rüther U, Wagner EF. Bone and haematopoietic defects in mice lacking c-fos. Nature 1992; 360:741-745.
185. Mak W, Shao X, Dunstan CR, Seibel MJ, Zhou H. Biphasic Glucocorticoid-Dependent Regulation of Wnt Expression and Its Inhibitors in Mature Osteoblastic Cells. Calcified Tissue International 2009; 85:538.
186. Wang Y, Li Y-P, Paulson C, Shao J-Z, Zhang X, Wu M, Chen W. Wnt and the Wnt signaling pathway in bone development and disease. Frontiers in bioscience (Landmark edition) 2014; 19:379-407.
187. Ponzetti M, Rucci N. Updates on Osteoimmunology: What's New on the Cross-Talk Between Bone and Immune System. Frontiers in Endocrinology 2019; 10.
188. Yoshida H, Hayashi S, Kunisada T, Ogawa M, Nishikawa S, Okamura H, Sudo T, Shultz LD, Nishikawa S. The murine mutation osteopetrosis is in the coding region of the macrophage colony stimulating factor gene. Nature 1990; 345:442-444.
189. Wiktor-Jedrzejczak W, Bartocci A, Ferrante AW, Jr., Ahmed-Ansari A, Sell KW, Pollard JW, Stanley ER. Total absence of colony-stimulating factor 1 in the macrophage-deficient osteopetrotic (op/op) mouse. Proc Natl Acad Sci U S A 1990; 87:4828-4832.
190. Kudo O, Sabokbar A, Pocock A, Itonaga I, Fujikawa Y, Athanasou NA. Interleukin-6 and interleukin-11 support human osteoclast formation by a RANKL-independent mechanism. Bone 2003; 32:1-7.
191. Blanchard F, Duplomb L, Baud'huin M, Brounais B. The dual role of IL-6-type cytokines on bone remodeling and bone tumors. Cytokine & Growth Factor Reviews 2009; 20:19-28.
192. Jensen J, Schultz RD. Effect of infection by bovine viral diarrhea virus (BVDV) in vitro on interleukin-1 activity of bovine monocytes. Veterinary Immunology and Immunopathology 1991; 29:251-265.

193. Shen X, He Z, Li H, Yao C, Zhang Y, He L, Li S, Huang J, Guo Z. Distinct Functional Patterns of Gene Promoter Hypomethylation and Hypermethylation in Cancer Genomes. PLOS ONE 2012; 7:e44822.
194. Okuneva O, Li Z, Körber I, Tegelberg S, Joensuu T, Tian L, Lehesjoki A-E. Brain inflammation is accompanied by peripheral inflammation in Cstb−/−mice, a model for progressive myoclonus epilepsy. Journal of Neuroinflammation 2016; 13:298.
195. Laitala-Leinonen T, Rinne R, Saukko P, Väänänen HK, Rinne A. Cystatin B as an intracellular modulator of bone resorption. Matrix Biol 2006; 25:149-157.
196. Manninen O, Puolakkainen T, Lehto J, Harittu E, Kallonen A, Peura M, Laitala-Leinonen T, Kopra O, Kiviranta R, Lehesjoki A-E. Impaired osteoclast homeostasis in the cystatin B-deficient mouse model of progressive myoclonus epilepsy. Bone reports 2015; 3:76-82.
197. Bossowska-Nowicka M, Mielcarska MB, Romaniewicz M, Kaczmarek MM, Gregorczyk-Zboroch KP, Struzik J, Grodzik M, Gieryńska MM, Toka FN, Szulc-Dąbrowska L. Ectromelia virus suppresses expression of cathepsins and cystatins in conventional dendritic cells to efficiently execute the replication process. BMC Microbiology 2019; 19:92.
198. Choi S-W, Yeon J-T, Park K-I, Lee CH, Youn BS, Oh J, Lee MS. VapB as a regulator of osteoclastogenesis via modulation of PLCγ2-Ca2+-NFAT signaling. FEBS Letters 2012; 586:263-269.
199. Silbernagel N, Walecki M, Schäfer MK-H, Kessler M, Zobeiri M, Rinné S, Kiper AK, Komadowski MA, Vowinkel KS, Wemhöner K. The VAMP-associated protein VAPB is required for cardiac and neuronal pacemaker channel function. The FASEB Journal 2018; 32:6159-6173.
200. Porter B, Ridpath J, Calise D, Payne H, Janke J, Baxter D, Edwards J. Hypomyelination associated with bovine viral diarrhea virus type 2 infection in a longhorn calf. Veterinary pathology 2010; 47:658-663.
201. Fernandez A, Hewicker M, Trautwein G, Pohlenz J, Liess B. Viral antigen distribution in the central nervous system of cattle persistently infected with bovine viral diarrhea virus. Veterinary Pathology 1989; 26:26-32.
202. Hewicker-Trautwein M, Liess B, Trautwein G. Brain Lesions in Calves following Transplacental Infection with Bovine-virus Diarrhoea Virus. Journal of Veterinary Medicine, Series B 1995; 42:65-77.
203. Joensuu T, Tegelberg S, Reinmaa E, Segerstråle M, Hakala P, Pehkonen H, Korpi ER, Tyynelä J, Taira T, Hovatta I. Gene expression alterations in the cerebellum and granule neurons of Cstb−/− mouse are associated with early synaptic changes and inflammation. PloS one 2014; 9:e89321.
204. Kabashi E, El Oussini H, Bercier V, Gros-Louis F, Valdmanis PN, McDearmid J, Mejier IA, Dion PA, Dupre N, Hollinger D, Sinniger J, Dirrig-Grosch S, et al. Investigating the contribution of VAPB/ALS8 loss of function in amyotrophic lateral sclerosis. Human Molecular Genetics 2013; 22:2350-2360.
205. Anagnostou G, Akbar MT, Paul P, Angelinetta C, Steiner TJ, de Belleroche J. Vesicle associated membrane protein B (VAPB) is decreased in ALS spinal cord. Neurobiology of Aging 2010; 31:969-985.
206. Teuling E, Ahmed S, Haasdijk E, Demmers J, Steinmetz MO, Akhmanova A, Jaarsma D, Hoogenraad CC. Motor neuron disease-associated mutant vesicle-

associated membrane protein-associated protein (VAP) B recruits wild-type VAPs into endoplasmic reticulum-derived tubular aggregates. Journal of Neuroscience 2007; 27:9801-9815.
207. Nosten-Bertrand M, Errington ML, Murphy KP, Tokugawa Y, Barboni E, Kozlova E, Michalovich D, Morris RG, Silver J, Stewart CL, Bliss TV, Morris RJ. Normal spatial learning despite regional inhibition of LTP in mice lacking Thy-1. Nature 1996; 379:826-829.
208. Mayeux-Portas V, File SE, Stewart CL, Morris RJ. Mice lacking the cell adhesion molecule Thy-1 fail to use socially transmitted cues to direct their choice of food. Curr Biol 2000; 10:68-75.
209. Bradley JE, Ramirez G, Hagood JS. Roles and regulation of Thy-1, a context-dependent modulator of cell phenotype. BioFactors (Oxford, England) 2009; 35:258-265.
210. Schubert W, Yang XY, Yang TTC, Factor SM, Lisanti MP, Molkentin JD, Rincón M, Chow C-W. Requirement of transcription factor NFAT in developing atrial myocardium. Journal of Cell Biology 2003; 161:861-874.
211. Graef IA, Chen F, Crabtree GR. NFAT signaling in vertebrate development. Current opinion in genetics & development 2001; 11:505-512.
212. Kirkbride CA. Viral agents and associated lesions detected in a 10-year study of bovine abortions and stillbirths. Journal of Veterinary Diagnostic Investigation 1992; 4:374-379.
213. Breshears M, Johnson B. Systemic reactive angioendotheliomatosis-like syndrome in a steer presumed to be persistently infected with bovine viral diarrhea virus. Veterinary pathology 2008; 45:645-649.
214. Ghobadi MZ, Mozhgani S-H, Farzanehpour M, Behzadian F. Identifying novel biomarkers of the pediatric influenza infection by weighted co-expression network analysis. Virology journal 2019; 16:1-10.
215. Lubick KJ, Robertson SJ, McNally KL, Freedman BA, Rasmussen AL, Taylor RT, Walts AD, Tsuruda S, Sakai M, Ishizuka M, Boer EF, Foster EC, et al. Flavivirus Antagonism of Type I Interferon Signaling Reveals Prolidase as a Regulator of IFNAR1 Surface Expression. Cell host & microbe 2015; 18:61-74.
216. Riera J, Rodríguez R, Carcedo MT, Campa VM, Ramos S, Lazo PS. Isolation and characterization of nudC from mouse macrophages, a gene implicated in the inflammatory response through the regulation of PAF-AH(I) activity. FEBS Letters 2007; 581:3057-3062.
217. Miller BA, Zhang M-Y, Gocke CD, De Souza C, Osmani AH, Lynch C, Davies J, Bell L, Osmani SA. A homolog of the fungal nuclear migration gene nudC is involved in normal and malignant human hematopoiesis. Experimental Hematology 1999; 27:742-750.
218. Rogers LK, Velten M. Maternal inflammation, growth retardation, and preterm birth: Insights into adult cardiovascular disease. Life Sciences 2011; 89:417-421.
219. Barker DJP, Osmond C. Infant mortality, childhood nutrition, and ischaemic heart disease in England and Wales. The Lancet 1986; 327:1077-1081.
220. Lewis AJ, Austin E, Knapp R, Vaiano T, Galbally M. Perinatal Maternal Mental Health, Fetal Programming and Child Development. Healthcare 2015; 3:1212-1227.

221. Arora N, Sadovsky Y, Dermody TS, Coyne CB. Microbial Vertical Transmission during Human Pregnancy. Cell host & microbe 2017; 21:561-567.
222. Zhao B, Ivashkiv LB. Negative regulation of osteoclastogenesis and bone resorption by cytokines and transcriptional repressors. Arthritis Research & Therapy 2011; 13:234.
223. Takeuchi T, Shimakawa G, Tamura M, Yokosawa H, Arata Y. ISG15 regulates RANKL-induced osteoclastogenic differentiation of RAW264 cells. Biol Pharm Bull 2015; 38:482-486.
224. Triunfol M. Microcephaly in Brazil: confidence builds in Zika connection. The Lancet Infectious Diseases 2016; 16:527-528.
225. Al-Haddad BJ, Oler E, Armistead B, Elsayed NA, Weinberger DR, Bernier R, Burd I, Kapur R, Jacobsson B, Wang C. The fetal origins of mental illness. American journal of obstetrics and gynecology 2019; 221:549-562.
226. de Vries LS. Viral infections and the neonatal brain. In: Seminars in pediatric neurology, vol. 32: Elsevier; 2019: 100769.
227. Lee SH, Shin JH, Choi BM, Kim Y-K. A Case of Cytomegalovirus Infection in a Neonate with Osteopetrosis. Pediatric Infection & Vaccine 2016; 23:72-76.
228. Katsafiloudi M, Gombakis N, Hatzipantelis E, Tragiannidis A. Osteopetrorickets in An Infant with Coexistent Congenital Cytomegalovirus Infection. Balkan J Med Genet 2020; 23:107-110.
229. Ye Z, Wang L, Yang T, Chen L, Wang T, Chen L, Zhao L, Zhang S, Zheng Z, Luo L. Maternal Viral Infection and Risk of Fetal Congenital Heart Diseases: A Meta-Analysis of Observational Studies. Journal of the American Heart Association 2019; 8:e011264.
230. Weiner CM, Smirnova NP, Webb BT, Van Campen H, Hansen TR. Interferon stimulated genes, CXCR4 and immune cell responses in peripheral blood mononuclear cells infected with bovine viral diarrhea virus. Res Vet Sci 2012; 93:1081-1088.
231. Senger PL. Pathways to pregnancy and parturition. Current Conceptions, Inc., 1615 NE Eastgate Blvd.; 1997.
232. Brett KE, Ferraro ZM, Yockell-Lelievre J, Gruslin A, Adamo KB. Maternal–fetal nutrient transport in pregnancy pathologies: the role of the placenta. International journal of molecular sciences 2014; 15:16153-16185.
233. Mettlen M, Chen P-H, Srinivasan S, Danuser G, Schmid SL. Regulation of clathrin-mediated endocytosis. Annual review of biochemistry 2018; 87:871-896.
234. Hackett BA, Cherry S. Flavivirus internalization is regulated by a size-dependent endocytic pathway. Proceedings of the National Academy of Sciences 2018; 115:4246-4251.
235. Cooke LD, Tumbarello DA, Harvey NC, Sethi JK, Lewis RM, Cleal JK. Endocytosis in the placenta: An undervalued mediator of placental transfer. Placenta 2021.
236. Lecot S, Belouzard S, Dubuisson J, Rouillé Y. Bovine viral diarrhea virus entry is dependent on clathrin-mediated endocytosis. Journal of virology 2005; 79:10826-10829.
237. Wickham H, Francois R, Henry L, Muller K. dplyr: A Grammar of Data Manipulation. In, R Package version 1.0.6 ed; 2021.

238. Wickham H. ggplot2: Elegant Graphics for Data Analysis. . In: Springer-Verlag; 2016.
239. Wickham H. tidyr: Tidy Messy Data. In, R package version 1.1.3 ed; 2021.
240. Love MI, Huber W, Anders S. Moderated estimation of fold change and dispersion for RNA-seq data with DESeq2. Genome Biology 2014; 15:550.
241. Scherer C, Flores E, Weiblen R, Caron L, Irigoyen L, Neves J, Maciel M. Experimental infection of pregnant ewes with bovine viral diarrhea virus type-2 (BVDV-2): effects on the pregnancy and fetus. Veterinary microbiology 2001; 79:285-299.
242. Barry JS, Anthony RV. The pregnant sheep as a model for human pregnancy. Theriogenology 2008; 69:55-67.
243. Peter AT. Bovine placenta: a review on morphology, components, and defects from terminology and clinical perspectives. Theriogenology 2013; 80:693-705.
244. Yockey LJ, Iwasaki A. Interferons and Proinflammatory Cytokines in Pregnancy and Fetal Development. Immunity 2018; 49:397-412.
245. Broeks MH, Shamseldin HE, Alhashem A, Hashem M, Abdulwahab F, Alshedi T, Alobaid I, Zwartkruis F, Westland D, Fuchs S. MDH1 deficiency is a metabolic disorder of the malate–aspartate shuttle associated with early onset severe encephalopathy. Human genetics 2019; 138:1247-1257.
246. Mitchell M, Cashman KS, Gardner DK, Thompson JG, Lane M. Disruption of mitochondrial malate-aspartate shuttle activity in mouse blastocysts impairs viability and fetal growth. Biology of reproduction 2009; 80:295-301.
247. Wookey AF, Chollangi T, Yong HE, Kalionis B, Brennecke SP, Murthi P, Georgiou HM. Placental vitamin D-binding protein expression in human idiopathic fetal growth restriction. Journal of Pregnancy 2017; 2017.
248. Takino J-i, Sato T, Hiraishi I, Nagamine K, Hori T. Alterations in Glucose Metabolism Due to Decreased Expression of Heterogeneous Nuclear Ribonucleoprotein M in Pancreatic Ductal Adenocarcinoma. Biology 2021; 10:57.
249. Kayisli UA, Demir R, Erguler G, Arici A. Vasodilator-stimulated phosphoprotein expression and its cytokine-mediated regulation in vasculogenesis during human placental development. Molecular human reproduction 2002; 8:1023-1030.
250. Luther J, Milne J, Aitken R, Matsuzaki M, Reynolds L, Redmer D, Wallace J. Placental growth, angiogenic gene expression, and vascular development in undernourished adolescent sheep. Biology of reproduction 2007; 77:351-357.
251. McMinn J, Wei M, Schupf N, Cusmai J, Johnson E, Smith A, Weksberg R, Thaker H, Tycko B. Unbalanced placental expression of imprinted genes in human intrauterine growth restriction. Placenta 2006; 27:540-549.
252. Yu Y, Singh U, Shi W, Konno T, Soares MJ, Geyer R, Fundele R. Influence of murine maternal diabetes on placental morphology, gene expression, and function. Archives of physiology and biochemistry 2008; 114:99-110.
253. Edwards AK, Dunlap KA, Spencer TE, Satterfield MC. Identification of Pathways Associated with Placental Adaptation to Maternal Nutrient Restriction in Sheep. Genes 2020; 11:1031.
254. Wen H, Abbasi S, Kellems R, Xia Y. mTOR: a placental growth signaling sensor. Placenta 2005; 26:S63-S69.

255. Dimasuay KG, Aitken EH, Rosario F, Njie M, Glazier J, Rogerson SJ, Fowkes FJ, Beeson JG, Powell T, Jansson T. Inhibition of placental mTOR signaling provides a link between placental malaria and reduced birthweight. BMC medicine 2017; 15:1-11.
256. Liang Q, Luo Z, Zeng J, Chen W, Foo S-S, Lee S-A, Ge J, Wang S, Goldman SA, Zlokovic BV. Zika virus NS4A and NS4B proteins deregulate Akt-mTOR signaling in human fetal neural stem cells to inhibit neurogenesis and induce autophagy. Cell stem cell 2016; 19:663-671.
257. Lum F-M, Narang V, Hue S, Chen J, McGovern N, Rajarethinam R, Tan JJ, Amrun SN, Chan Y-H, Lee CY. Trimester-specific Zika virus infection affects placental responses in women. bioRxiv 2019:727081.
258. Wek RC. Role of eIF2α kinases in translational control and adaptation to cellular stress. Cold Spring Harbor Perspectives in Biology 2018; 10:a032870.
259. Yung H-w, Calabrese S, Hynx D, Hemmings BA, Cetin I, Charnock-Jones DS, Burton GJ. Evidence of placental translation inhibition and endoplasmic reticulum stress in the etiology of human intrauterine growth restriction. The American journal of pathology 2008; 173:451-462.
260. Holder B, Jones T, Sancho Shimizu V, Rice TF, Donaldson B, Bouqueau M, Forbes K, Kampmann B. Macrophage exosomes induce placental inflammatory cytokines: a novel mode of maternal–placental messaging. Traffic 2016; 17:168-178.
261. Jacinto E, Loewith R, Schmidt A, Lin S, Rüegg MA, Hall A, Hall MN. Mammalian TOR complex 2 controls the actin cytoskeleton and is rapamycin insensitive. Nature cell biology 2004; 6:1122-1128.
262. Szabo S, Xu Y, Romero R, Fule T, Karaszi K, Bhatti G, Varkonyi T, Varkonyi I, Krenacs T, Dong Z. Changes of placental syndecan-1 expression in preeclampsia and HELLP syndrome. Virchows Archiv 2013; 463:445-458.
263. Pricop L, Salmon JE. Redox regulation of Fcγ receptor-mediated phagocytosis: implications for host defense and tissue injury. Antioxidants and Redox Signaling 2002; 4:85-95.
264. Mah MM, Roverato N, Groettrup M. Regulation of Interferon Induction by the Ubiquitin-Like Modifier FAT10. Biomolecules 2020; 10:951.
265. Kandel-Kfir M, Garcia-Milan R, Gueta I, Lubitz I, Ben-Zvi I, Shaish A, Shir L, Harats D, Mahajan M, Canaan A. IFNγ potentiates TNFα/TNFR1 signaling to induce FAT10 expression in macrophages. Molecular immunology 2020; 117:101-109.
266. Jovanović M, Stefanoska I, Radojcić L, Vićovac L. Interleukin-8 (CXCL8) stimulates trophoblast cell migration and invasion by increasing levels of matrix metalloproteinase (MMP) 2 and MMP9 and integrins alpha5 and beta1. Reproduction (Cambridge, England) 2010; 139:789-798.
267. Zhou Y, Genbacev O, Fisher SJ. The human placenta remodels the uterus by using a combination of molecules that govern vasculogenesis or leukocyte extravasation. Annals of the New York Academy of Sciences 2003; 995:73-83.
268. Nie A, Sun B, Fu Z, Yu D. Roles of aminoacyl-tRNA synthetases in immune regulation and immune diseases. Cell death & disease 2019; 10:1-14.

269. Yu YC, Han JM, Kim S. Aminoacyl-tRNA Synthetases and amino acid signaling. Biochimica et Biophysica Acta (BBA)-Molecular Cell Research 2020:118889.
270. Jiang L, Jones J, Yang X-L. Human diseases linked to cytoplasmic aminoacyl-tRNA synthetases. Biology of Aminoacyl-tRNA Synthetases 2020; 48:277.
271. Williams TF, Mirando AC, Wilkinson B, Francklyn CS, Lounsbury KM. Secreted Threonyl-tRNA synthetase stimulates endothelial cell migration and angiogenesis. Scientific reports 2013; 3:1-7.
272. Li J, Li Y, Zhou X, Wei L, Zhang J, Zhu S, Zhang H, Gao X, Sharifu LM, Wang S. Upregulation of IL-15 in the placenta alters trophoblasts behavior contributing to gestational diabetes mellitus. Cell & Bioscience 2021; 11:1-15.
273. MacPhee DJ, Mostachfi H, Han R, Lye SJ, Post M, Caniggia I. Focal adhesion kinase is a key mediator of human trophoblast development. Laboratory investigation 2001; 81:1469-1483.
274. Kemp MW. Preterm birth, intrauterine infection, and fetal inflammation. Frontiers in immunology 2014; 5:574.
275. Lahra MM, Jeffery HE. A fetal response to chorioamnionitis is associated with early survival after preterm birth. American journal of obstetrics and gynecology 2004; 190:147-151.
276. Toti P, De Felice C, Occhini R, Schuerfeld K, Stumpo M, Epistolato MC, Vatti R, Buonocore G. Spleen depletion in neonatal sepsis and chorioamnionitis. American journal of clinical pathology 2004; 122:765-771.
277. Kuypers E, Willems MG, Jellema RK, Kemp MW, Newnham JP, Delhaas T, Kallapur SG, Jobe AH, Wolfs TG, Kramer BW. Responses of the spleen to intraamniotic lipopolysaccharide exposure in fetal sheep. Pediatric research 2015; 77:29-35.
278. Van Campen H, Bishop JV, Abrahams VM, Bielefeldt-Ohmann H, Mathiason CK, Bouma GJ, Winger QA, Mayo CE, Bowen RA, Hansen TR. Maternal Influenza A Virus Infection Restricts Fetal and Placental Growth and Adversely Affects the Fetal Thymic Transcriptome. Viruses 2020; 12:1003.
279. Lewis SM, Williams A, Eisenbarth SC. Structure and function of the immune system in the spleen. Science immunology 2019; 4.
280. Pereira L. Congenital viral infection: traversing the uterine-placental interface. Annual review of virology 2018; 5:273-299.
281. Austin KJ, Carr AL, Pru JK, Hearne CE, George EL, Belden EL, Hansen TR. Localization of ISG15 and conjugated proteins in bovine endometrium using immunohistochemistry and electron microscopy. Endocrinology 2004; 145:967-975.

Appendix

Appendix Table 1: Primers utilized for RT-qPCR

Gene	Sequence	Accession	Efficiency
GAPDH	FW: TGACCCCTTCATTGACCTTC REV: CGTTCTCTGCCTTGACTGTG	NM_001034034.2	96%
YWHAZ	FW: CGGACACAGAACATCCAGTC REV: TCCAAGATGACCTACGGGCT	NM_174814.2	102%
18S	FW: GAACGAGACTCTGGGCATGC REV: CTGAACGCCACTTGTCCCTC	NR_036642	102%
RIGI	FW: GAGCACTGGTGGATGCCTTA REV: GCTGTCTCTGTTGGTTCGGA	XM_024996055.1	157%
IRF7	FW: GCCTCCTGGAAAACCAACTT REV: CCTTATGAGGGTCGGTAGGGG	NM_001105040.1	127%
NFKB	FW: CGAGGTTCGGTTCTACGAGG REV: TGCAGGAACACGGGTTACAGG	NM_001102101.1	134%
IFNB	FW: TCCAGCACATCTTCGGCATT REV: TTCCCTAGGTGGGGAACGAT	NM_174350.1	104%
ISG15	FW: GGTATCCGAGCTGAAGCAGTT REV: ACCTCCCTGCTGTCAAGGT	NM_174366	115%
STAT4	FW: TTCTTCCCATGTCGCCAAGT REV: AACCAGATGTGATTGTTGGCA	NM_001083692.2	104%
IFI30	FW: GCATGCAGCTCTTGCACATC REV: GGCCCCAAGAGTTCTTACCC	NM_001101251.2	131%
LMP2	FW: ATCTACCTGGCCACCATCAC REV: AGGAGAGTCCGAGGAAGGAG	NM_001034388	115%
LMP7	FW: ACTGGAAGGCAGCACAGAGT REV: ATTGTGCTTAGTGGGGCATC	NM_001040480	124%
CD4	FW: GGGCAGAACGGATGTCTCAA REV: ATAGGTCTTCTGGAGCCGGT	NM_001103225.1	110%
CD8a	FW: TACATCTGGGCTCCCTTGGT REV: CCACAGGCCTGGGACATTTG	NM_174015.1	130%
CD8b	FW: AGCTGAGTGTGTTGATGTTCT REV: TTCTGAGTCACCTGGGTTGG	NM_001105344.2	93%
CD79b	FW: TGATTCCCGGGCTCAACAAC REV: CTGCCAGATCCGGGAACAAG	XM_002696068.6	160%

Appendix Table 2: Antibodies used for western blotting

Target	Dilution in 2% Blocking Buffer	Source
ISG15	1:20,000	Hansen lab; [281]
CD4	1:1,000	Abcam ab25804
CD79b	1:500	Abcam ab134147
ACTB HRP	1:2,000	Santa Cruz Biotechnology SC-47778
Donkey anti Mouse HRP Secondary	1:2,000	Santa Cruz Biotechnology SC-2314
Donkey anti Rabbit HRP Secondary	1:2,000	Santa Cruz Biotechnology SC-2077
Goat anti Mouse	1:5,000	Abcam ab97040

Appendix Table 3: Antibodies used for immunohistochemistry

Target	Antigen Retrieval Method	Dilution	Source
CD3	Citrate, pH 6.0	1:40	DAKO
CD79a	EDTA, pH 9.0	1:200	DAKO

Appendix Table 4: Differentially methylated genes and associated pathways as identified by IPA

Pathway	Gene Symbol	p Value	Log2 Fold Change
Signaling by Rho Family GTPases	ARHGEF2	0.0000458	-32.448
	ARHGEF7	0.00000701	-32.454
	ARHGEF9	0.000000626	26.627
	ARHGEF19	0.00000593	-31.791
	BAIAP2	0.0000899	-28.663
	CDC42EP4	0.000106	-34.586
	CDH3	0.0000511	-30.189
	CDH4	0.0000774	-26.417
	CDH5	0.0000218	-38.261
	CDH11	0.0000302	-30.643
	CDH13	0.000103	30.566
	CDH22	0.0000146	-36.218
	GNA12	0.0000568	-27.296
	GNAI2	0.000000415	-26.772
	GNAT1	0.000000226	-39.154
	GNB1L	0.00000053	-30.228
	GNG7	0.0000895	-27.143
	GNG13	0.000000275	29.342
	MAP2K2	0.000087	26.989
	MYL9	6.67E-09	-40.861
	MYL10	0.0000203	-31.216
	PAK3	0.000000101	26.667
	PARD3	0.00000254	-30.532
	PRKCZ	0.000026	27.506
	RAC3	0.00000027	-39.765
	RHOQ	0.0000573	-28.857
	SEPTIN1	0.0000209	-30.906
	SEPTIN5	0.0000461	-30.27
	SEPTIN8	0.00000403	-26.382
	SEPTIN9	0.000106	-31.778
Human Embryo Stem Cell Pluripotency	FGF4	0.0000605	27.055
	FOXO1	0.000161	29.167
	FZD1	0.0000185	27.788
	FZD5	0.00000477	-30.645
	FZD9	0.000104	-28.133
	HNF1A	0.00000151	-34.928
	NTF3	0.0000244	-27.719

	NTF4	0.00000352	27.428
	NTRK1	0.00000709	31.423
	NTRK2	0.0000056	-27.273
	PDGFRB	0.0000002	-33.937
	PDPK1	0.0000128	-38.274
	S1PR5	0.00000453	-27.527
	SMAD3	0.00000175	-26.471
	SMAD6	0.0000366	-25.875
	TCF4	0.000000724	-31.841
	TCF7	0.00000728	-29.221
	WNT2B	5.99E-09	-31.67
	WNT7A	0.000000401	-44.149
Wnt/B-Catenin Signaling	CCND1	0.00000547	-31.886
	CDH3	0.0000511	-30.189
	CDH5	0.0000218	-38.261
	DKK3	0.000109	-29.292
	FZD1	0.0000185	27.788
	FZD5	0.00000477	-30.645
	FZD9	0.000104	-28.133
	HNF1A	0.00000151	-34.928
	LRP5	0.000165	-31.54
	PPARD	0.00000563	-33.171
	PPP2R3A	0.0000565	32.252
	RARA	0.00000666	-30.138
	RPS27A	0.000000665	-26.263
	SFRP1	0.000135	-25.551
	SOX8	0.0000944	-28.618
	SOX9	0.00000843	-32.791
	TCF4	0.000000724	-31.841
	TCF7	0.00000728	-29.221
	WNT2B	5.99E-09	-31.67
	WNT7A	0.000000401	-44.149
Protein Kinase A Signaling	CNGA3	3.55E-08	-30.777
	DUSP18	4.34E-08	-36.414
	DUSP26	0.0000037	-30.593
	FICD	0.000115	-27.503
	GNAI2	0.000000415	-26.772
	GNB1L	0.00000053	-30.228
	GNG7	0.0000895	-27.143

	GNG13	0.000000275	29.342
	HNF1A	0.00000151	-34.928
	MAP2K2	0.000087	26.989
	MAP3K1	0.000000522	-29.31
	MYL9	6.67E-09	-40.861
	MYL10	0.0000203	-31.216
	NFATC1	0.0000843	33.466
	NFATC2	3.03E-10	35.288
	PDE4D	0.0000226	-27.461
	PLCL2	0.00000118	-39.466
	PRKAG2	0.000000151	-40.906
	PRKCD	0.00000902	25.606
	PRKCZ	0.000026	27.506
	PRKD1	1.78E-08	46.465
	PTPN3	0.000000138	-27.957
	PTPRE	0.00000485	-36.331
	PTPRJ	0.0000816	25.29
	PTPRS	0.00000665	-33.202
	PTPRU	0.000000244	-34.17
	SMAD3	0.00000175	-26.471
	TCF4	0.000000724	-31.841
	TCF7	0.00000728	-29.221
	TH	0.000000111	-26.677
	TNNI2	0.0000011	-41.468
	YWHAH	1.97E-08	32.258
PI3K/AKT Signaling	BCL2	0.0000468	-26.444
	CCND1	0.00000547	-31.886
	CDKN1A	0.000143	29.825
	FOXO1	0.000161	29.167
	GAB2	0.000149	25.988
	GDF15	0.000000655	-33.046
	IKBKB	0	35.484
	IL1R1	0.0000502	31.056
	IL21R	0.0000249	27.322
	IL31RA	0.0000425	-32.106
	IL3RA	0.0000486	27.877
	IL6R	0.0000309	34.295
	IL9R	0.0000721	-27.756
	MAP2K2	0.000087	26.989

	PDPK1	0.0000128	-38.274
	PPP2R3A	0.0000565	32.252
	YWHAH	1.97E-08	32.258
Calcium Signaling	ATP2B2	0.00000131	42.22
	ATP2B3	0.00000206	31.199
	CACNA1G	0.000178	26.674
	CACNA1I	0.0000646	32.271
	CACNA2D2	0.000109	-31.43
	CACNA2D4	0.000136	-32.204
	CACNG5	0	60.119
	CHRNG	0.000000127	-43.727
	GRIN2B	0.00000194	-34.509
	GRIN2C	1.33E-09	51.686
	HDAC7	0.00000727	-33.704
	MEF2D	0.00000268	-38.069
	MYL9	6.67E-09	-40.861
	NFATC1	0.0000843	33.466
	NFATC2	3.03E-10	35.288
	PRKAG2	0.000000151	-40.906
	SLC8A2	0.000051	29.132
	TNNI2	0.0000011	-41.468
	TNNT2	0.0000266	-36.701
STAT3 Pathway	BCL2	0.0000468	-26.444
	CDKN1A	0.000143	29.825
	IL1R1	0.0000502	31.056
	IL21R	0.0000249	27.322
	IL31RA	0.0000425	-32.106
	IL3RA	0.0000486	27.877
	IL6R	0.0000309	34.295
	IL9R	0.0000721	-27.756
	MAP2K2	0.000087	26.989
	NTRK1	0.00000709	31.423
	NTRK2	0.0000056	-27.273
	PDGFRB	0.0000002	-33.937
	SOCS3	0.0000739	-30.058
	VEGFA	8.7E-09	-25.49
mTOR Signaling	EIF3F	1.97E-08	-39.326
	EIF3M	0.000169	-27.535
	EIF4G3	0.0000641	-26.507

	GNB1L	0.00000053	-30.228
	IRS1	1.83E-08	-42.523
	PDPK1	0.0000128	-38.274
	PPP2R3A	0.0000565	32.252
	PRKAG2	0.000000151	-40.906
	PRKCD	0.00000902	25.606
	PRKCZ	0.000026	27.506
	PRKD1	1.78E-08	46.465
	PROK1	0.0000704	-29.412
	PRR5	0.0000639	-31.02
	RAC3	0.00000027	-39.765
	RHOQ	0.0000573	-28.857
	RPS27A	0.000000665	-26.263
	RPS6KA4	0.00000118	-28.205
	VEGFA	8.7E-09	-25.49
Phospholipase C Signaling	ARHGEF2	0.0000458	-32.448
	ARHGEF7	0.00000701	-32.454
	ARHGEF9	0.000000626	26.627
	ARHGEF19	0.00000593	-31.791
	CD247	0.000000195	-43.459
	GNB1L	0.00000053	-30.228
	GNG7	0.0000895	-27.143
	GNG13	0.000000275	29.342
	HDAC7	0.00000727	-33.704
	MAP2K2	0.000087	26.989
	MEF2D	0.00000268	-38.069
	MPRIP	4.46E-08	29.603
	MYL9	6.67E-09	-40.861
	MYL10	0.0000203	-31.216
	NFATC1	0.0000843	33.466
	NFATC2	3.03E-10	35.288
	PRKCD	0.00000902	25.606
	PRKCZ	0.000026	27.506
	PRKD1	1.78E-08	46.465
	RAC3	0.00000027	-39.765
	RHOQ	0.0000573	-28.857
Wnt/Ca + Pathway	FZD1	0.0000185	27.788
	FZD5	0.00000477	-30.645
	FZD9	0.000104	-28.133

	NFATC1	0.0000843	33.466
	NFATC2	3.03E-10	35.288
	PLCL2	0.00000118	-39.466
	ROR1	0.00000767	-25.843
Role of Macrophages, Fibroblasts and Endothelial Cells in Rheumatoid Arthritis	CCND1	0.00000547	-31.886
	CEBPA	0.0000006	-27.174
	CEBPD	0.000000245	-35.964
	CSF1	0.0000138	-30.283
	DKK3	0.000109	-29.292
	F2RL1	0	-25.563
	FZD1	0.0000185	27.788
	FZD5	0.00000477	-30.645
	FZD9	0.000104	-28.133
	HNF1A	0.00000151	-34.928
	IKBKB	0	35.484
	IL1R1	0.0000502	31.056
	IL6R	0.0000309	34.295
	LRP5	0.000165	-31.54
	LTA	0.000011	28.303
	MAP2K2	0.000087	26.989
	MIF	2.23E-09	-36.14
	NFATC1	0.0000843	33.466
	NFATC2	3.03E-10	35.288
	PLCL2	0.00000118	-39.466
	PRKCD	0.00000902	25.606
	PRKCZ	0.000026	27.506
	PRKD1	1.78E-08	46.465
	PROK1	0.0000704	-29.412
	PRSS2	0.00000338	33.955
	SFRP1	0.000135	-25.551
	SOCS3	0.0000739	-30.058
	TCF4	0.000000724	-31.841
	TCF7	0.00000728	-29.221
	TRAF1	0.000083	-26.325
	TRAF2	5.02E-08	-44.481
	VEGFA	8.7E-09	-25.49
	WNT2B	5.99E-09	-31.67
	WNT7A	0.000000401	-44.149
	CACNA1G	0.000178	26.674

CCR5 Signaling in Macrophages	CACNA1I	0.0000646	32.271
	CACNA2D2	0.000109	-31.43
	CACNA2D4	0.000136	-32.204
	CACNG5	0	60.119
	CD247	0.000000195	-43.459
	GNAI2	0.000000415	-26.772
	GNB1L	0.00000053	-30.228
	GNG7	0.0000895	-27.143
	GNG13	0.000000275	29.342
	PRKCD	0.00000902	25.606
	PRKCZ	0.000026	27.506
	PRKD1	1.78E-08	46.465
IL8 Signaling	BCL2	0.0000468	-26.444
	CCND1	0.00000547	-31.886
	CCND3	0.0000367	32.689
	GNA12	0.0000568	-27.296
	GNAI2	0.000000415	-26.772
	GNB1L	0.00000053	-30.228
	GNG7	0.0000895	-27.143
	GNG13	0.000000275	29.342
	IKBKB	0	35.484
	ITGAM	0.00000562	-37.012
	LASP1	0.0000229	-29.825
	MAP2K2	0.000087	26.989
	MYL9	6.67E-09	-40.861
	PRKCD	0.00000902	25.606
	PRKCZ	0.000026	27.506
	PRKD1	1.78E-08	46.465
	PROK1	0.0000704	-29.412
	RAC3	0.00000027	-39.765
	RHOQ	0.0000573	-28.857
	VEGFA	8.7E-09	-25.49
IL15 Signaling	DDR1	0.0000131	-31.571
	EPHA2	0.0000548	27.319
	EPHA8	0.00000473	-33.98
	EPHB4	0.000000871	-32.17
	HCK	0.000000045	-25.692
	MATK	0.0000384	-30.36
	NTRK1	0.00000709	31.423

	NTRK2	0.0000056	-27.273
	PDGFRB	0.0000002	-33.937
	PRKCZ	0.000026	27.506
	RET	0.000113	-26.441
	ROR1	0.00000767	-25.843
	TNK1	0.00000321	-27.988
	TYRO3	0.00000123	33.07
Regulation of IL2 Expression in Activated and Anergic T Lymphocytes	CARD11	0.00000129	-39.841
	CD247	0.000000195	-43.459
	IKBKB	0	35.484
	MAP2K2	0.000087	26.989
	MAP3K1	0.000000522	-29.31
	NFATC1	0.0000843	33.466
	NFATC2	3.03E-10	35.288
	SMAD3	0.00000175	-26.471
	VAV1	0.0000207	-25.581
	VAV2	0.00000511	-30.417
IL1 Signaling	GNA12	0.0000568	-27.296
	GNAI2	0.000000415	-26.772
	GNAT1	0.000000226	-39.154
	GNB1L	0.00000053	-30.228
	GNG7	0.0000895	-27.143
	GNG13	0.000000275	29.342
	IKBKB	0	35.484
	IL1R1	0.0000502	31.056
	MAP3K1	0.000000522	-29.31
	PRKAG2	0.000000151	-40.906
B Cell Activator Factor Signaling	IKBKB	0	35.484
	MAP3K1	0.000000522	-29.31
	NFATC1	0.0000843	33.466
	NFATC2	3.03E-10	35.288
	TRAF1	0.000083	-26.325
	TRAF2	5.02E-08	-44.481
CXCR4 Signaling	GNA12	0.0000568	-27.296
	GNAI2	0.000000415	-26.772
	GNAT1	0.000000226	-39.154
	GNB1L	0.00000053	-30.228
	GNG7	0.0000895	-27.143
	GNG13	0.000000275	29.342

	MAP2K2	0.000087	26.989
	MYL9	6.67E-09	-40.861
	MYL10	0.0000203	-31.216
	PAK3	0.000000101	26.667
	PRKCD	0.00000902	25.606
	PRKCZ	0.000026	27.506
	PRKD1	1.78E-08	46.465
	RAC3	0.00000027	-39.765
	RHOQ	0.0000573	-28.857
PKCO (theta) in T Cells	CACNA1G	0.000178	26.674
	CACNA1I	0.0000646	32.271
	CACNA2D2	0.000109	-31.43
	CACNA2D4	0.000136	-32.204
	CACNG5	0	60.119
	CARD11	0.00000129	-39.841
	CD247	0.000000195	-43.459
	IKBKB	0	35.484
	MAP3K1	0.000000522	-29.31
	NFATC1	0.0000843	33.466
	NFATC2	3.03E-10	35.288
	RAC3	0.00000027	-39.765
	VAV1	0.0000207	-25.581
	VAV2	0.00000511	-30.417
Leukocyte Extravasation Signaling	ARHGAP1	0.00000702	30.549
	ARHGAP6	0	33.645
	CDH5	0.0000218	-38.261
	CLDN7	0.000000126	-27.487
	CTTN	0.000149	-29.468
	GNAI2	0.000000415	-26.772
	ITGAM	0.00000562	-37.012
	MAP2K2	0.000087	26.989
	MMP23B	4.96E-08	26.59
	PRKCD	0.00000902	25.606
	PRKCZ	0.000026	27.506
	PRKD1	1.78E-08	46.465
	THY1	0.0000126	-30.846
	TIMP4	0.0000513	-30.518
	VAV1	0.0000207	-25.581
	VAV2	0.00000511	-30.417

CD27 Signaling	BID	6.91E-08	-34.444
	IKBKB	0	35.484
	MAP2K2	0.000087	26.989
	MAP3K1	0.000000522	-29.31
	SIVA1	0.00000889	-33.165
	TRAF2	5.02E-08	-44.481
Axonal Guidance Signaling	ABLIM2	0.0000124	-27.816
	ADAMTS17	0.000000307	28.571
	ARHGEF7	0.00000701	-32.454
	BAIAP2	0.0000899	-28.663
	EFNA2	0.0000149	-30.054
	EFNB2	0.0000121	-25.806
	EPHA2	0.0000548	27.319
	EPHA8	0.00000473	-33.98
	EPHB4	0.000000871	-32.17
	FZD1	0.0000185	27.788
	FZD5	0.00000477	-30.645
	FZD9	0.000104	-28.133
	GDF7	0.0000112	25.317
	GLI2	0.00005	-28.683
	GLIS1	0.0000394	-25.615
	GNA12	0.0000568	-27.296
	GNAI2	0.000000415	-26.772
	GNAT1	0.000000226	-39.154
	GNB1L	0.00000053	-30.228
	GNG7	0.0000895	-27.143
	GNG13	0.000000275	29.342
	KEL	3.92E-10	-42.144
	MAP2K2	0.000087	26.989
	MMP23B	4.96E-08	26.59
	MYL9	6.67E-09	-40.861
	MYL10	0.0000203	-31.216
	NFATC1	0.0000843	33.466
	NFATC2	3.03E-10	35.288
	NRP1	0.00000902	-34.295
	NTF3	0.0000244	-27.719
	NTF4	0.00000352	27.428
	NTNG1	0.0000281	-34.21

	NTRK1	0.00000709	31.423
	NTRK2	0.0000056	-27.273
	PAK3	0.000000101	26.667
	PAPPA	9.65E-08	-27.826
	PITRM1	0.00007	-32.997
	PLCL2	0.00000118	-39.466
	PLXNA1	0.000000311	-32.653
	PLXNB2	0.000000611	26.217
	PLXND1	0.0000016	-26.927
	PRKAG2	0.000000151	-40.906
	PRKCD	0.00000902	25.606
	PRKCZ	0.000026	27.506
	PRKD1	1.78E-08	46.465
	PROK1	0.0000704	-29.412
	RAC3	0.00000027	-39.765
	RGS3	0.00000871	-28.085
	RTN4R	0.0000186	-30.695
	SEMA3B	0.0000021	-34.329
	SEMA4C	0.00000134	28.812
	SEMA6C	0.000000288	-31.167
	SHANK2	0.00000211	-28.148
	SLIT1	0.0000265	-30.552
	SRGAP3	0.0000439	-31.05
	TUBB6	0.0000882	-26.264
	UNC5D	0.0000988	-28.789
	VEGFA	8.7E-09	-25.49
	WNT2B	5.99E-09	-31.67
	WNT7A	0.000000401	-44.149
Synaptogenesis Signaling Pathway	ARHGEF7	0.00000701	-32.454
	CDH3	0.0000511	-30.189
	CDH4	0.0000774	-26.417
	CDH5	0.0000218	-38.261
	CDH11	0.0000302	-30.643
	CDH13	0.000103	30.566
	CDH22	0.0000146	-36.218
	COMP	0.0000684	-26.749
	CPLX1	1.59E-10	35.445
	EFNA2	0.0000149	-30.054
	EFNB2	0.0000121	-25.806

	EPHA2	0.0000548	27.319
	EPHA8	0.00000473	-33.98
	EPHB4	0.000000871	-32.17
	GRIN2B	0.00000194	-34.509
	GRIN2C	1.33E-09	51.686
	GRM4	0.0000145	-29.01
	HCK	0.000000045	-25.692
	MAPT	0.00000131	-35.156
	NAPA	0.00000914	-28.494
	NLGN4Y	0.0000759	-31.819
	NRXN2	3.23E-08	-34.61
	NTRK2	0.0000056	-27.273
	PRKAG2	0.000000151	-40.906
	PRKCD	0.00000902	25.606
	STXBP2	0.00000732	25.779
	SYT2	9.45E-08	-32.407
	SYT7	0.000143	29.894
	SYT8	0.0000757	-30.037
	THBS1	0.0000462	-31.27
	THBS2	0.000135	-25.092
	TIAM1	0.000000545	34.146
CREB Signaling in Neurons	CACNA1G	0.000178	26.674
	CACNA1I	0.0000646	32.271
	CACNA2D2	0.000109	-31.43
	CACNA2D4	0.000136	-32.204
	CACNG5	0	60.119
	GNA12	0.0000568	-27.296
	GNAI2	0.000000415	-26.772
	GNAT1	0.000000226	-39.154
	GNB1L	0.00000053	-30.228
	GNG7	0.0000895	-27.143
	GNG13	0.000000275	29.342
	GRIK4	0.0000246	-32.898
	GRIN2B	0.00000194	-34.509
	GRIN2C	1.33E-09	51.686
	GRM4	0.0000145	-29.01
	MAP2K2	0.000087	26.989
	PLCL2	0.00000118	-39.466
	PRKAG2	0.000000151	-40.906

	PRKCD	0.00000902	25.606
	PRKCZ	0.000026	27.506
	PRKD1	1.78E-08	46.465
Alpha Adrenergic Signaling	GNAI2	0.000000415	-26.772
	GNB1L	0.00000053	-30.228
	GNG7	0.0000895	-27.143
	GNG13	0.000000275	29.342
	MAP2K2	0.000087	26.989
	PRKAG2	0.000000151	-40.906
	PRKCD	0.00000902	25.606
	PRKCZ	0.000026	27.506
	PRKD1	1.78E-08	46.465
	SLC8A2	0.000051	29.132
Synaptic Long Term Depression	CACNA1G	0.000178	26.674
	CACNA1I	0.0000646	32.271
	CACNA2D2	0.000109	-31.43
	CACNA2D4	0.000136	-32.204
	CACNG5	0	60.119
	GNA12	0.0000568	-27.296
	GNAI2	0.000000415	-26.772
	GNAT1	0.000000226	-39.154
	GRM4	0.0000145	-29.01
	MAP2K2	0.000087	26.989
	PLCL2	0.00000118	-39.466
	PPP2R3A	0.0000565	32.252
	PRKCD	0.00000902	25.606
	PRKCZ	0.000026	27.506
	PRKD1	1.78E-08	46.465
Factors Promoting Cardiogenesis in Vertebrates	FZD1	0.0000185	27.788
	FZD5	0.00000477	-30.645
	FZD9	0.000104	-28.133
	HNF1A	0.00000151	-34.928
	LRP5	0.000165	-31.54
	PRKCD	0.00000902	25.606
	PRKCZ	0.000026	27.506
	PRKD1	1.78E-08	46.465
	TBX5	0.0000536	-30.091
	TCF4	0.000000724	-31.841
	TCF7	0.00000728	-29.221

Role of NFAT in Cardiac Hypertrophy	CACNA1G	0.000178	26.674
	CACNA1I	0.0000646	32.271
	CACNA2D2	0.000109	-31.43
	CACNA2D4	0.000136	-32.204
	CACNG5	0	60.119
	GNAI2	0.000000415	-26.772
	GNB1L	0.00000053	-30.228
	GNG7	0.0000895	-27.143
	GNG13	0.000000275	29.342
	HDAC7	0.00000727	-33.704
	MAP2K2	0.000087	26.989
	MAP3K1	0.000000522	-29.31
	MEF2D	0.00000268	-38.069
	PLCL2	0.00000118	-39.466
	PRKAG2	0.000000151	-40.906
	PRKCD	0.00000902	25.606
	PRKCZ	0.000026	27.506
	PRKD1	1.78E-08	46.465
	SLC8A2	0.000051	29.132
Cardiac Hypertrohpy Signaling (enhanced)	FGF4	0.0000605	27.055
	FGF9	0.0000816	-28.675
	FGF19	0.000104	-33.907
	FICD	0.000115	-27.503
	FZD1	0.0000185	27.788
	FZD5	0.00000477	-30.645
	FZD9	0.000104	-28.133
	GNA12	0.0000568	-27.296
	GNAI2	0.000000415	-26.772
	GNG7	0.0000895	-27.143
	HDAC7	0.00000727	-33.704
	IKBKB	0	35.484
	IL1R1	0.0000502	31.056
	IL21R	0.0000249	27.322
	IL31RA	0.0000425	-32.106
	IL3RA	0.0000486	27.877
	IL6R	0.0000309	34.295
	IL9R	0.0000721	-27.756
	LTA	0.000011	28.303
	MAP2K2	0.000087	26.989

	MAP3K1	0.000000522	-29.31
	MEF2D	0.00000268	-38.069
	MYOCD	0.000017	-26.206
	NFATC1	0.0000843	33.466
	NFATC2	3.03E-10	35.288
	PDE4D	0.0000226	-27.461
	PLCL2	0.00000118	-39.466
	PRKAG2	0.000000151	-40.906
	PRKCD	0.00000902	25.606
	PRKCZ	0.000026	27.506
	PRKD1	1.78E-08	46.465
	WNT2B	5.99E-09	-31.67
	WNT7A	0.000000401	-44.149
Role of Osteoblasts, Osteoclasts, and Chondrocytes in Rheumatoid Arthritis	ALPL	0.000000117	-30
	BCL2	0.0000468	-26.444
	COL1A1	1.71E-08	-39.864
	CSF1	0.0000138	-30.283
	DKK3	0.000109	-29.292
	FOXO1	0.000161	29.167
	FZD1	0.0000185	27.788
	FZD5	0.00000477	-30.645
	FZD9	0.000104	-28.133
	GSN	1.56E-10	-46.107
	HNF1A	0.00000151	-34.928
	IKBKB	0	35.484
	IL1R1	0.0000502	31.056
	LRP5	0.000165	-31.54
	NFATC1	0.0000843	33.466
	NFATC2	3.03E-10	35.288
	SFRP1	0.000135	-25.551
	SMAD6	0.0000366	-25.875
	TCF4	0.000000724	-31.841
	TCF7	0.00000728	-29.221
	TRAF2	5.02E-08	-44.481
	WNT2B	5.99E-09	-31.67
	WNT7A	0.000000401	-44.149
Osteoarthritis Pathway	ALPI	0	-55.556
	ALPL	0.000000117	-30
	ANKH	0.000102	-28.289

	FADD	0.00000322	-34.409
	FZD1	0.0000185	27.788
	FZD5	0.00000477	-30.645
	FZD9	0.000104	-28.133
	GLI2	0.00005	-28.683
	GLIS1	0.0000394	-25.615
	HNF1A	0.00000151	-34.928
	IL1R1	0.0000502	31.056
	NOTCH1	0.00000187	-34.821
	PPARD	0.00000563	-33.171
	PRKAG2	0.000000151	-40.906
	PROK1	0.0000704	-29.412
	SDC4	0.0000511	-28.767
	SMAD3	0.00000175	-26.471
	SMAD6	0.0000366	-25.875
	SOX9	0.00000843	-32.791
	TCF4	0.000000724	-31.841
	TCF7	0.00000728	-29.221
	VEGFA	8.7E-09	-25.49
Actin Cytoskeleton Signaling	ARHGEF7	0.00000701	-32.454
	BAIAP2	0.0000899	-28.663
	FGF4	0.0000605	27.055
	FGF9	0.0000816	-28.675
	FGF19	0.000104	-33.907
	GNA12	0.0000568	-27.296
	GSN	1.56E-10	-46.107
	MAP2K2	0.000087	26.989
	MATK	0.0000384	-30.36
	MPRIP	4.46E-08	29.603
	MYL9	6.67E-09	-40.861
	MYL10	0.0000203	-31.216
	PAK3	0.000000101	26.667
	RAC3	0.00000027	-39.765
	SSH1	0.00000135	-30.209
	SSH3	0.000000328	35.212
	TIAM1	0.000000545	34.146
	VAV1	0.0000207	-25.581

Appendix Table 5 Differentially expressed proteins from infected maternal caruncles compared to non-infected controls.

Symbol	Gene Name	Log2 Fold Change	P Value
Day 82			
ISG15	Ubiquitin-like protein ISG15	5.53	0.00069509
DDB1	DNA Damage Binding Protein 1	-4.78	0.02528178
IFIT1	Interferon Induced Transmembrane Protein 1	4.72	0.05161388
MX1	Isoform 2 of Interferon-induced GTP-binding protein Mx1	3.95	0.07539347
Day 89			
GC	Gc-Globulin	-5.07	0.04842978
HNRNPM	Heterogeneous Nuclear Ribonucleoprotein M	-4.35	0.04842978
MDH1	Malate Dehydrogenase	-5.15	0.07060752
Day 97			
GATM	Glycine amidinotransferase, mitochondrial	5.49	0.00313715
RPL21	60S ribosomal protein L21 (Fragment)	4.67	0.02434566
MVP	Major vault protein	4.59	0.07372129
NPEPPS	Aminopeptidase	4.61	0.07372129
PTMA	Prothymosin alpha	4.36	0.07372129
RAB1B	Ras-related protein Rab-1B	5.13	0.07372129
CYP1B1	Cytochrome P450 Family 1 Subunite B Member 1	4.38	0.07454121
	Day 82		
ISG15	Ubiquitin-like protein ISG15	5.53	0.00069509
DDB1	DNA Damage Binding Protein 1	-4.78	0.02528178
IFIT1	Interferon Induced Transmembrane Protein 1	4.72	0.05161388
MX1	Isoform 2 of Interferon-induced GTP-binding protein Mx1	3.95	0.07539347
	Day 89		
GC	Gc-Globulin	-5.07	0.04842978
HNRNPM	Heterogeneous Nuclear Ribonucleoprotein M	-4.35	0.04842978
MDH1	Malate Dehydrogenase	-5.15	0.07060752
	Day 97		
GATM	Glycine amidinotransferase, mitochondrial	5.49	0.00313715
RPL21	60S ribosomal protein L21 (Fragment)	4.67	0.02434566
MVP	Major vault protein	4.59	0.07372129
NPEPPS	Aminopeptidase	4.61	0.07372129
PTMA	Prothymosin alpha	4.36	0.07372129
RAB1B	Ras-related protein Rab-1B	5.13	0.07372129
CYP1B1	Cytochrome P450 Family 1 Subunite B Member 1	4.38	0.07454121
	Day 190		
SCIN	Adseverin	4.38995449	0.00843574
CORO1A	Coronin-1A	4.02738356	0.02169867
HP1BP3	Heterochromatin protein 1-binding protein 3	3.78771547	0.02169867
JSP	Ig-like domain-containing protein	4.04202994	0.02169867
B2M	Beta-2-microglobulin	3.9518327	0.02169867
SRI	Sorcin	3.5952223	0.02169867
AFP	Alpha-fetoprotein	-3.8076588	0.02372424
EPCAM	Epithelial cell adhesion molecule	-3.8794277	0.02372424

STAT1	Signal transducer and activator of transcription	4.0273822	0.02570405
N/A	Uncharacterized protein	4.01258486	0.02951494
FBN1	Fibrillin-1	-3.8408455	0.03156163
FHL1.1	Four and a half LIM domains 1	3.87210412	0.03156163
HSD17B11	Hydroxysteroid (17-beta) dehydrogenase 11	-3.9246607	0.03156163
LOC100847119	Uncharacterized protein	3.8389378	0.03156163
AP1M2	AP-1 complex subunit mu-2	-3.6848013	0.03696187
CD163	Scavenger receptor cysteine-rich type 1 protein M130	3.67945948	0.03696187
H2AZ2	Histone H2A	-3.9742329	0.03696187
QARS1	Glutamine--tRNA ligase	3.67945948	0.03696187
UBE2M	NEDD8-conjugating enzyme Ubc12	3.47876415	0.03696187
WARS1	Tryptophan--tRNA ligase, cytoplasmic	3.71645358	0.03696187
A1BG	Alpha-1B-glycoprotein	-3.6244793	0.04242728
EIF4G2	Eukaryotic translation initiation factor 4 gamma 2	-3.5149164	0.05229842
FCGRT	Fc fragment of IgG receptor and transporter	3.50013613	0.05240313
PTK2	Non-specific protein-tyrosine kinase	-3.4597888	0.05557735
ITGA3	Integrin alpha-3	-3.6192085	0.06377844
RPL11	60S ribosomal protein L11	-3.3828479	0.06377844
HNRNPH1	Heterogeneous nuclear ribonucleoprotein H1	2.47393797	0.0649692
PLEKHF1	PLEKHF1 protein	-3.3223227	0.06817555
CTSC	Dipeptidyl peptidase 1	3.24556407	0.07464957
PLA2G15	Phospholipase A2 group XV	-3.1994386	0.07464957
TARS1	Threonine--tRNA ligase 1, cytoplasmic	3.22002905	0.07464957
UBE2L3	Ubiquitin-conjugating enzyme E2 L3	3.22002905	0.07464957
FBLN2	Fibulin 2	-3.3713063	0.07495173
NA..22	HIT domain-containing protein	-3.1930808	0.07495173
DPP7	DPP7 protein	3.16756182	0.075572
TWF1	Twinfilin-1	3.16756175	0.07564675
ARPC5	Actin-related protein 2/3 complex subunit 5	-3.3223008	0.08434275
EIF4A1	Eukaryotic initiation factor 4A-I	-2.2421108	0.08434275
C8H9orf64	Queuosine salvage protein	-3.3015479	0.08633313
BLMH	Bleomycin hydrolase	-3.000511	0.08695447
ARL6IP5	PRA1 family protein 3	-3.2374359	0.09208944
CARHSP1	Calcium regulated heat stable protein 1, 24kDa	-3.2374359	0.09208944
LARS1	Leucyl-tRNA synthetase	-3.215416	0.09462893
DHRS11	Dehydrogenase/reductase SDR family member 11	2.94812073	0.09636454
PTGR2	Prostaglandin reductase 2	-3.0757491	0.09636454
Day 245			
C15H11orf34	Placenta-expressed transcript 1 protein	-4.1151729	0.00100145
EIF4B	Eukaryotic translation initiation factor 4B	-5.4750607	0.00100145
FAF2	FAS-associated factor 2	-5.4597891	0.00100145

SF3B3	Splicing factor 3B subunit 3	-4.9346107	0.00148497
PMM1	Phosphomannomutase	-4.9179942	0.00154181
IDH2	Isocitrate dehydrogenase [NADP], mitochondrial	-3.6386211	0.00186964
XPO1	Exportin 1	-5.2179502	0.00285243
NA..21	Ig-like domain-containing protein	4.96843145	0.00300263
NA..4	sp|ALBU_HUM	-5.5630035	0.00385456
WARS1	Tryptophan--tRNA ligase, cytoplasmic	5.45374892	0.00385456
CACYBP	Calcyclin-binding protein	-5.4046887	0.00416384
PDCD6IP	Programmed cell death 6 interacting protein	-5.4516867	0.00458377
IGF2BP1	IGF-II mRNA-binding protein 1	-5.3723952	0.00552274
MIF	Macrophage migration inhibitory factor	4.29617899	0.00701342
TNNC2	Troponin C type 2 (Fast)	4.38742927	0.00764953
HMOX1	Heme oxygenase (biliverdin-producing)	-4.646562	0.00776377
TBCB	Tubulin-folding cofactor B	-4.6055569	0.00776377
RPS17	40S ribosomal protein S17	-4.5916125	0.00789858
ALB	Albumin	-3.9152751	0.00827914
ATP2A3	Calcium-transporting ATPase	-5.0846924	0.00844846
CORO2A	Coronin-2A	-5.0846943	0.00844846
NME2	Nucleoside diphosphate kinase B	2.98744437	0.00844846
AIFM1	Apoptosis inducing factor mitochondria associated 1	-4.9708478	0.011827
ATP5PB	ATP synthase F(0) complex subunit B1, mitochondrial	-4.9271531	0.011827
PSMD3	26S proteasome non-ATPase regulatory subunit 3	-4.9160091	0.011827
CAPZA2	F-actin-capping protein subunit alpha-2	-4.8820694	0.01203581
CSRP1	Cysteine and glycine-rich protein 1	-3.8847302	0.01291722
STK3	Non-specific serine/threonine protein kinase	-4.7249928	0.01541996
CA2	Carbonic anhydrase 2	-4.6327045	0.01995438
CAPG	Macrophage-capping protein	-4.2088398	0.01995438
EIF5B	Eukaryotic translation initiation factor 5B	-4.3975981	0.01995438
FUBP1	Far upstream element binding protein 1	-4.6991606	0.01995438
HSD17B11	Hydroxysteroid (17-beta) dehydrogenase 11	-4.6861175	0.01995438
TMPO	Thymopoietin	-4.6596464	0.01995438
MARCKS	Myristoylated alanine-rich C-kinase substrate	-3.374604	0.02108851
SF3A1	Splicing factor 3A subunit 1	-4.5772073	0.02108851
FN1	Fibronectin	-3.44193	0.02221179
PSMC6	26S proteasome regulatory subunit 10B	-4.3101209	0.02221179
ATP6V1A	H(+)-transporting two-sector ATPase	3.29256501	0.02228254
KIF5B	Kinesin-like protein	-4.5341128	0.02398492
GNS	N-acetylglucosamine-6-sulfatase	-4.4746337	0.02411405
SFN	14-3-3 protein sigma	-4.9379545	0.02411405
SYNCRIP	Synaptotagmin binding cytoplasmic RNA interacting protein	-4.1214529	0.02411405
ARMC10	Armadillo repeat containing 10	-4.4438792	0.02730365

FNBP1L	Formin-binding protein 1-like	-4.3642005	0.02730365
NDUFB10	NADH dehydrogenase [ubiquinone] 1 beta subcomplex subunit 10	-4.3642005	0.02730365
NDUFS1	NADH-ubiquinone oxidoreductase 75 kDa subunit, mitochondrial	-4.3966183	0.02730365
NT5E	5'-nucleotidase	2.66196162	0.02730365
PCBP2	Poly(rC) binding protein 2	-4.8233979	0.02730365
PDS5B	PDS5 cohesin associated factor B	-4.4125603	0.02730365
S100A16	Protein S100-A16	-4.3805027	0.02730365
SYPL1	Synaptophysin like 1	4.3681208	0.02730365
H2AZ2	Histone H2A	-4.7748994	0.02792349
HP1BP3	Heterochromatin protein 1-binding protein 3	3.7945661	0.02792349
RDX	Radixin	-4.5045752	0.02866966
OGDH	2-oxoglutarate dehydrogenase, mitochondrial	-4.1176364	0.02877409
AP1B1	AP complex subunit beta	-4.5193442	0.02969472
COL6A3	Collagen type VI alpha 3 chain	-3.1729364	0.02969472
ISOC1	Isochorismatase domain-containing protein 1	-4.1143013	0.03286646
ARPC1A	Actin-related protein 2/3 complex subunit 1A	-4.1901579	0.03770758
GARS1	Diadenosine tetraphosphate synthetase	-4.0545903	0.03770758
CAB39	Calcium-binding protein 39	-4.1715421	0.03884415
ATIC	Bifunctional purine biosynthesis protein ATIC	-3.9292402	0.03985335
BTF3L4	Transcription factor BTF3	-4.1526671	0.03985335
CCAR2	Cell cycle and apoptosis regulator 2	-4.1526714	0.03985335
LGALS1	Galectin-1	-2.8036092	0.03985335
PREB	Prolactin regulatory element binding	-4.1526714	0.03985335
SLC25A24	Calcium-binding mitochondrial carrier protein SCaMC-1	-4.1526671	0.03985335
CYRIB	CYFIP-related Rac1 interactor B	-4.0945686	0.04266807
MANF	Mesencephalic astrocyte-derived neurotrophic factor	-4.0945686	0.04266807
RBBP4	Histone-binding protein RBBP4	-4.4591242	0.04266807
ARHGDIA	Rho GDP-dissociation inhibitor 1	-2.6887539	0.0427486
PAG10	Peptidase A1 domain-containing protein	-4.3963896	0.04725858
DDX1	ATP-dependent RNA helicase DDX1	-4.2796213	0.05007123
FMNL1	Formin like 1	-4.2621333	0.05009545
HNRNPUL 2	Heterogeneous Nuclear Ribonucleoprotein U Like 2	-4.2621333	0.05009545
PHB	Prohibitin	-2.8708752	0.05009545
PDE1B	Phosphodiesterase	-3.8820799	0.05260931
CMPK1	UMP-CMP kinase	-3.7508991	0.05316187
DDX31	RNA helicase	-4.2968325	0.05587138
PRDX1	Peroxiredoxin-1	-2.9313837	0.05587138
PSMD13	26S proteasome non-ATPase regulatory subunit 13	-4.2620881	0.05587138
RIDA	2-iminobutanoate/2-iminopropanoate deaminase	3.67663663	0.05587138
COL12A1	Collagen alpha-1(XII) chain	-2.467174	0.05806077
CYFIP1	Cytoplasmic FMR1-interacting protein	-4.0131562	0.05806077

DDX39A	RNA helicase	-2.8411356	0.05806077
DHX15	RNA helicase	-3.8820186	0.05806077
EIF1	Eukaryotic translation initiation factor 1	-3.6929109	0.05806077
EIF4G3	Eukaryotic translation initiation factor 4 gamma 3	-4.0745238	0.05806077
ETFA	Electron transfer flavoprotein subunit alpha	-2.855311	0.05806077
PDHB	Pyruvate dehydrogenase E1 component subunit beta, mitochondrial	-4.2083186	0.05806077
PSMD11	26S proteasome non-ATPase regulatory subunit 11	3.75840233	0.05806077
SAFB	SAFB protein	-3.8820186	0.05806077
UNC45A	Unc-45 myosin chaperone A	-3.8820186	0.05806077
WDR5	WD repeat-containing protein 5	-4.2083005	0.05806077
EFTUD2	116 kDa U5 small nuclear ribonucleoprotein component	-4.1524641	0.05846101
ELOC	Elongin-C	-3.9920944	0.05846101
GCLC	Glutamate--cysteine ligase	-3.8354702	0.05846101
PAG2	Pregnancy-associated glycoprotein 2	-3.271847	0.05846101
CAPN6	Calpain 6	-2.8416484	0.06516806
RAB25	Ras-related protein Rab-25	-4.0744612	0.06624461
SLC7A8	Solute carrier family 7 member 8	-4.0744612	0.06624461
FZD4	Frizzled-4	-4.0542828	0.06714457
MYO6	Unconventional myosin-6	-4.0542828	0.06714457
PAICS	AIR carboxylase	-4.0542828	0.06714457
RANBP2	E3 SUMO-protein ligase RanBP2	-4.0338185	0.06935429
BoLA.DRA	BoLA-DR-alpha	4.0100282	0.07400143
MTPN	Myotrophin	4.0100282	0.07400143
N/A	Uncharacterized protein	4.0100282	0.07400143
SCIN	Adseverin	4.0100282	0.07400143
GDA	Guanine deaminase	3.97985048	0.0768946
NA..31	BOLA class I histocompatibility antigen, alpha chain BL3-7	3.97985048	0.0768946
NA..33	Ig-like domain-containing protein	3.97985048	0.0768946
HDGF	Hepatoma-derived growth factor	2.75935694	0.07828351
THY1	Thy-1 cell surface antigen	-3.9489212	0.07828351
CSRP2	Cysteine and glycine-rich protein 2	-3.9489156	0.07857139
HNRNPH1	Heterogeneous nuclear ribonucleoprotein H1	3.04727557	0.07901574
PROS1	Vitamin K-dependent protein S	-3.6739584	0.07901574
C1QBP	Complement component 1 Q subcomponent-binding protein, mitochondrial	-2.6465995	0.08244787
PGM2	Phosphoglucomutase 2	2.28978645	0.08794468
DYNC1I2	Cytoplasmic dynein 1 intermediate chain 2	-3.7872119	0.0885953
MCM3	DNA replication licensing factor MCM3	-3.7625543	0.09091614
ARF6	ADP-ribosylation factor 6	-3.8114141	0.09505082
METAP2	Methionine aminopeptidase 2	-3.8114141	0.09505082
GNG12	Guanine nucleotide-binding protein G(I)/G(S)/G(O) subunit gamma-12	3.83770815	0.09578323
PTK2	Non-specific protein-tyrosine kinase	-3.7374516	0.09578323

IQGAP2	IQ motif containing GTPase activating protein 2	-3.7871645	0.09773814
AP3B1	AP-3 complex subunit beta-1	-3.7374091	0.09799238
C8H9orf64	Queuosine salvage protein	-3.7625066	0.09799238
CAPRIN1	Caprin-1	-3.7374152	0.09799238
CTSS	Cathepsin S	3.65794599	0.09799238
DPP3	Dipeptidyl peptidase 3	-3.7374091	0.09799238
GLOD4	Glyoxalase domain-containing protein 4	-3.7374091	0.09799238
ITGA2	Integrin alpha-2	-2.6079887	0.09799238
PCMT1	Protein-L-isoaspartate(D-aspartate) O-methyltransferase	-3.7625003	0.09799238
RSU1	Ras suppressor protein 1	-3.7374091	0.09799238
SLC6A11	Transporter	-3.6325129	0.09799238
TMEM109	Transmembrane protein 109	-3.6859278	0.09799238
UBR4	Ubiquitin protein ligase E3 component n-recognin 4	-3.7625003	0.09799238
VKORC1L1	Vitamin-K-epoxide reductase (warfarin-sensitive)	-3.6325129	0.09799238
LAP3	Cytosol aminopeptidase	2.83877044	0.09871953

Appendix Table 6: Significant pathways and proteins in infected fetal cotyledons vs. controls, as identified by IPA.

Symbol	Protein Name	Log2 Fold Change	P Value
Day 89			
TPM1	Tropomyosin alpha-1 chain	5.7252824	0.00500916
GALK1	Galactokinase	5.14377577	0.01161287
HADHA	Enoyl-CoA hydratase	4.86281892	0.01161287
HMGB2	High mobility group protein B2	4.44533623	0.01161287
HPX	Hemopexin	-5.184079	0.01161287
N/A	Ig-like domain-containing protein	-5.1305227	0.01161287
PSMD2	26S proteasome non-ATPase regulatory subunit 2	5.10234559	0.01161287
ARCN1	Coatomer subunit delta	4.861271	0.01813422
EIF5	Eukaryotic translation initiation factor 5	4.842988	0.02186776
GOT1	Aspartate aminotransferase, cytoplasmic	4.02054879	0.02533946
H2AC21	Histone H2A	4.30044596	0.02533946
NAPA	Alpha-soluble NSF attachment protein	4.42426475	0.02533946
SERPINA3.7	Serpin A3-7	-5.2615095	0.02533946
MCM3	DNA replication licensing factor MCM3	4.61293409	0.0266234
ACAA2	3-ketoacyl-CoA thiolase, mitochondrial	4.3527633	0.04628822
AKR7A2	Aldo_ket_red domain-containing protein	4.37455123	0.04628822
MX1	Isoform 2 of Interferon-induced GTP-binding protein Mx1	4.8991289	0.04628822
N/A	Uncharacterized protein	3.12330224	0.04628822
PYGB	Alpha-1,4 glucan phosphorylase	4.35243084	0.04628822
SEPTIN9	Septin 9	4.37455123	0.04628822
VASP	Vasodilator-stimulated phosphoprotein	4.71160863	0.04628822
ATIC	Bifunctional purine biosynthesis protein ATIC	4.6050773	0.05563543
HBB	Hemoglobin subunit beta	3.09264704	0.05563543
THSD4	PLAC domain-containing protein	4.69431141	0.05563543
ALDOC	Fructose-bisphosphate aldolase	4.63600479	0.06359686
CASP6	Caspase-6	-4.1463276	0.0668167
GNG12	Guanine nucleotide-binding protein G(I)/G(S)/G(O) subunit gamma-12	-4.5173677	0.0668167
HNRNPH3	Heterogeneous nuclear ribonucleoprotein H3	4.29393682	0.0668167
ISG15	Ubiquitin-like protein ISG15	4.50385405	0.0668167
RPS17	40S ribosomal protein S17	4.57127077	0.0668167
TMED2	RNP24	4.51009911	0.0668167
TMED4	Transmembrane p24 trafficking protein 4	4.03476177	0.0668167
VWA5A	von Willebrand factor A domain containing 5A	4.03476177	0.0668167
PSMA6	Proteasome subunit alpha type-6	4.27678888	0.06689308
S100A11	Protein S100	4.47818049	0.06965272
SLC25A6	ADP/ATP translocase 3	-3.0471126	0.09021742
TACSTD2	Tumor associated calcium signal transducer 2	4.24465617	0.09637597
TM9SF3	Transmembrane 9 superfamily member	4.24465617	0.09637597

ISYNA1	Inositol-3-phosphate synthase 1	4.26184128	0.09744892
Day 97			
DDB1	DNA damage-binding protein 1	-5.4093821	0.00086434
RAB11B	Ras-related protein Rab-11B	-4.1351544	0.00086434
RPS10	40S ribosomal protein S10	-5.0980242	0.00086434
PREP	Post-proline cleaving enzyme	-4.9999922	0.00115356
SFN	14-3-3 protein sigma	-5.5774167	0.00191905
H2AC21	Histone H2A	-5.2479162	0.00480666
UQCRC1	Cytochrome b-c1 complex subunit 1, mitochondrial	-4.6724173	0.00526666
ISYNA1	Inositol-3-phosphate synthase 1	-4.9657736	0.00859799
BLVRB	Flavin reductase (NADPH)	-4.8073446	0.0104492
N/A	Uncharacterized protein	-4.8073446	0.0104492
PA2G4	Proliferation-associated 2G4	-4.8201688	0.0104492
PABPC4	Polyadenylate-binding protein	-5.0334105	0.0129497
UBE2V2	Ubiquitin-conjugating enzyme E2 variant 2	4.62934937	0.01376931
ARPC3	Actin-related protein 2/3 complex subunit 3	-4.4093817	0.01815732
EPCAM	Epithelial cell adhesion molecule	-4.4429341	0.01815732
FLII	FLII actin remodeling protein	-4.4093817	0.01815732
GNAI3	G protein subunit alpha i3	-4.9307242	0.01815732
HYOU1	Hypoxia up-regulated 1	-4.5235522	0.01815732
PCNA	Proliferating cell nuclear antigen	-4.5235523	0.01815732
PYGL	Alpha-1,4 glucan phosphorylase	-4.4093816	0.01871788
EHD2	EH-domain containing 2	-4.2288097	0.02629811
HEXB	Beta-hexosaminidase	-4.2288097	0.02629811
NID1	NID1 protein	-4.5698441	0.02629811
PGRMC2	Progesterone receptor membrane component 2	-4.2479185	0.02629811
PPP2R1A	Serine/threonine-protein phosphatase 2A 65 kDa regulatory subunit A alpha isoform	-4.2667772	0.02716836
S100A16	Protein S100-A16	-4.4429319	0.03962277
SEC61A1	Protein transport protein Sec61 subunit alpha isoform 1	3.92599388	0.03962277
EIF5	Eukaryotic translation initiation factor 5	-3.954188	0.04327656
RPS7	40S ribosomal protein S7	-4.3575407	0.04327656
AKR7A2	Aldo_ket_red domain-containing protein	-3.9307291	0.04370727
FETUB	Fetuin-B	-3.0995302	0.04370727
CLIC4	Chloride intracellular channel protein 4	3.10962258	0.05019413
DDX17	RNA helicase	-4.1699143	0.05019413
FBN2	Fibrillin 2	-4.137493	0.05019413
HADHB	Trifunctional enzyme subunit beta, mitochondrial	-3.8073469	0.05019413
IGF2R	Cation-independent mannose-6-phosphate receptor	2.84608595	0.05019413
PAFAH1B3	Platelet-activating factor acetylhydrolase IB subunit alpha1	-4.1292725	0.05019413
RPL10A	60S ribosomal protein L10a	-3.213773	0.05019413
RPS5	40S ribosomal protein S5	-4.1292725	0.05019413

TARDBP	TAR DNA-binding protein 43	-4.1497365	0.05019413
VASP	Vasodilator-stimulated phosphoprotein	-4.1898138	0.05019413
SERBP1	SERPINE1 mRNA binding protein 1	-4.0874525	0.05261922
ERP44	Endoplasmic reticulum resident protein 44	-3.700432	0.05329122
OGDH	2-oxoglutarate dehydrogenase, mitochondrial	-3.0931036	0.05329122
PDCD6IP	Programmed cell death 6 interacting protein	-4.1085136	0.05329122
PSMB5	Proteasome subunit beta type-5	-4.0660787	0.05329122
ADK	Adenosine kinase	-3.9541863	0.05675903
AP2M1	AP-2 complex subunit mu	-3.6438486	0.05675903
CLTB	Isoform Non-brain of Clathrin light chain B	-3.9541863	0.05675903
DSTN	Actin-depolymerizing factor	-3.9541863	0.05675903
NDUFA9	NADH dehydrogenase [ubiquinone] 1 alpha subcomplex subunit 9, mitochondrial	-3.9772699	0.05675903
PSMC2	26S proteasome regulatory subunit 7	-3.9999899	0.05675903
TPM2	Isoform 2 of Tropomyosin beta chain	-2.8916187	0.05675903
STC1	Stanniocalcin-1	-3.9068807	0.06045774
PEPD	Peptidase D	3.93072993	0.06179424
NUCB2	Nucleobindin 2	-3.8826332	0.06196085
LRPAP1	LDL receptor related protein associated protein 1	-3.8579712	0.06296429
PHLDA2	Pleckstrin homology-like domain family A member 2	-3.8579712	0.06296429
PSMC3	Proteasome 26S subunit, ATPase 3	-3.8579712	0.06296429
EMILIN1	Elastin microfibril interfacer 1	3.70043364	0.06979796
GALK1	Galactokinase	-3.7548781	0.07224171
RPS26	40S ribosomal protein S26	-3.7548781	0.07224171
GLB1	Beta-galactosidase	-3.7548781	0.07241233
CP	Ceruloplasmin	-3.7004304	0.0808064
TACSTD2	Tumor associated calcium signal transducer 2	-3.7004304	0.0808064
UCHL3	Ubiquitin carboxyl-terminal hydrolase isozyme L3	-3.672416	0.08369431
VPS26A	Vacuolar protein sorting-associated protein 26A	-3.672416	0.08369431
NPEPPS	Aminopeptidase	-3.643847	0.08692714
SPTBN1	Spectrin beta chain	-3.643847	0.08692714
ATP2A2	Calcium-transporting ATPase	-3.5849536	0.08775227
COPZ1	Coatomer subunit zeta-1	-3.5849536	0.08775227
LTBP4	Latent transforming growth factor beta binding protein 4	-3.5849536	0.08775227
SEC22B	SEC22 homolog B, vesicle trafficking protein	-3.5849536	0.08775227
NME2	Nucleoside diphosphate kinase B	2.78135778	0.09841427
PAK2	Non-specific serine/threonine protein kinase	-3.4918444	0.09841427
RAC1	Ras-related C3 botulinum toxin substrate 1	-3.4918444	0.09841427
SRGN	Serglycin	-3.4918444	0.09841427
TPD52	Tumor Protein D52	-3.4918444	0.09841427
YARS1	Tyrosine--tRNA ligase	-3.4918444	0.09841427
Day 190			

CYP17A1	Steroid 17-alpha-hydroxylase/17,20 lyase	-4.123286	0.01921249
N/A	Uncharacterized protein	4.06080507	0.01965788
NUCB1	Nucleobindin-1	-3.7899999	0.01965788
PPP2R1A	Serine/threonine-protein phosphatase 2A 65 kDa regulatory subunit A alpha isoform	-3.695111	0.01965788
YWHAH	14-3-3 protein eta	-2.6052634	0.01965788
NA..13	sp|K22E_HUM	3.86855752	0.02386618
SOD3	Superoxide dismutase [Cu-Zn]	-4.0130567	0.02386618
SLC25A1	Tricarboxylate transport protein, mitochondrial	-3.4358794	0.02778926
TMED2	RNP24	3.7026263	0.02778926
SFN	14-3-3 protein sigma	-2.7642771	0.02986332
IFI44L	Interferon induced protein 44 like	3.79565982	0.0388512
IFITM1	Interferon Induced Transmembrane Protein 1	3.66802733	0.0436384
ITGA3	Integrin alpha-3	-3.4114719	0.0436384
JSP	Ig-like domain-containing protein	3.35279942	0.04773004
ISG15	Ubiquitin-like protein ISG15	3.60719775	0.05202859
HNRNPR	HNRNPR protein	-3.5639624	0.05328273
NA..21	Beta-2-microglobulin	3.50004164	0.05399233
LAMB2	Laminin Subunit Beta 2	-3.5430025	0.06095442
OAS1X	2'-5' oligoadenylate synthase	3.45393667	0.06095442
P4HA1	Prolyl 4-hydroxylase subunit alpha-1	-3.4986817	0.06160823
THBS1	Thrombospondin-1	-3.3587155	0.0636607
NA..14	sp|K1C10_HUM	3.14559159	0.07421613
APOA4	Apolipoprotein A-IV	-3.34122	0.08387758
FBN2	Fibrillin 2	-3.2680731	0.08456228
LRPAP1	LDL receptor related protein associated protein 1	-3.1730517	0.08456228
ILF3	Interleukin enhancer binding factor 3	-2.9274472	0.09371253
CAPN1	Calcium-activated neutral proteinase 1	-3.0264152	0.09451766
CYB5A	Cytochrome b5	-2.8585412	0.09451766
GPX1	Glutathione peroxidase 1	3.02550584	0.09451766
HRG	Histidine-rich glycoprotein	-3.1619413	0.09451766
OAS1Y	2'-5' oligoadenylate synthase	3.10754262	0.09451766
SEC61A1	Protein transport protein Sec61 subunit alpha isoform 1	-3.1804534	0.09567207
BLMH	Bleomycin hydrolase	-2.8293722	0.09748399

Table of Abbreviations

Acronym	Full Name
ACAA2	3 Ketoacyl CoA Thiolase
ADAR	Adenosine Deaminase Acting on RNA
AFP	Alphafetoprotein
AKAP2	AKAP2 C Domain Containing Protein
ALDPC	Fructose Biphosphate Aldolase
ALS	Amyotrophic Lateral Sclerosis
AP1	Activator Protein Transcriptional Complex
APC	Antigen Presenting Cell
ARS	Aminoacyl-tRNA synthetases
BDV	Border Disease (sheep)
BRD	Bovine Respiratory Disease
BVDV	Bovine Viral Diarrhea Virus
C/EBP1A	CCAAT/enhancer Binding Protein Alpha
CALM	Calmodulin
CD	Cluster of Differentiation
CLR	C Type Lectin Receptors
CME	Clathrin Mediated Endocytosis
CMV	Human Cytomegalovirus
CNN2	Calponin 2
cp	Cytopathic (BVDV)
CSFV	Classical Swine Fever Virus
CSFV	Colony Stimulating Factor
CSH	Chorionic Somatomammotropin
CSRP1	Cysteine and Glycine Rich Protein 1
CSTB	CSTB Protein
CXCL	Chemokine Ligand
CXCR	Chemokine Receptor
CYP1B1	Cytochrome P450 Family 1 Subfamily B Member 1
DAMPS	Damage Assoicated Molecular Patters
DDB1	DNA Damage Binding Protein 1
DDX58/RIGI	DExD/H-Box Helicase 58/Retinoic Acid Inducible Gene 1
DHRS11	Methylglycoxal Degradation III
DKK1	Dickkopf WNT Signaling Pathway Inhibitor 1
DMR	Differentially Methylated Regions
dsRNA	Double Stranded RNA

EC	Endothelial Cell
EIF2	Eukaryotic Initiation Factor 4A-1
EIF4G2	Eukaryotic Initiation Factor 4G-2
EPM1	Progressive Myoclonus Epilepsy of Unverricht-Lundborg Type
FDR	False Discovery Rate
GAPDH	Glyceraldehyde-3-Phosphate Dehydrogenase
GATM	Glycine Amidinotransferase Mitochondrial
GC	GC-globulin
GEO	Gene Expression Omnibus
H&E	Hematoxylin and Eosin
HADHA	Enoyl CoA Hydratase
HELLP	Hemolysis, Elevated Liver Enzymes, and Low Platelet Count
Hep2	Human Epithelial
HNRNPM	Heterogeneous Nuclear Ribonucleoprotein M
HNRPC	Heterogenous Nuclear Ribonucleoprotein C
HSV	Herpes Simplex Virus
IACUC	Institutional Animal Care and Use Committee
IFI30	IFI30 Lysosomal Thiol Reuctase
IFIT1	Interferon Induced Protein with Tetratricopeptide Repeats 1
IFITM1	Interferon Induced Transmembrane Protein 1
IFN	Interferon
IHC	Immunohistochemistry
IKBKB	Inhibitor of Nuclear Factor Kappa B Kinase Subunit Beta
IL	Interleukin
IPA	Ingenuity Pathway Analysis
IRES	Internal Ribosome Entry Site
IRF7	Interferon Regulatory Factor 7
IRI16	Interferon Gamma Inducible Protein
ISG	Interferon Stimulated Gene
ISGF	Interferon Stimulated Gene Factor
ITGAM	Integrin Subunit Alpha M
IUGR	Intrauterine Growth Restriction
JAK	Janus Kinase
Jiv	J Domain Protein Interacting with Viral Protein
KV	Killed Vaccine
LARS1	Leucyl-tRNA Synthetase
LC-MS	Liquid Chromatography Mass Spectrometry
MDBK	Madin-Darby Bovine Kidney

MDH1	Malate Dehydrogenase
MEF2D	Myocyte Enhancer Factor 2D
MEM	Minimal Essential Media
MHC	Major Histocompatibility Complex
MLV	Modified Live Viral
MVP	Major Vault Protein
MX1	Isoform 2 of Interferon Induced GTP Binding Protein MX1
ncp	Noncytopathic (BVDV)
NFAT	Nuclear Factor of Activate T Cells
NFKB	Nuclear Factor Kappa B
NIBP	NIK- and IKKB Binding Protein
NOD	Nucleotide Binding Oligomerization Domains
NPEPPS	Aminopeptidase
NUDC	Nuclear Migration Protein NUDC
OAS1	2'-5'-Oligoadenylate Synthetase 1
ORF	Open Reading Frame
PALS	Periarteriolar Sheath
PAMP	Pattern Associated Molecular Patterns
PBMC	Peripheral Blood Mononuclear Cells
PEPD	Peptidase D
PGCA1B	PPARG Coactivator 1 Beta
PI	Persistent Infection
PKC	Protein Kinase C
PPARG	Peroxisome Proliferator Activated Receptor Gamma
PRR	Pattern Recognition Receptor
PSMA2	Proteasome Subunit Type 2
PSMA6	Proteasome Subunit Alpha Type 6
PSMB8/9	Proteasome Subunit Beta
PTGR2	Prostaglandin Reductase 2
PTK2	Protein Tyrosine Kinase
PTMA	Prothymosin Alpha
PYGB	Alpha 1,4 Glucan Phosphorlase
QARS1	Glutamine-tRNA Ligase
RAB1B	Ras-Related Protein Rab-1B
RANKL	Receptor Activator of Nuclear Factor Kappa B Ligand
RdRp	RNA Dependent RNA Polymerase
RPL21	60S Ribosomal Protein L21
RRBS	Reduced Representation Bisulphite Sequencing

RT-qPCR	Reverse Transcription Quantitative Polymerase Chain Reaction
SD	Standard Deviation
SEM	Standard Error Mean
SNRPF	Small Nuclear Ribonucleoprotein F
SpC	Spectral Counts
STAT	Signal Transducer and Activator of Transcription
TAP1	Transporter Associated with Antigen Processing
TARS1	Threonine-tRNA Ligase 1
TBX5	T Box Transcription Factor 5
TCF	T Cell Factor
Th	T Helper Cell
THY1	Thy-1 Cell Surface Antigen
TLR	Toll Like Receptor
TMA7	Translation Machinery Associated Protein 7
TMOD3	Tropomodulin 3
TNFA	Tumor Necrosis Factor Alpha
TNFB	Tumor Necrosis Factor Beta
TRAF	TNF Receptor Associated Factor
Treg	T Regulatory Cell
tRNA	Transfer RNA
TWF1	Twinfilin
UTR	Untranslated Region
VAPB	Vesicle Associated Membrane Protein B
VASP	Vasodilator Stimulated Phophoprotein
VAV1	Vav Guanine Nucleotide Exchange Factor 1
VEGF	Vascular Endothelial Growth Factor
Vero	African Green Monkey Kidney Cells
WARS1	Tryptophan-tRNA ligase
YWHAZ	Tyrosine 3-Monooxygenase
ZIKV	Zika Virus